NISTIR 89-3912

ELECTROMECHANICAL PROPERTIES OF SUPERCONDUCTORS FOR HIGH-ENERGY PHYSICS APPLICATIONS Part II

J. W. Ekin
L. F. Goodrich
S. L. Bray
N. F. Bergren
R. B. Goldfarb

NISTIR 89-3912

ELECTROMECHANICAL PROPERTIES OF SUPERCONDUCTORS FOR HIGH-ENERGY PHYSICS APPLICATIONS Part II

J. W. Ekin
L. F. Goodrich
S. L. Bray
N. F. Bergren
R. B. Goldfarb

Electromagnetic Technology Division
Center for Electronics and Electrical Engineering
National Engineering Laboratory
National Institute of Standards and Technology
Boulder, Colorado 80303-3328

November 1989

U.S. DEPARTMENT OF COMMERCE, Robert A. Mosbacher, Secretary

National Institute of Standards and Technology, Raymond G. Kammer, Acting Director

CONTENTS

ELECTROMECHANICAL PROPERTIES OF SUPERCONDUCTORS FOR HIGH-ENERGY PHYSICS APPLICATIONS

J.W. Ekin, L.F. Goodrich, S.L. Bray, N.F. Bergren, R.B.Goldfarb
Electromagnetic Technology Division
National Institute of Standards and Technology
Boulder, Colorado 80303-3328

This report presents data on superconductor performance under mechanical load. The data are needed for setting mechanical design constraints and measuring the electro-mechanical performance of NbTi superconductors for DOE high-energy physics magnet applications. The effect of axial tensile stress, applied at room temperature, on the critical current of NbTi superconductor strands has been measured. The data show a simple result that the effect on the critical current is independent of the temperature at which the stress is applied; this allows the existing 4 K data base to be used to determine critical current degradation from room temperature fabrication stress, from cool-down stress introduced by differential contraction, and from 4 K stress generated by the Lorentz force when the magnet is energized. A study of the critical-current variations along NbTi strands extracted from a Rutherford cable has been made also. The results show that the principal mechanical degradation is extremely localized at the regions where the NbTi strand is bent around the edge of the cable. For example, only 3% of the total strand length can contribute 92% of the total strand voltage. A further study has been made of the effects of bending strain on the critical current of NbTi conductors. The degradation of the critical current from bending strain is much greater at low values of electric field than at high, suggesting that irregularity of the filament cross-sectional area introduced by bending may be the source of the I_c degradation. The bend tolerance of a NbTi conductor can be enhanced by increasing the local copper-to-super-conductor area ratio. Measurements of the permeability, saturation magnetization, and intrinsic coercivity of several high-permeability steel alloys were made. The overall differences of saturation magnetization and in-trinsic coercivity between cold-rolled steel samples were not significant.

Key words: bending strain; cable; coercivity; critical current; electromechanical; magnetic properties; NbTi; permeability; Rutherford cable; saturation magnetization; SSC; Superconducting Super Collider.

Summary

This report presents data on superconductor performance under mechanical load. The data are needed for setting mechanical design constraints and measuring the electromechanical performance of NbTi superconductors for DOE high-energy physics magnet applications. The main objective of the program is to develop strategies leading to the most tolerant strain damage limits in these conductors and, therefore, the least overall performance degradation in magnet applications.

In an earlier report from this program (NBS Internal Report # NBSIR 86-3061), several basic aspects of the electromechanical degradation problem were studied. Highlights of that report include the following:

*The critical current (I_c) degradation in NbTi from transverse compressive stress is comparable to that from axial tension.

*Results on superconductor strands extracted from keystoned Rutherford cables indicate that the principal source of critical-current degradation occurs at the narrow keystone edge, not at strand crossover points along the flat region of the cable.

*An approximate quantitative relationship was established between filament sausaging and the shape of the electric-field vs. current (E vs. I) characteristic, given by n where $E \propto I^n$).

Highlights of this report include the following:

The first measurements of the effect of axial tensile stress, applied at room temperature, on the critical current of NbTi superconductor strands have been measured. The data show a simple result that the effect on the critical current is independent of the temperature at which the stress is applied; this allows the existing 4 K data base to be used to determine critical current degradation from room temperature fabrication stress, from cool-down stress introduced by differential contraction, and from 4 K stress generated by the Lorentz force when the magnet is energized.

A study of the critical-current variations along NbTi strands extracted from a Rutherford cable has been made. The results show that the principal mechanical degradation is extremely localized at the regions where the NbTi strand is bent around the edge of the cable. For example, only 3% of the total strand length can contribute 92% of the total strand voltage. The degree of variation depends on the orientation of the applied magnetic field. However, the overall voltage is nearly independent of the field angle. All conductors tested showed small resistive voltages associated with current transfer in the regions of deformation.

A systematic study of the effects of bending strain on the critical current of NbTi conductors has been performed. The I_c degradation decreases with increasing magnetic field, suggesting that the source of degradation is not an intrinsic degradation of H_{c2}, as with the elastic axial-strain effect. The degradation of the critical current from bending strain is much greater at low values of electric field than at high, suggesting that irregularity of the

filament cross-sectional area introduced by bending may be the source of the I_c degradation. By testing a series of similarly fabricated NbTi wires, we found that the bend tolerance of a NbTi conductor can be enhanced by increasing the local copper-to-superconductor area ratio (LAR). Improved bend tolerance also correlates with using a filament diffusion barrier material made of vanadium, instead of Nb or Nb/CuNi. The dependence of the bend degradation on LAR represents a mechanical limit to reduction of the LAR when controlling filament-sausaging effects.

Many high-energy-physics accelerators use high-permeability steel for the return flux path of the superconducting magnets. Measurements of the permeability, saturation magnetization, and intrinsic coercivity (H_c) of several high-permeability steel alloys were made. Values of H_c at 76 K ranged from 110 A/m (1.4 Oe) for cold-rolled samples to 170 A/m (2.1 Oe) for hot-rolled samples. The results were independent of whether the field was parallel or perpendicular to the rolling direction. H_c was slightly larger at liquid-nitrogen temperature than at room temperature. At liquid-helium temperature, H_c is expected to be slightly higher still. The overall differences of saturation magnetization and intrinsic coercivity between cold-rolled steel samples were not significant.

Effect of room temperature stress on the critical current of NbTi

S. L. Bray and J. W. Ekin

National Institute of Standards and Technology

Electromagnetic Technology Division

Boulder, Colorado 80303

ABSTRACT

The effect of axial tensile stress, applied at room temperature, on the critical current of NbTi superconducting wire was measured and compared with the effect of tensile stress applied at liquid-helium temperature ($\sim$4 K). The results of these measurements indicate that the effect on the critical current is independent of the temperature at which the stress is applied. Thus, the existing 4 K data base can be used to determine I_c degradation from room temperature fabrication stress, from cool-down stress introduced by differential contraction, and from 4 K stress generated by the Lorentz force when the magnet is energized. To generalize these results for arbitrary matrix-to-superconductor volume ratios, the data are presented in terms of the stress on the NbTi portion of the composite conductor. Methods for determining the stress on the NbTi from the total composite load are presented.

INTRODUCTION

Superconducting composites used in the construction of large-scale magnets may be subjected to several sources of mechanical stress. These stresses occur within three different temperature ranges: room temperature, the transition between room and liquid-helium temperatures, and liquid-helium temperature (~4 K). At room temperature the sources of stress are associated with the fabrication of the magnet; they are predominantly winding tension and bending stress arising from cabling and conductor-winding operations. In the transition between room temperature and 4 K, stress on the superconductor arises from differential thermal contraction between the superconductor and other materials that compose the magnet. Finally, at 4 K the source of stress is the Lorentz force that is generated when the magnet is energized.

Until now, critical-current degradation in NbTi from uniaxial stress has been measured only for stresses introduced at liquid-helium temperature.[1-3] This paper presents the results of the first measurements of the effect on critical current of tensile stress applied at room temperature. The results indicate a simple general relationship: the stress effect on the critical current of NbTi is independent of the temperature at which the stress is applied. The results should be useful in setting limits on the acceptable tensile stress resulting from the combined effects of fabrication, differential thermal contraction, and Lorentz force, particularly in large magnet systems. This result has implications for the fundamental understanding of the source of the stress effect on the upper critical field (Hc_2) and critical-current density (J_c).

EXPERIMENTAL APPARATUS

The superconductor used in this experiment is a multifilamentary NbTi sample, containing 648 filaments in a copper matrix. The characteristics of the sample are presented in Table I.

Tensile stress is applied to a 28 cm long straight sample of the conductor by a servohydraulic feedback load system having the capability of load, stroke, or strain control. The background magnetic field is applied perpendicular to the direction of stress by a 7 T radial-access solenoidal magnet. Current is supplied to the sample by a 1000 A, controllable battery supply. Details of the apparatus are described in Ref. 2.

EXPERIMENTAL PROCEDURE

The experimental procedure consists of two separate tests. The first test (4 K test) is conducted entirely at liquid-helium temperature and serves as a baseline for the room-temperature stress test. The sample is cooled to liquid-helium temperature under no load, and then the critical current is measured as a function of magnetic field and stress applied at liquid-helium temperature. In the second test (room-temperature test) another sample of the same wire from the same spool as the first sample is stressed to a selected level at room temperature and then lowered to liquid-helium temperature while the load is maintained constant by the servohydraulic load system. Once temperature equilibrium is reached at 4 K, the critical current is measured at several applied magnetic fields.

In order to compare the room-temperature stress effect with the 4 K stress effect in a generic way, the results are presented here in terms of the stress on the NbTi portion of the composite. Comparisons in terms of overall composite stress are specific to only one conductor because of the variations

in the copper-to-superconductor volume ratio for different conductors. The
relative portions of the total load carried by the Cu matrix and the NbTi
depend primarily on their volume ratio and their mechanical properties;
however, copper creep and loading history can also somewhat affect the
relative loading. For these reasons, the I_c-degradation data are presented in
terms of NbTi stress. The method for applying these results to an arbitrary
conductor is discussed in the PRACTICAL APPLICATION section.

RESULTS

The results of these tests are presented graphically in Fig. 1 where
normalized critical current (I_c/I_{cm}) is plotted versus the stress on the NbTi
component of the composite (NbTi Stress). The normalized critical current is
calculated by dividing the critical current (I_c) measured at a particular load
and magnetic field by the maximum critical current (I_{cm}) measured at no load
and at the same magnetic field. The result (I_c/I_{cm}) is expressed as a
percent.

I_{cm} is measured after the sample is unloaded from its room-temperature
stress point. This procedure is justified by comparisons made between the
measured critical currents for the unloaded room-temperature samples and
virgin samples of the same wire that have not been loaded. These comparisons
show that, within the sample-to-sample variation measured for the virgin wire,
the critical-current recovery of the unloaded room-temperature samples is
complete.

For comparison, the plot contains data points from a 4 K test and three
room-temperature tests at three magnetic fields and various stress levels.
The solid symbols correspond to the room-temperature tests and the open
symbols correspond to the 4 K test. The close agreement between the 4 K and

room-temperature data points indicate that the stress effect on NbTi is independent of the temperature at which the stress is applied. The largest disagreement between the 4 K and the room-temperature data occurs at the maximum room-temperature stress level (~1.6 GPa) where the NbTi filaments are just starting to yield (at room temperature). Here the room-temperature data points are consistently slightly lower than the 4 K data points. The maximum discrepancy occurs at 7 T where the critical current is approximately 7% lower for stress applied at room temperature than for stress applied at 4 K. This difference is less than the uncertainty of the room-temperature measurement.

METHOD OF DETERMINING NbTi STRESS

As stated above, the comparisons of I_c degradation for stress applied at room temperature versus 4 K shown in Fig. 1 are based upon the stress state of just the NbTi portion of the conductor. The NbTi stress was used to make the results more generic and not dependent on a specific copper-to-superconductor ratio. Because direct measurement of the stress on the NbTi portion of the composite is not practical, a method of extracting this information from the available composite stress data is required. In the Appendix we discuss the detailed breakdown of each component's load-strain relationship for relating overall composite stress to the stress experienced by just the NbTi filaments. An example of the use of the technique is shown in Fig. 2. The heavy lines in Fig. 2 show the stress-strain curve for the composite upon repeated loading and unloading. The repeated loading portions of the curve between zero load and the upper envelope has been omitted for clarity. [These portions of the curve are equivalent to the A-to-C segment of the composite curve of Fig. 5 in Appendix A and are not required for constructing the NbTi curve.]

The two other curves shown in Fig. 2, the "Cu" curve and the "NbTi" curve, are derived from the composite curve by using the technique described in the Appendix. This technique, however, is only applicable in the area labeled "Linear Region." The lower nonlinear portion of the "Composite" curve is due to yielding of the Cu, while the upper nonlinearity is due to yielding of the NbTi. Consequently, extrapolation is necessary in order to determine the NbTi load outside this linear region. This extrapolation is possible based on two assumptions: one, that the "NbTi" load curve is linear below its yield point and, two, that the "Cu" load curve is linear above its yield point. Both of these assumptions are supported by independent stress-strain data on these materials.[4]

The Cu load points, indicated by triangular symbols in Fig. 2, are determined by taking the difference between the composite and NbTi load curves. The line defined by these symbols is then extended to the maximum strain of the composite curve, again assuming linearity of the Cu curve above the yield point. Finally, the upper portion of the NbTi curve is constructed by taking the difference between the composite and Cu load curves. This general technique was used to determine the NbTi stresses for both the room temperature and the 4 K data that are presented in Fig. 1; (Fig. 2 shows only the 4 K data).

PRACTICAL APPLICATION

Figure 3 is a plot of normalized I_c versus NbTi stress for a number of magnetic fields at 4 K, and it can be used to estimate the effect of stress at room temperature. However, the stress on the NbTi portion of the conductor must first be determined. Ideally, this should be achieved as described above by measuring the room-temperature composite load-versus-strain characteristic

of the conductor and then constructing the associated NbTi load-versus-strain

curve. Due to the specialized equipment required for making these stress

measurements, this technique may, in some cases, be impractical.

Alternatively, a method for estimating the NbTi stress without the aid of

these measurements may be used.

Figure 4 is a plot of NbTi stress versus composite stress for several Cu-

to-NbTi volume ratios. The dashed curve (Cu:NbTi = 1.77:1) is based on the

conductor used in these tests. The other curves were derived by using various

Cu-to-NbTi volume ratios. These curves are based on a linear model (equation

1 below) of the composite load-versus-strain characteristic and they are

sensitive to the material properties used in the model. The material

properties of the conductor tested here were used in generating these curves

and the values of these parameters are given below, following their

definitions. For NbTi superconductors in general, these curves may be used to

estimate, at least to first order, the NbTi stress and the resulting I_c

degradation due to room-temperature loading. If the material properties of a

conductor are known, they may be used in the following equation to more

accurately estimate the NbTi stress:

$$\sigma_{NbTi} = \frac{E_{NbTi} [\ L/A_c - \epsilon_{ym}(1-f)(E_{Cu}-M_{Cu})]}{fE_{NbTi} + (1-f)M_{Cu}} + \sigma_p, \qquad [1]$$

where

σ_{NbTi} = the tensile stress on the NbTi

E_{NbTi} = the modulus of elasticity for the NbTi (6×10^{10} N/m^2)

L = the composite load

A_c = the cross-sectional area of the conductor (0.33 mm^2)

f = the volume of NbTi in the conductor divided by the total conductor
   volume

E_{Cu} = the modulus of elasticity for the Cu (7×10^{10} N/m^2)

M_{Cu} = the slope of the stress-versus-strain curve, above its yield point,
   for the Cu matrix (3×10^9 N/m^2)

σ_p = the residual pre-stress on the NbTi due to the manufacturing process
   (1×10^8 N/m^2)

ϵ_{ym} = the composite strain at matrix yield (0.002)

This equation is applicable only beyond the Cu yield point, which is the
region where the effect of stress on the I_c becomes large. For strain levels
that are below the Cu yield point the I_c degradation is negligible.

CONCLUSIONS

The results of these tests indicate that the effect on critical current of
tensile stress applied to NbTi superconductors at room temperature is the same
as that of stress applied at 4 K. Thus, we have the simple result that
degradation from room-temperature loading can be determined from the existing
4 K stress-effect data base given in Fig. 3. To generalize the results for
arbitrary matrix-to-superconductor volume ratios, the data in Fig. 3 are
presented in terms of NbTi stress, which can be determined using the methods
outlined in the text. Because room-temperature and 4 K stress have an
equivalent effect on I_c, we think that Fig. 3 can also be used to estimate the
effect of stress at intermediate temperatures generated by differential
thermal contraction between the different conductor and magnet materials
during cool-down. Presently, the typical level of tensile stress applied to
NbTi composites during magnet fabrication ranges from about 40 to 180 MPa. At
these stresses the resulting I_c degradation is negligible. The data presented

here are useful in defining the acceptable limits of tensile stress in forthcoming magnet designs where increased winding tension may be necessary for restricting conductor motion at high Lorentz forces. For the conductor measured in this study, a 5% degradation in I_c occurs at a composite tensile stress of approximately 550 MPa at 5 T and 390 MPa at 9 T.

APPENDIX: METHOD TO DETERMINE STRESS ON THE NbTi COMPONENT

Figure 5 is an idealized representation of the load-versus-strain characteristic for a NbTi and Cu composite over a single load cycle. Three separate load curves are shown in this figure: one for the NbTi filaments, one for the Cu matrix, and one for the overall composite. The NbTi curve is a straight line with a positive load intercept (point α) and no hysteresis between loading and unloading (the arrows on the curves indicate the loading sequence). This reflects the assumption of perfect elastic behavior of the NbTi for the strains measured here. The positive load intercept α represents the small residual tensile stress on the NbTi; this stress is a result of the manufacturing process. Similarly, the Cu curve shows a small negative (compressive) load intercept (point a). The Cu curve is linear up to point b, where the Cu begins to yield. There is a transition region between points b and c followed by another linear region between point c and point d, the maximum-strain point. This portion of the curve (c-d) is based on the assumption that the yield strength of the Cu increases linearly with increasing strain. As the load decreases to zero at point e the curve is linear, again indicating elastic behavior. The load becomes compressive after point e and, again, the Cu goes through another transition region followed by a linear region. At point g the load on the Cu is equal to the load on the NbTi and represents the unloaded state of the overall composite. The composite curve is simply the algebraic summation of the NbTi and Cu curves.

The dashed lines in Fig. 5 are extensions of the linear portions of the load curves and are needed for constructing the NbTi load curve from the composite curve. A fundamental assumption made in drawing the Cu load curve

is that of symmetry between the compressive and tensile mechanical properties.

In particular, the curve indicates that the distances from point d to e and from point e to f are equal. This equality shows that the distances from point D to E and from point E to F on the composite curve are also equal. In turn, this allows the determination of the load experienced by the NbTi (point E) simply by bisecting the line between points D and F. Additional points can be similarly determined by loading the conductor to higher levels and unloading.

References:

1. J. W. Ekin, F. R. Fickett, and A. F. Clark, Proc. Int. Cryog. Mat. Conf. (Aug. 1975), Adv. Cryog. Eng. 22, 449 (1977).

2. J. W. Ekin "Mechanical properties and strain effects in superconductors" Chapt. 7, p. 455 in Superconductor Materials Science, edited by S. Foner and B. B. Schwartz, Plenum Press, New York (1981).

3. J. W. Ekin, IEEE Trans. Mag. 23, 1634 (1987).

4. R. P. Reed, R. P. Mikesell, A. F. Clark, Adv. in Cryog. Eng. 22, 463 (1977).

Table I. Multifilamentary NbTi sample characteristics

Strand diameter	0.648 mm
Filament diameter	16 μm
Number of filaments	648
(single stack construction)	
Copper-to-superconductor volume ratio	1.77
Twist pitch	1.27 cm
Superconductor area	0.119 mm^2
Total area	0.330 mm^2
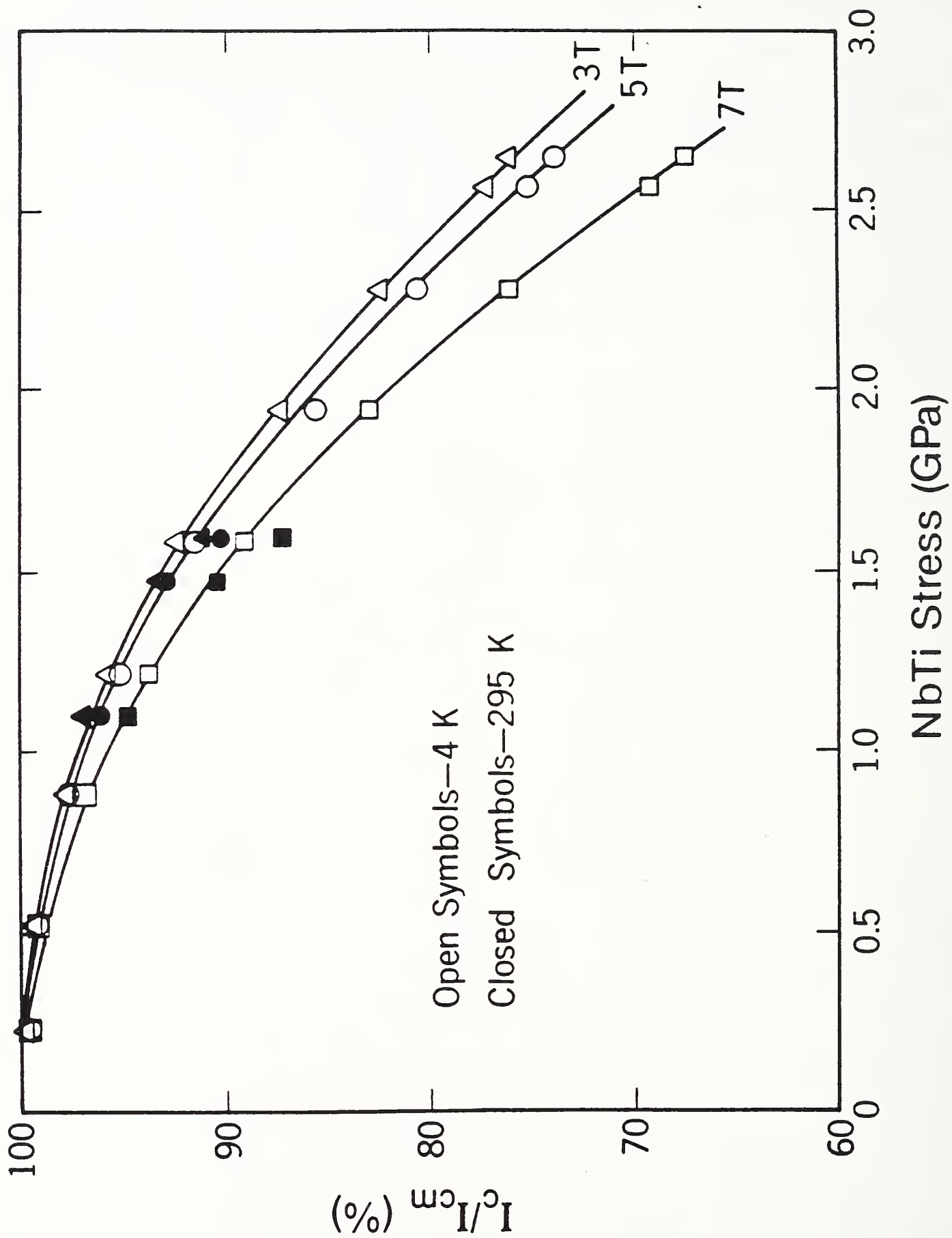
Fig. 1. Normalized critical current (I_c/I_{cm}) vs. tensile stress on NbTi portion of conductor (NbTi Stress) at magnetic fields from 3 to 7 T. The open and solid data points show the near equivalence of the effect of stress

18
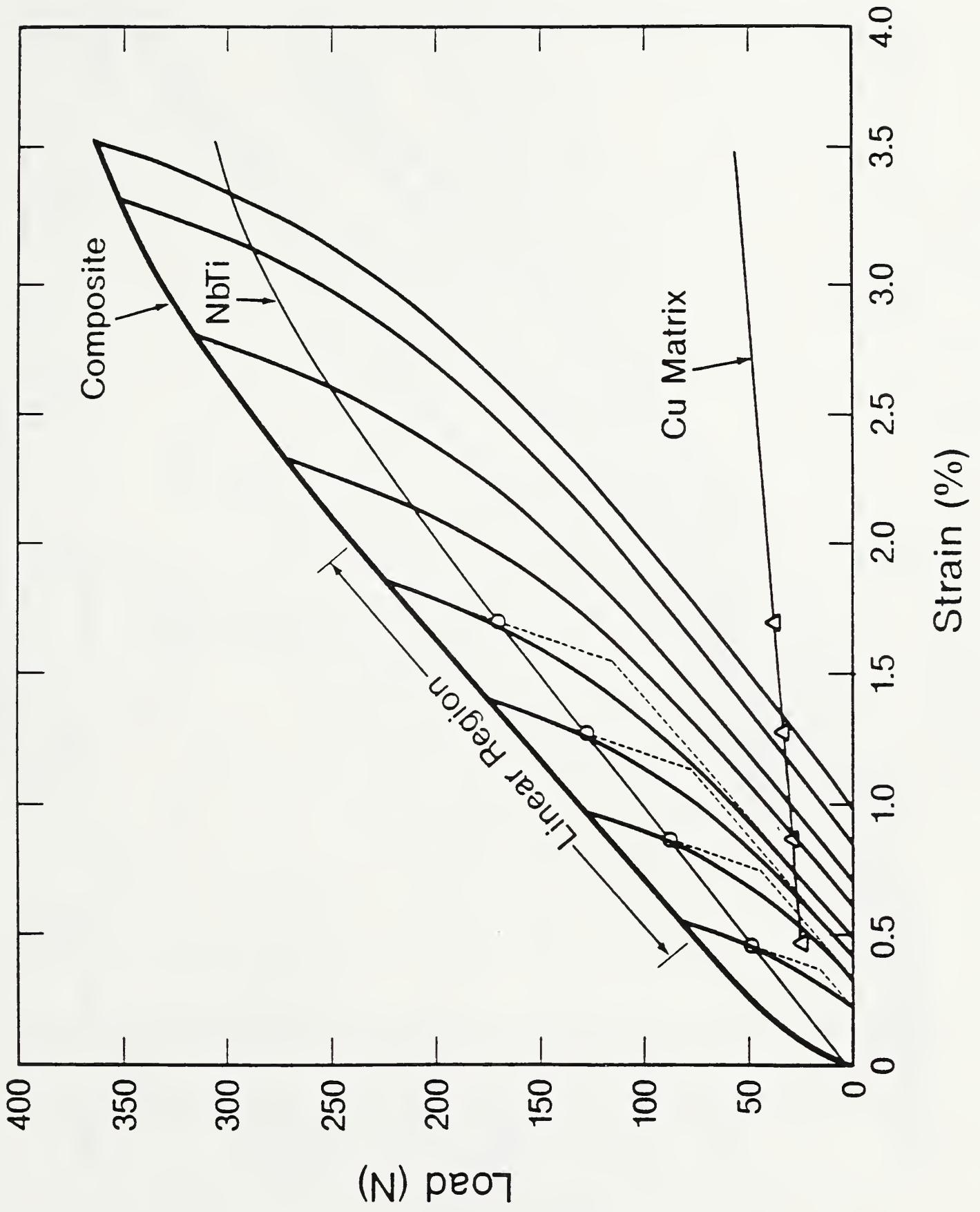
Fig. 2. Load vs. strain characteristics at 4 K for composite conductor and derived characteristics for its individual components, NbTi and Cu.
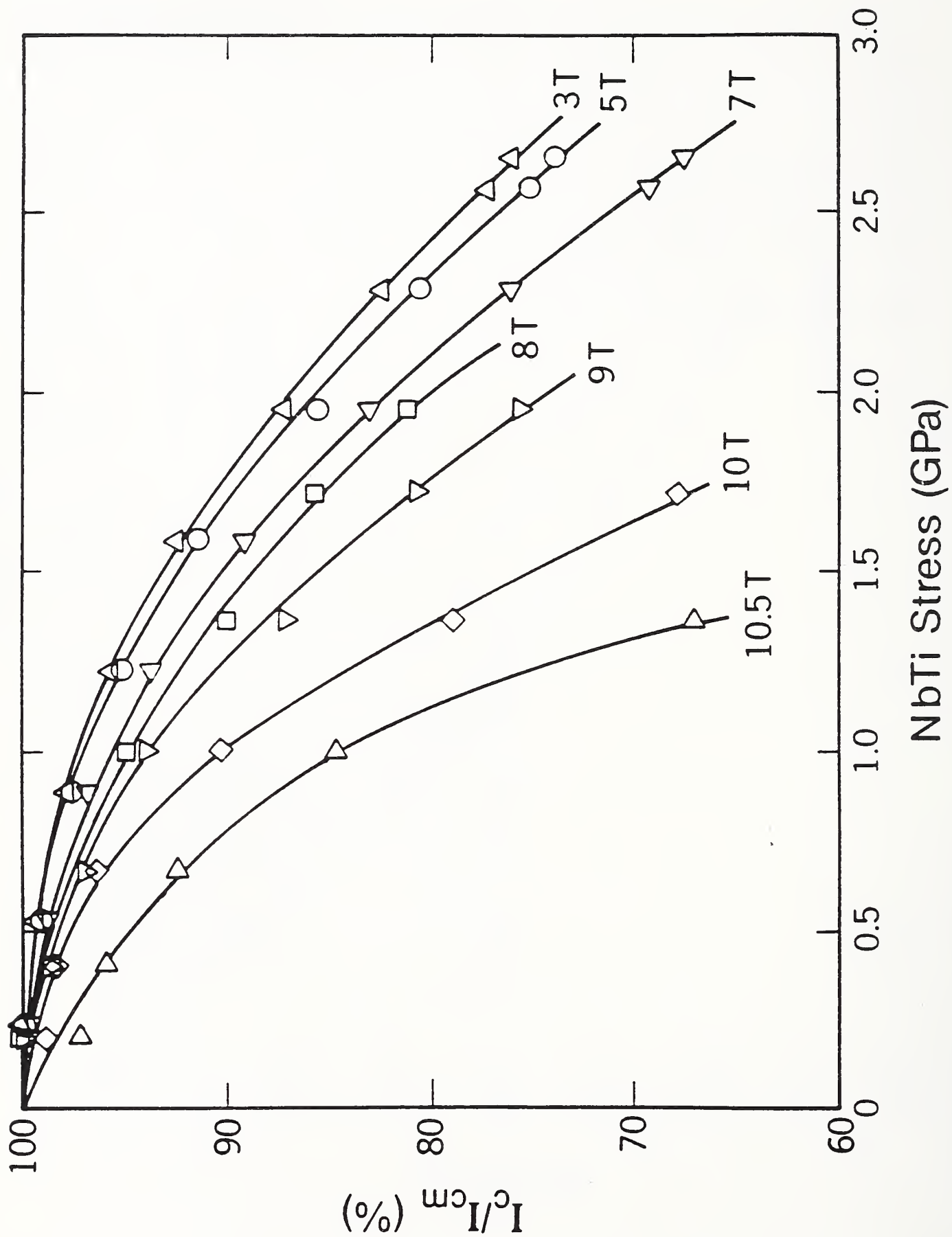
Fig. 3. Normalized critical current (I_c/I_{cm}) vs. axial tensile stress on NbTi portion of conductor (NbTi Stress) at magnetic fields from 3 to 10.5 T for generalized use in estimating the effect of stress on critical current of NbTi.
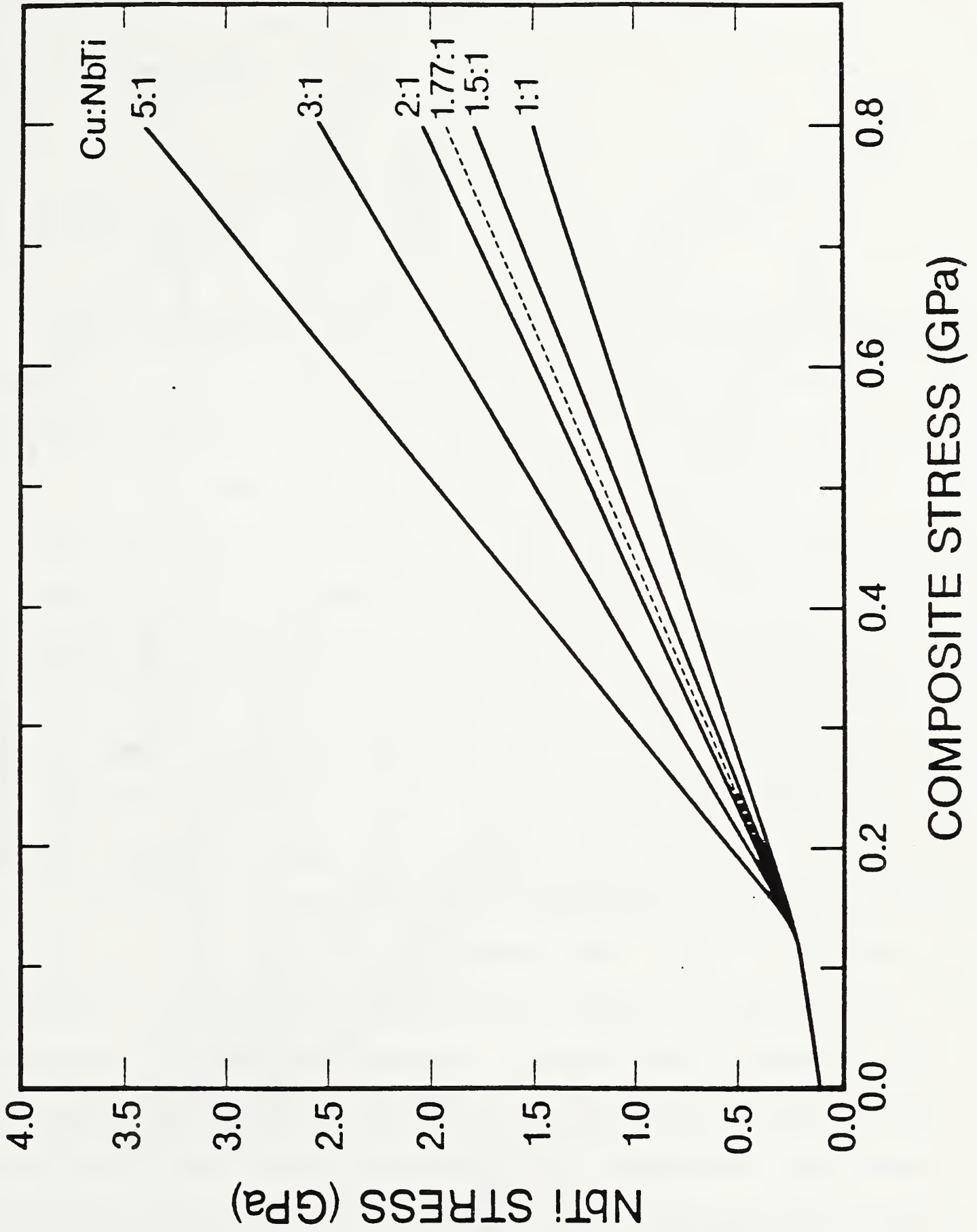
Fig. 4. NbTi stress vs. composite stress characteristics for several Cu:NbTi ratios to approximately determine the NbTi stress required for use of Fig.
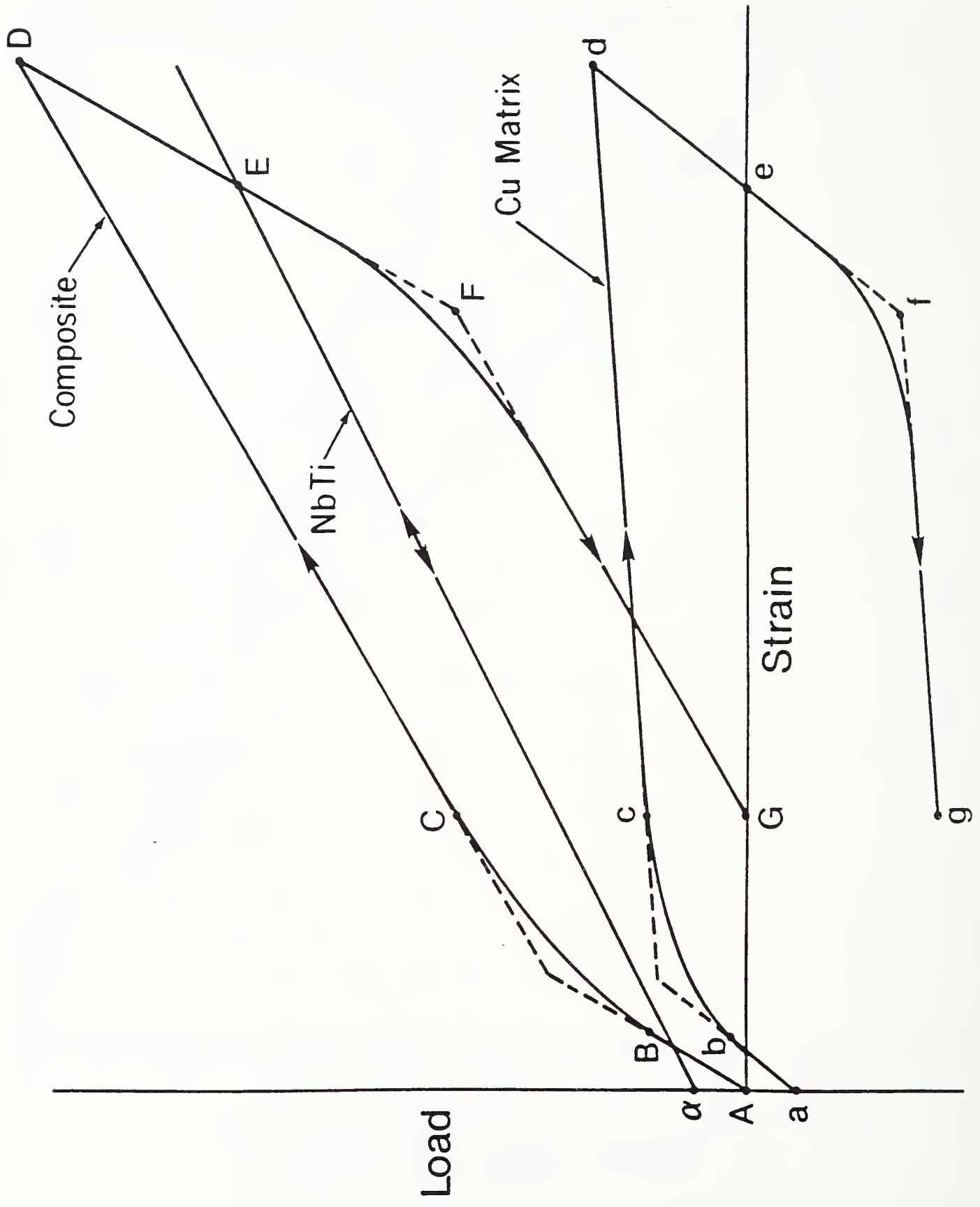
21

Fig. 5. Load vs. strain characteristics for composite conductor and its individual components, NbTi and Cu.

ELECTROMAGNETIC CHARACTERISTICS OF NbTi STRANDS EXTRACTED FROM RUTHERFORD
CABLES

by L. F. Goodrich and S. L. Bray

A. SUMMARY

The electromagnetic properties of NbTi strands extracted from Rutherford
cables were studied to clarify the effect of mechanical deformation, caused by
the cabling process, on the current capacity of the strands. The mechanical
abuse that these conductors are subjected to present a number of measurement
concerns that are not normally encountered in the testing of superconductors.
Consequently, a major portion of this study was aimed at determining how the
measurement and data-analysis techniques should be adjusted for these
conductors to allow a more complete and accurate determination of their
current capacities. Four different cables, all of which are prototypes for
the Superconducting Super Collider's dipole magnets were studied. The
extracted cable strands were instrumented to allow measurement of the voltage
across several key regions of mechanical deformation as a function of current
and the orientation of the applied magnetic field. The resulting data are
presented in several forms besides critical current in order to more
thoroughly characterize the conductors' electromagnetic properties. The cable
strands show very localized reductions in current capacity that are well
correlated with the regions of high mechanical deformation. For example, at a
particular field orientation, the voltage across a portion of the strand that
is only 3% of the total strand length contributes 92% of the total strand
voltage. Two applied magnetic-field orientations, parallel and perpendicular

to the cable's width, have pronounced effects on the electrical properties of the strand. Both of these magnetic field orientations will arise in application.

Although there is a pronounced irregularity in the voltage along the pitch length of these conductors and the degree of the irregularity depends on the orientation of the applied magnetic field, the overall voltage of the entire pitch length is comparatively constant. This is the result of a statistical effect where a particular field angle that is detrimental to some of the strand segments is equally beneficial to others. The measured critical currents for these strands are only a weak function of the field angle, and they are well correlated with the quench currents. Since certain field angles result in large reductions in the critical current of individual strand segments, this indicates that the local degradations do not act as weak links in limiting the current capacity of the strand to the reduced level of the most degraded segments. This tolerance for local critical-current degradation depends upon the strand's good longitudinal thermal conductivity, and any reduction in this local cooling capacity might limit the strand's current capacity to that of the weak link.

An important characteristic of all the conductors that were tested in this study is an intrinsic current transfer that is apparently associated with their mechanical deformation. In other words, at high-enough currents and magnetic fields, the deformation of the cable strands results in a periodic redistribution of the current among the superconducting filaments; as a consequence, there are small resistive voltages associated with these

conductors. This characteristic definitely affects the measurement of these conductors, and it may affect their performance in application.

The conductors tested in this study represent a continuing evolution in design that is aimed at increasing the strand material's precabled current capacity while decreasing its sensitivity to mechanical deformation. The results of these tests indicate that considerable progress is being made toward this goal.

B. INTRODUCTION

The measurements presented here are a continuation of earlier studies[1] of NbTi cable strands extracted from Rutherford-type cables (cables provided by the Lawrence Berkeley Laboratory). These are prototype cables for high-energy physics applications. Specifically, they were designed for use in the inner and outer windings of the Superconducting Super Collider's (SSC) dipole magnets. The main emphasis of these studies is the effect of mechanical deformation, during manufacture, on the cable's current capacity. In addition to the bending deformation required to achieve the cable's twist pitch, the cables are compacted into a keystone shape. These mechanical deformations result in a very localized degradation in the electrical properties of the cable strands. The deformation of the cable strands results in a periodic geometry with the various segments of the strands defined by the degree and type of deformation. The desired products of the current studies is information that will lead to methods for reducing the current-capacity degradation associated with the manufacture of superconducting cables, and the

determination of specific measurement considerations that will result in a more complete and accurate determination of that current capacity.

For all the measurements, the orientation of the applied magnetic field was perpendicular to the cable's longitudinal axis. The angle of the applied field about this axis was varied from 0° to 360° with special emphasis given to the 0° (parallel to the cables width) and 90° (perpendicular) orientations. The reasons for emphasizing these field directions are twofold. First, there is a pronounced effect on the strands[1] electrical properties in these orientations and, second, both of these field orientations arise in a dipole magnet.

The mechanical deformation of the cable strands during the cabling process results in localized variations in the conductor's current capacity. The sources of this variation fall into two categories, cross-sectional area differences and angular effects. The cross-sectional variation of the superconducting filaments is due to necking and serrated yielding of the NbTi filaments. Under the second category, angular effects, the orientation of the applied magnetic field with respect to the various segments of the strand (pitch angle effect[2]) and their mechanically deformed cross sections (aspect ratio effect[3]) varies along the strand.

Several types of data are presented in order to emphasize different characteristics of the cable strands. A number of different cables, manufactured with different virgin wire (source wire for the cable strands) materials and cabling techniques, were studied. These data allow comparisons of the various cables. An overall critical current, defined as the critical

current (I_c) determined by adding the voltage contributions of each segment of the strand and then dividing this voltage by the sum of the strand segment lengths to arrive at an effective electric field, is presented as a function of the applied field angle. This information is useful in examining the cumulative effect of variations in the spatial orientation and the aspect ratio of different strand segments at different field angles. The concept of an overall I_c is also useful for comparing the strand's I_c with the I_c of the virgin wire from which the cable was manufactured. These comparisons indicate the I_c degradation introduced by the cabling process. The variation of the electric field along the strand's longitudinal axis, or the electric-field profile, is presented as a measure of the wire's local current capacity. In order to assess the relative contribution to the total voltage of different strand segments, the voltage distribution at fixed magnetic field angles along the conductor's length is also presented. In addition, plots of I_c versus position along the cable strand's length are presented to provide a comparison of the different strand segments in a more conventional form than the electric-field or differential-voltage plots do. Finally, the voltage of the strand segments and of the overall strand, at a fixed current, are presented as a function of the applied magnetic-field angle to exhibit which field orientations are critical for different strand segments and for the overall strand.

C. SAMPLES

Four different cables, denoted as W, X, Y, and Z, were studied. Detailed specifications for these cables are given in Table 1. Cables W, X, and Y are

all outer-winding SSC conductors, whereas cable Z is an inner-winding conductor. Cable W was re-rolled through a turkshead (for resizing) after it had been cabled. The re-rolled cable is a worst-case situation that was studied to more clearly identify the degradation features. Cable X is similar to W; however, it was not subjected to as much mechanical deformation and is a more typical example of late-1985 to early-1986 prototype outer cables. Cable Y (1987) is an evolution of cable X where the cabling techniques were refined in an attempt to reduce current-capacity degradation. Finally, cable Z is similar to cable Y with respect to the cabling technique, but it is an inner, rather than an outer, cable.

Single-strand samples of each cable were obtained by cutting an appropriate length of the cable and then separating the strands. Initially, the strands were difficult to remove from the cable without causing additional mechanical damage. However, after several strands were removed, the cable structure relaxes and additional strands may be removed without damage. These undamaged strands were selected for the measurements.

Table 1. Parameters for each of the four cables

Parameter	W	X	Y	Z
Cable No.	SC297	SC305	SC361	SC362
Billet No.	5212-3	5914	5954-4	5955-2
Number of strands per cable	30	30	30	23
Pitch length, mm	69	69	69	79
Cable width, mm	9.7	9.7	9.7	9.3
Cable mid-thick, mm	1.17	1.17	1.17	1.46
Keystone angle, deg	1.24	1.24	1.24	1.6
Filament twist, cm^{-1}	0.8	0.8	0.8	0.8
Filament dia., μm	16	5	6	6
Number of filaments	648	6006	4162	7249
Virgin wire dia, mm	0.65	0.65	0.65	0.808
Cu/superconductor ratio	1.77/1	1.64/1	1.78/1	1.40/1

D. EXPERIMENTAL DETAILS

Figure 1 is a cross-sectional view of a typical cable showing its key regions. Three regions of the cable were studied: the thin edge, the face (top or bottom), and the thick edge. Each of these regions was divided with voltage taps into three approximately equal-length, adjacent segments. The three segments of each cable edge were denoted as the central flat edge and the two corners. These edge segments had separations of 2 mm for the outer cable and 2.5 mm for the inner cable. The voltage taps along the face of the cable had voltage tap separations of about 10 mm for the outer cable (11 mm for the inner cable) and did not include any of the corner region.

Figure 2 shows the instrumented portion of a cable strand and the location of the voltage taps along the strand's length. The two key orientations of the applied magnetic field relative to the strand's face, 0° and 90°, are also shown. In this view, the cable's face is in the plane of the figure. Voltage taps on the sample were made using three flat quads (miniature four-conductor flat cable) of four #32-gauge wires. Within each quad, three adjacent segments could be measured with a minimum of induced voltage. The end leads of adjacent quads were connected to the same tap to allow complete coverage of the sample. An additional voltage-tap pair was connected to the sample so that it spanned an entire cable pitch including all of the other voltage-tap pairs. In order to encompass an entire pitch length, the span of this overall voltage-tap pair extended beyond the thick- and thin-edge taps by about one-half the face length at each end. Data presented for these extreme strand positions were derived by subtracting the sum of the measured segment voltages from the overall voltage and then assuming that the voltages for the two end

regions were equal. The quad leads were soldered to twisted-pair leads near the bottom of the sample test fixture. In this position, the soldered joints were immersed in liquid helium during data acquisition. The twisted pairs were continuous from the bottom of the test fixture to the voltmeter's input cables. The junction between the voltage-tap leads and the nanovoltmeter's input leads were maintained isothermal by small bags of lead shot placed under and on top of the junction.

The sample holders are 1/2 in diameter 316 stainless steel rods with a machined longitudinal channel that is slightly wider than the width of the cable. The walls and bed of this channel are insulated with a thin layer of epoxy formed with a TFE (polytetrafluoroethylene) impressioner. The sample is mounted in the holder with a thin layer of epoxy between its lower face and the bed of the sample-holder groove. Small epoxy bridges are then applied across the sample's upper face, leaving the majority of the upper face directly exposed to the helium bath while still providing some mechanical support. The ends of the sample extend past the ends of the stainless-steel rod to allow attachment to the current contacts. The sample holder and longitudinal axis of the sample strand are held perpendicular to the field of a radial access, split-pair magnet. The sample is rotated about its longitudinal axis resulting in various transverse orientations of the applied field, as identified in Figures 1 and 2.

All the measurements were conducted below standard atmospheric pressure (due to the low ambient pressure at the altitude of the test site), resulting in an equilibrium liquid-helium temperature of ~4.02 K. The I_c densities for these samples at 4.22 K would be about 6% less at 5 T and 12% less at 8 T than

those reported here. The I_c densities for these conductors were calculated using the NbTi cross-sectional area, which was determined using the copper-to-superconductor ratio.

Two four-channel, digital-processing, storage oscilloscopes were simultaneously used for data acquisition. Five channels were used to monitor the sample's voltage taps with analog nanovoltmeters, and a sixth channel was used to monitor the sample current. These signals were measured and averaged at a number of different current levels (point method). The resulting data points were then analyzed to construct the sample's voltage-current characteristic. This procedure is different from the more typical procedure where the current is ramped continuously with time while the voltage and current are recorded. The point method has some advantages over the ramp method. The point method allows for a longer time-averaged voltage to be measured (this is beneficial if voltage noise is a problem) without greatly increasing the time required for taking a complete V-I curve. This is achieved by selecting a distribution of current-bias points that results in a more precise measurement. This requires taking a few widely spaced points in the low-current portion of the curve to establish the base line and then taking a progressively closer-spaced point distribution as the current increases toward I_c. The point method greatly reduces the effect of inductive voltage and sample motion. The disadvantages are that it takes longer because the voltage has to settle for each data point and the general shape of the voltage-current curve has to be known *a priori* in order to determine the positions of the data-acquisition points along the V-I curve.

During data analysis, the effects of voltage offsets, changes in thermoelectric voltage, and current-transfer voltage were determined. The

voltage offsets and changes in thermoelectric voltage were determined using the initial and final zero-current points of the waveforms. The thermoelectric voltage corrections were made assuming a constant drift with time. This correction was generally only a few nanovolts per centimeter. The current-transfer voltages were determined using the low-current portion of the waveforms. These current-transfer voltages may partially be an artifact of the measurement method since only a 64 mm length of the sample was in full magnetic field; however, the local voltage data indicate that there is also an intrinsic component of the current-transfer voltage. There is a further discussion of current transfer later in this report. Generally, the current-transfer voltage was quite small because the current contacts were long (~4 cm) and were located more than 6 cm from the nearest voltage tap. A current-transfer correction was made in the determination of the I_c, but no correction was made on the electric-field or differential-voltage data.

E. RESULTS

The first three conductors measured in this study, designated as cables W, X, and Y, represent an evolution in the cable fabrication process aimed at reducing cabling's detrimental effect on the critical current density (J_c) of the finished cable as compared to that of the virgin wire.[4] An evolution has also occurred in the design and processing of the virgin wire.[5] This evolution can be characterized by a decrease in filament size aimed at reducing ac losses while attempting to maintain J_c. Initially, increased wire drawing that was used to reduce the filament size of wire X in comparison with wire W resulted in lower J_c for the virgin wire. Later, improved

33

manufacturing processes that were used for wire Y resulted in a substantial restoration of the J_c. Cable Z is an inner cable that was manufactured and cabled using techniques similar to those used for cable Y.

Overall Critical Current

Critical-current measurements were made on the virgin wires from which each cable was manufactured. Three pairs of voltage taps, each pair spanning about 10 mm, were connected to the specimens. This allowed for a check of I_c homogeneity with position. Critical-current measurements were also made as a function of the applied magnetic-field angle. This allowed for a test of I_c homogeneity with respect to field angle. The average I_c of the virgin wire was used to determine the relative degradation of each cable. The typical I_c variation among voltage taps was ±0.3% at 5 T and ±0.5% at 8 T for cables W, X, and Y. The I_c variation among voltage taps for cable Z was about ±2.2% at 5 and 8 T. A reason for this large variation in the case of sample Z is not evident. For cables X and Y, the I_c variation of a given tap with respect to field angle (0° to 360°) was measured to be about ±0.6% at 5 T.

Figures 3 and 4 show comparisons between the overall I_c density of the extracted cable strands and the virgin wires from which they were constructed. The data presented in these plots is tabulated in table 2. Figure 3 shows this comparison for each of the four conductors for applied magnetic-field angles of 0° and 90° at 5 T. For cable strands W, X, and Y, there is a consistent increase in J_c at 0°, although the virgin wire's J_c decreased between wires W and X. Recal dangling that cable W is a worst-case situation with respect to the cabling operation. The higher J_c for strand X is due to

34

the greatly reduced mechanical deformation of the strand. Cable Y shows a greater mechanical degradation of its J_c than cable W, but, again, it shows an increased strand J_c due to its high virgin-wire J_c. For cable strand X, the mechanical degradation of J_c was somewhat higher at 90° than at 0° and, consequently, its J_c was less than strand W's. This increased degradation at 90° was not present in the case of strand Y and it showed a higher J_c than its two predecessors. Strand Z was very similar to strand Y.

The 8 T plot, Fig. 4, shows an increase in the strand's J_c between W and Y but there is a decrease between W and X. Comparison between the 5 and 8 T J_c degradation for strands W, X, and Y shows a reduced sensitivity to mechanical deformation at the higher magnetic field for all the strands. The virgin wire W, which has larger diameter filaments, had a higher relative J_c at 8 T than did wires X and Y. This lower J_c dependency (sensitivity) of wire W to magnetic field results in a higher strand J_c for W than for X. Comparing the Jc degradation of strand Z at 5 and 8 T shows a reverse trend of higher sensitivity to mechanical deformation at the higher magnetic field. At 8 T, strand Z has a considerably higher J_c degradation than strand Y.

Table 2. Cable degradation and critical current density (A/mm^2) at 0.1 μV/cm

| | | 5 T | | | |
| Cable | | Critical current density | | Cable degradation | |
	virgin	0°	90°	0°	90°
W	2827	2378	2469	-15.9%	-12.7%
X	2464	2442	2383	-0.9%	-3.3%
Y	3043	2835	2887	-6.8%	-5.1%
Z	2933	2738	2713	-6.6%	-7.5%

| | | 8 T | | | |
| Cable | | Critical current density | | Cable degradation | |
	virgin	0°	90°	0°	90°
W	1306	1183	1194	-9.4%	-8.6%
X	1036	1051	1014	+1.4%	-2.1%
Y	1239	1218	1210	-1.7%	-2.3%
Z	1257	1121	1092	-10.8%	-13.1%

Electric-Field Profile

Plots of the electric field versus position along the cable strand's length, or the electric field profile, are presented for all four conductors at two magnetic fields (5 and 8 T) and two orientations (0° and 90°) in figures 5-18. At the top of each plot, located outside the axes, is an outline of the cable strand's geometry positioned to correlate with the horizontal or position axis. The cable outline is labeled to indicate the position of the thin edge, the face, and the thick edge relative to the horizontal axis. The local electric field was calculated by dividing the measured voltage across a strand segment by its length. The discrete data points, therefore, represent the average electric field over the strand segment. The horizontal positions of the data points are at the centers of each strand segment. The lines connecting the data points are intended as a visual aid and not an interpolation between the data points. The actual electric-field profile might have much greater extremes than those indicated by the averaged data points shown in these plots.

There is an electric-field criterion associated with each of these plots. This is an overall electric-field criterion arrived at by dividing the voltage across one cable pitch by the sum of the segment lengths. Consequently, the current associated with different plots or different curves within a plot are not the same. This is necessary to compare different cables within the same plot and to present data taken at different magnetic fields and orientations in a comparable manner. In other words, each curve represents the electric-field profile of a cable strand at a selected I_c criterion, and that criterion is consistent for all curves within a particular plot. In examining these

plots, recognize the inverse relationship between the electric field and I_c: a large local electric field indicates a small local I_c.

Figures 5, 6, 7, and 8 are electric-field profiles for the outer cables W, X, and Y at 5 T and 0°. The data in each of these four plots represents a different electric-field criterion. The dominant elements in the structure of these curves are the pronounced peaks located at the centers of the thin and thick edges. In general, the major peak is at the thin edge. The imbalance between the two peaks is greatest for cable W, the oldest of the three cables, and progressively less for cables X and Y. This demonstrates a trend toward a more uniform electric-field profile as these conductors have been refined. The first cable, W, has the lowest electric field at the thick edge of the three cables.

The negative electric fields shown in the plots indicate negative measured voltages, not negative resistances. These negative voltages are projection voltages[6,7] associated with current redistribution among the filaments. The strongest evidence of intrinsic (not associated with the location of the current contact) transverse currents within the strand is a region of negative voltage bounded by regions of large positive voltages. The curve for cable Y is the best example of this structure. This type of structure is present in the center of these plots. This location indicates that the current redistribution is caused by the longitudinal variation in the relative current-carrying capacity of the filaments rather than being caused by current injection at the current contact. Thus, voltages associated with this type of redistribution will occur periodically along the entire length of the cable strand.

Although the negative voltages are the most obvious indication of current redistribution, there are other indicators within the data curves. These indicators have the same general character as the negative voltages with the exception of polarity. The best example of this structure is the center segment (at about 3.5 cm) of cable Y. At low currents, the voltage associated with this hump in the electric field profile increases rapidly with increasing current, and indicates an intrinsic I_c. At higher currents, this voltage becomes a weak function of the current as indicated by the curves of Figs. 6, 7, and 8. This behavior is evidenced by the relative size of this central hump in the electrical-field profile, for increasing current, in comparison with the dominant edge peaks. This is further evidence of intrinsic current redistribution among the conductor's filaments.

Figures 9, 10, 11, and 12 are the electric-field profiles for cables W, X, and Y at a magnetic field of 5 T and an orientation of 90°. In comparison with the 0° data, the extremes of the electric field profile are smaller in these plots. This is due to the effects of pitch angle and aspect ratio when the center of the strand edges are in a favorable position relative to the 90° orientation of the applied magnetic field. This effect is most evident for cables X and Y where the peak in the electric field, observed at the central edges in the 0° plots, is suppressed in the 90° case. Comparison of the 0° and 90° curves for cable W also shows a reduction in the peak electric field but to a lesser degree than for the other cables. Although the peak electric field has switched from the center to the corners of the thin edge for cables X and Y in this orientation, the peak still occurs near the region of greatest mechanical deformation, the thin edge. Current redistribution and the resulting current-transfer voltage are lower for this field orientation, as

evidenced by the reduced negative voltage and more uniform electric field profile.

Figures 13 and 14 are plots of the electric field for cables W, X, and Y at an applied magnetic field of 8 T and orientations of 0° and 90°. These 8 T plots are very similar to the 5 T plots. For the 0° orientation, the peaks of the electric field profile are again at the edges of the strand, with the larger peak occurring at the thin edge. At 90°, cables X and Y show peaks at the corners of the thin edge and a strong suppression of the electric field at the center of the thin edge. Cable W has a reduced peak at the center of its thin edge at 8 T as it did at 5 T. The 8 T data is presented only at the 0.1 μV criterion, but it is typical of the similarities between the 5 and 8 T data at all criteria.

The electric field profile for cable Z, the inner cable, is presented in Figs. 15, 16, 17, and 18. Comparing these curves with those of the other cables indicates a strong similarity to cables X and Y. At 0°, and both magnetic fields, the peaks in the electric field profile are comparable, with the thin edge showing a slightly higher electric field. Once again, at 90° and at both fields, the peaks in the profile switch from the center of the edges to the corners. If a general statement can be made it might be that cable Z's profile is more uniform than that of X and Y.

Differential Voltage Profile

Figures 19-26 are similar to the electric-field profiles in that they also exhibit the electrical properties of the cable strand as a function of

the position along its length. In this case, the differential voltage across the various strand segments is plotted as a function of position. The plateaus, or peak levels, in the curves represent the voltage across the indicated strand segments at the indicated overall I_c. As was the case for the electric-field plots, the lines connecting these data are only a visual aid. Vertical lines, rather than smooth curves were selected because they more accurately portray the differential nature of these data and more clearly define the positions of the different strand segments.

The plots show that there is a considerable variation in the lengths of the various strand segments. Herein lies the significance of these plots, which show the relative contribution of the separate strand segments to the overall voltage. In other words, because of the variation in segment length, the electric field shows only the relative current capacity of the segments, not each segment's contribution to the total voltage and the resulting overall I_c. For this reason, a comparison between the electric field and differential voltage profiles shows that the voltage peaks at the strand edges is less than that at the strand faces. This is due to the greater length of the face segments. Moreover, the edges, although highly degraded, are a small portion of the total pitch length of the strand and, therefore, have a limited effect on the overall I_c.

This comparison between the two types of plots raises a question regarding which of these parameters, local electric field or total voltage, has the greatest practical importance. Several factors, including the sample's longitudinal thermal conductivity, determine which of these parameters are most indicative of the strand's current capacity. For the samples and

conditions existing in these measurements, the total voltage seems to determine the current capacity of the conductor. This is evidenced by a close agreement between the measured overall I_c and the maximum achieved currents (quench currents). For a sample that has poor longitudinal thermal conductivity, the short-edge segments might act as weak links, limiting the current capacity at a total strand voltage below that required to reach the overall I_c criterion.

In general, the differential-voltage plots indicate many of the same strand characteristics as do the electric-field plots. For all cables in the 0° orientation, the majority of the voltage is concentrated at the edges of the cable with the central portions dominant. At 90°, the voltage concentration increases at the corners of the edges in comparison with the centers. The striking difference between these plots and the electric-field plots is the contribution of the face segments at 90°. A comparison between the 90°, 8 T, plots for cable Z (Figs. 18 and 26) illustrates this difference. The electric field profile shows peaks at the corners of the strand edges with a relatively small contribution from the faces. On the other hand, the differential voltage profile shows that the majority of the voltage is contributed by the face segments. This trend is evident for all but cable W where the center of the thin edge remains the dominant segment.

Critical Current Profile

Figures 27-34 are plots of I_c versus strand position. The horizontal lines bounded by data symbols represent the average I_c of the indicated strand segment over the length of the segment. The vertical lines are, again,

intended only as a visual aid. Two data symbols are shown for each data point to indicate the region over which each I_c data point is averaged. The breaks in the curves indicate missing I_c data points for the corresponding strand segments. Missing I_c data occur for regions where I_c was higher than the quench current of the sample; thus, missing data implies relatively high I_c for those regions. Cable W has the most missing points because of its larger range of local critical currents. A low electric-field criterion, 0.05 μV/cm, was selected to reduce the number of missing points. A current-transfer voltage correction was made in the determination of I_c.

The curves of I_c versus position for the outer cables, X and Y, show a smaller variation at 90° than at 0°. Because the combination of the pitch angle and aspect ratio is advantageous to the more mechanically deformed edges at 90°, I_c is more balanced. In a previous measurement of a W strand,[8] the thin edge was shunted with another superconductor in order to allow the I_c of the other segments to be measured. Those measurements showed that the variation in I_c was also smaller at 90° than at 0°. There are some problems with local I_c measurements because of the intrinsic current-transfer voltage which was mentioned in the section of this report on electric-field profiles. The voltage-current characteristic of this type of current transfer, where the voltage rises abruptly and then plateaus, is difficult to separate from an intrinsic I_c characteristic. This type of current-transfer voltage caused the relatively low measured I_c for the center of the cable face in Fig. 29. The reduction in the measured I_c of this strand segment is artificial in the sense that it was caused not by the strand segment itself, but rather was caused by the mechanical deformation and resulting current redistribution associated with an adjacent strand segment.

The I_c-versus-position data for the inner cable, Z, also shows a smaller variation at 90° than at 0° with the exception of one point on Fig. 34. This point was a corner on the thin edge that had a negative transfer voltage at 0° (missing, high I_c) and apparently an intrinsic, positive transfer voltage at 90°, which may have contributed to the lower measured I_c.

Differential Voltage Versus Angle

Plots of the differential voltage versus magnetic-field angle for various positions along the cable strand's length are presented for all four conductors at 5 T and a given current, Fig. 35-38. At the top of each plot, located outside the axes, is an outline of the cable strand's geometry; in this case it does not correlate with the horizontal axis. The cable outline is labeled to indicate the position of the thin edge, the face, and the thick edge. The data-point symbols are located, horizontally, at the center of each segment on the cable outline. The discrete data points on the plot, therefore, represent the differential voltage over each strand segment at a given angle. The lines connecting the data points are intended as a visual aid and not an interpolation between the data points. This is especially true between the angles -180 and -105° because of the widely spaced data points. A plus symbol was used for the total differential (overall) voltage of one cable pitch length. The same data symbols were chosen for equivalent positions along the thick and thin edges, with open symbols for the thin edge and filled symbols for the thick edge. The differential-voltage curves for the end segments of the strand, indicated by the circular data symbols, are equal for the two segments because of the way in which they were derived. Separate data were not available for these two segments; rather, the total voltage of the

44

two segments was available and, based on their equivalent positions, their voltages were assumed to be equal.

It is difficult to follow all of the curves, but these plots reveal significant features. In Fig. 35 (cable W) the differential voltage of the center of the thin edge is where most of the total voltage drop occurs for angles around 0°. Two of the positions along the face have a negative differential voltage at all angles. The rest of the positions show little structure with angle and have relatively small differential voltage. The peak in the total differential voltage at 0 and -180° indicates the lowest I_c, the relative minimums at about ±45° are regions of larger I_c, and the relative peaks at ±90° are local minima in I_c.

Figure 36 (cable X) has some other features. The lowest I_c was at ±90° rather than 0°. The center of the thin edge still contributes the majority of the total differential voltage around 0°. The corners of the thin edge contribute the most to the total differential voltage near ±90°. The maximum for each of these corners occurs at angles slightly shifted to one side or the other of 90°. This is due to the difference in the average pitch angle of each corner segment. Some positions have a negative differential voltage at some angles and a positive differential voltage at other angles.

A comparison between Fig. 37 (cable Y) and Fig. 35 (cable W) shows a strong similarity between the overall voltage curves. Both curves show a large peak at 0°; however, unlike cable W, where almost all of the voltage is due to the central thin edge, the peak in the overall curve for cable Y is the product of contributions from several strand segments. Most notable, there is

45

a significant contribution to the overall voltage at 0° from the central thick edge.

The overall curve of Fig. 38 (cable Z) is similar to that of Fig. 36 (cable X) with maximum differential voltages at ±90°, minimums at ±45°, and a local maximum at 0°. In the case of cable X, the local maximum at 0° is primarily due to the central thin edge. On the other hand, in the case of cable Z, the 0° local maximum is due to approximately equal contributions from both the thick and thin central edges.

Close examination of the overall voltage curves of Figs. 35-38 shows several instances of 180° asymmetry. The most prominent example of this asymmetry can be seen by comparing the overall voltages for cable Z at +90° and -90°. The overall voltage at +90° is significantly higher than at -90°. A number of the individual segment curves for cable Z show this same ±90° asymmetry; therefore this effect is probably a characteristic of the conductor and not a measurement error. Similar asymmetries exist in the individual segment curves for the other three cables W, X, and Y.

This phenomenon may be due to a transverse asymmetry in the deformation of the cable strand. This condition, in conjunction with the asymmetry of the total magnetic field (the vector summation of the applied field and the strand's self field) over the strand's cross section, might result in applied field angles that are favorably or detrimentally oriented with respect to the local deformation of the filaments. This may explain the asymmetry in the differential-voltage curves.

46

F. DISCUSSION

The main objective of this work is to determine the current capacity of
several different cable strands with the ultimate goal an increased
understanding of the sources and degree of current-capacity degradation in
these conductors. Typically, I_c of a conductor is an accepted practical
measure of its current capacity. However, for these conductors, there are
some difficulties in relating I_c to the actual current capacity of the cable
strands. Owing to the electrical inhomogeneity of the strands caused by the
cabling operation, there is a large variation in I_c along the strand's length.
The problem is determining what current level in this fairly broad range of
critical currents best reflects the strand's practical current capacity.

One approach is to assume a weak-link condition where the strand segment
that has the lowest I_c determines the overall current capacity of the strand.
A comparison between the actual quenching currents (the maximum observed
current prior to thermal runaway) and the weak-link critical currents shows
that the current capacity of the strand is significantly higher than the weak-
link I_c. This enhanced current capacity, above the weak-link I_c, is due to
the strand's relatively good stability.

At the other extreme, the current capacity of the strands could be assumed
to be equal to the overall I_c. For the conductors tested here, this would not
be a bad assumption, as evidenced by the close agreement between the overall
critical currents and the quenching currents. However, there are two problems
associated with simply measuring the overall I_c and assuming this to be the
strand's practical limit. First, the overall I_c gives no information about

47

the voltage distribution along the strand's length and, consequently, is not useful in understanding the sources of current degradation in the cable. Also, for conductors that are less stable than those tested here, the actual current limit might be close to the weak-link I_c and the overall I_c level could not be achieved.

Another factor associated with the I_c measurements for these cable strands is the presence of intrinsic current-transfer voltages that are caused by periodic current redistribution along the strand's length. This current transfer is apparently caused by the periodic mechanical deformation of the strand and, therefore, it is not isolated to the current contact area. In this sense it is intrinsic to the conductor (not a product of the measurement technique) and it presents a problem in data reduction and analysis. The problem that this intrinsic current-transfer voltage poses is whether or not it is appropriate to separate it from the flux-flow voltage for determining the I_c, as is the normal practice in the case of nondeformed conductors. In other words, because of its intrinsic nature, these current-transfer voltages play a role in determining the current capacity of the cable, not only in testing but in application as well, and, therefore, their presence should be reflected in the reported I_c value. In contradiction to this precept, the critical currents reported here were corrected for current-transfer voltages.

There are two reasons for this apparent inconsistency. First, for these measurements it was impossible to attribute all of the observed current transfer to intrinsic sources. Moreover, the relatively short length (64 mm) of the sample that resided in the full magnetic field may have led to nonintrinsic current transfer. This is why current-transfer corrections were

made to the overall-I_c data. Second, as previously explained, the intrinsic current-transfer voltages do not necessarily appear solely on the strand segments that produced them. This does not present a problem for overall-I_c measurements (if the current transfer is purely intrinsic) where only the magnitude of the voltage over one pitch length is important, not the specific sources of the voltage. However, for the localized-I_c measurements presented here, the comparison of the critical currents of the various strand segments is intended as a measure of the damage caused by mechanical deformation at different segments of the strand. Inclusion of current-transfer voltages, resulting from damage to adjacent strand segments, in the I_c criterion would distort the results of this comparison.

I_c data alone are insufficient for characterizing these conductors. For this reason the electric-field and differential-voltage data were presented. The electric-field data are the clearest indicator of the relative current capacity of the different strand segments. However, the limitation of the electric-field data is that they do not indicate the relative contribution of the various strand segments to the total conductor voltage because the segments are of different lengths. Consequently, the differential-voltage data are a necessary supplement to the electric-field data to fully characterize the conductors. Which of these data are the most indicative of the actual current capacity depends on the stability of the particular conductor. In the case of a stable conductor, the total voltage is an important determining factor of the strand's current capacity and, consequently, the voltage distribution along the strand shows which segments are the most detrimental to the current capacity. On the other hand, for a relatively unstable conductor, the local current capacity can be a limiting factor and, in this case, the electric-field data are more relevant.

49

Because of the electrical inhomogeneity of these conductors, stability may play a key role in determining their current capacity. This coupling between stability and current capacity increases the importance of the matrix material in the conductor design. For example, the use of CuNi for the cable's matrix material, although beneficial in reducing proximity-effect coupling[9] and improving the wire's drawing characteristics, might result in a considerable reduction in current capacity because of the relatively low thermal conductivity of the CuNi and resulting reduction in the cable's stability. Also, the increased electrical resistivity of a CuNi matrix would result in larger current-transfer voltages at current-redistribution sites. Another approach to reducing the proximity-effect coupling between filaments without substantially lowering the stability of the wire is a magnetic approach where Mn is added to the Cu matrix material.[9,10] The Mn reduces the proximity-effect coupling by promoting magnetic scattering of the electron pairs.

To optimize the current capacity of a superconducting cable, three main factors must be considered: the virgin wire's current capacity, its sensitivity to mechanical deformation, and the degree of deformation introduced by the cabling process. A truly optimal design would require the simultaneous determination of the conductor and cabling parameters that, in conjunction with each other, would result in the maximum current capacity of the finished cable. Although ideal, this approach is impractical. Also, the primary concern dictating the cables structural design is mechanical stability, not current capacity. This limits the amount that the cabling parameters can be varied to enhance the current capacity.

A second approach to this problem would be to simply optimize the virgin-wire parameters for maximum current capacity, optimize the cabling parameters for minimum strand deformation, and then assume that the wire's sensitivity to deformation will be acceptably low. It can be argued, however, that optimizing the virgin current capacity of the wire is likely to make it sensitive to mechanical deformation. In other words, if the virgin wire is truly optimized, then any change in the wire (mechanical deformation for example) must result in a degradation in its performance. For example, a comparison of cables X and Y in Figs. 3 and 4 shows that the increase in virgin-wire I_c density from cable X to cable Y is accompanied by an increase in mechanical degradation, although cabling had been improved for sample Y. This apparent increase in sensitivity to deformation may be caused by changes in the virgin-wire construction (matrix-filament configuration) that were necessary to improve its J_c.

A third approach to the problem of cable optimization would be based on an iterative design where a number of different virgin wires, all having relatively high current capacities but different design parameters (filament diameter, matrix-filament configuration, etc.), would be cabled using different parameters (strand diameter, number of strands, strand twist, etc.) and then measured for local degradation. The process would be repeated, with the wire and cabling parameters adjusted according to the results of the strand measurements, until an optimal combination of high virgin-wire current capacity and low mechanical degradation was approached. Unlike the first design method, this method might be practical and, unlike the second design method, this method addresses the interrelationship between the virgin wire's current capacity, its sensitivity to mechanical deformation, and the cabling

51

parameters. This iterative method might be a practical means of approaching an optimal cable design.

Measuring extracted cable strands rather than an entire cable is partially a matter of convenience; it does not require the high output current supply or the large test fixture that are necessary for cable measurements. In addition, for single-strand measurements, there is less uncertainty in the current measurement because all of the supplied current is carried by the single strand. For a cable measurement, however, the supplied current is distributed among all of the cable strands and not necessarily equally. Also, the lower output-current supplies that can be used for an extracted strand measurement typically are less noisy than the larger supplies required for cable measurements and, therefore, more sensitive voltage measurements can be made at the lower current levels.

A limitation of the extracted-strand measurements is that they do not indicate the effect, on an individual strand's current capacity, of localized magnetic field variations produced by adjacent cable strands (self-field effect). The exact duplication of the magnetic field that the conductors will encounter in application is beyond the scope of these measurements. The intent of these localized measurements is to determine the degree and sources of mechanical degradation of the strand, in general. Although the self-field effect will undoubtedly result in some variations in the local electrical characteristics of the cable, the salient features of the mechanical degradation, such as the locations of weak links and the critical magnetic-field orientation, will remain the same. Another electrical characteristic of the cable that is not duplicated by the extracted-strand measurements is

current transfer between adjacent cable strands. This interstrand current transfer might slightly enhance the stability of the cable as compared to that of an individual strand.[1]

All the measurements reported here were made on single specimens of each sample and, as a result, the measurements do not necessarily represent the global characteristics of the cables. Other specimens of samples W and X were measured at an earlier date and the results were reported elsewhere.[8] A second specimen of sample Y was measured during the present tests. The results for these other measurements were generally in good agreement with those reported here. Additionally, the dominant electromagnetic characteristics are consistent among the four samples. For example, the thin edge of the cable strand contributes significantly to the overall strand voltage for a magnetic-field orientation of 0° for all samples.

As changes are made in the cable design and manufacture, the degree and character of the mechanical degradation might change considerably. For example, these prototype cables were sized using a nonpowered turkshead, but the cables might be sized using a powered turkshead in mass production. A change of this type in the manufacturing process could significantly affect the degradation of the cable. By including periodic measurements of extracted strands as part of the cable development process, the effect of new design and manufacturing parameters on current capacity can be thoroughly evaluated.

An extremely large body of information is contained within the data plots presented here, and only a small portion of that information was specifically addressed. The presentation of this data serves two purposes; it demonstrates

the intricate and complex nature of these conductors and it documents the evolution and present status of the cable design.

G. CONCLUSIONS

Based on these measurements, some general conclusions can be stated regarding the electromagnetic character of these cables and its effect on their current capacities. Also, the measurements have implications regarding short sample testing of these cables.

The mechanical deformation of the cable strands associated with cabling can lead to very localized reductions in their current capacity. The widest spread in local current capacity occurs with the applied magnetic field parallel to the cable's width. The deformation geometry of the cable is such that the interaction between the applied magnetic field and a strand segment's aspect ratio or its pitch angle have the same tendency. In other words, a field angle that is either detrimental or beneficial to a strand segment's current capacity due to its aspect ratio is also detrimental or beneficial, respectively, due to its pitch angle. However, strand segments have different critical orientations, so the detrimental and beneficial effects of the field angle on those segments tend to cancel one another over the total length of the strand. Consequently, variations of the overall I_c and the quenching current, with the magnetic-field angle, are significantly less than the I_c variation for individual segments of the strand. For these conductors, the relevant I_c criterion may be a spatial average (the overall I_c) because the degradation in current capacity is concentrated over short regions of the

cable strand and local temperature rises are limited by strong end cooling. Any compromise in sample stability may lower I_c to that of the weak-link segment of the cable strand.

These results have several implications for short-sample I_c testing of cables. First, the data indicate that both magnetic-field orientations, parallel to the cable's width and perpendicular to its width, need to be tested in order to determine the limiting case for I_c. As shown above, the limiting magnetic-field orientation can be parallel or perpendicular to the cable's width and this is not known beforehand. Second, a large difference in current-capacity degradation can exist between the thick and thin cable edges; therefore, changing the direction of the test current (for each field orientation) can affect the measured I_c. This is due to a self-field effect where the location of the peak magnetic field depends on the current direction. Consequently, the peak-field location should be part of the data recorded for short-sample measurements of these conductors. These measurements that address the orientation of the applied field and the location of the peak field should be made periodically as part of the cable development. Also, because of their intrinsic nature, the current-transfer voltages that are associated with mechanical damage of the cable strands should be included in their characterization.

The wire from which these cables are made has evolved to the point where the virgin wire has a high current capacity and a relatively high tolerance to mechanical deformation. Considering the amount of mechanical deformation of the strands in the cabling process, the resulting degradation in current

capacity is surprisingly low. The maximum observed degradation of the overall I_c of the latest outer-winding cable, sample Y, was only 6.8%.

ACKNOWLEDGMENTS

REFERENCES

1. L. F. Goodrich, E. S. Pittman, J. W. Ekin, and R. M. Scanlan, "Studies of NbTi Strands Extracted from Coreless Rutherford Cables," IEEE Trans. on Magnetics, MAG 23, 1642, 1987.

2. A. F. Clark, L. F. Goodrich, F. R. Fickett, and J. V. Minervini, "Development of Standards for Superconductors, Interim Report Oct. 80 to Jan. 82", NBSIR 82-1678, National Bureau of Standards, Boulder, Colorado (July 1982).

3. L. F. Goodrich, W. P. Dube, E. S. Pittman, and A. F. Clark, "The Effect of Aspect Ratio on Critical Current in Multifilamentary Superconductors," Adv. Cryog. Eng. - Materials, Vol. 32, Plenum Press, New York (1986), p. 833-840.

4. J. Royet and R. M. Scanlan, "Manufacture of Keystoned Flat Superconducting Cables for Use in SSC dipoles," IEEE Trans. on Magnetics, MAG 23, 480, 1987.

5. D. C. Larbalestier, A. W. West, W. Starch, W. Warnes, P. Lee, W. K. McDonald, P. O'Larey, K. Hemachalam, B. Zeitlin, R. Scanlan, and C. Taylor, "High Critical Current Densities in Industrial Scale Composites Made From High Homogeneity Nb 46.5 Ti", IEEE Trans. on Magnetics, MAG 21, 269, 1985.

6. L. F. Goodrich, J. W. Ekin, F. R. Fickett, "Effect of Twist Pitch on Short-Sample V-I Characteristics of Multifilamentary Superconductors," Adv. Cryog. Eng. - Materials, Vol. 28, Plenum Press, New York (1981), p. 571-580.

7. L. F. Goodrich, "The Effect of Field Orientation on Current Transfer in Multifilamentary Superconductors," IEEE Trans. on Magnetics, MAG 19, 244, 1983.

8. J. W. Ekin, L. F. Goodrich, J. Moreland, E. S. Pittman, and A. F. Clark, "Electro-Mechanical Properties of Superconductors for High Energy Physics Applications," NBSIR 86-3061, National Bureau of Standards, Boulder, Colorado (December 1986).

9. E. W. Collings, "Stabilizer Design Considerations in Fine-Filament Cu/NbTi Composites," Adv. Cryog. Eng. - Materials, Vol. 34, Plenum Press, New York (1988), p. 867-877.

10. T. S. Kreilick, E. Gregory, J. Wong, R. M. Scanlan, A. K. Ghosh, W. B. Sampson, and E. W. Collings, "Reduction of Coupling in Fine Filamentary Cu-NbTi Composites by the Addition of Manganese to the Matrix," Adv. Cryog. Eng. - Materials, Vol. 34, Plenum Press, New York (1988), p. 895-900.
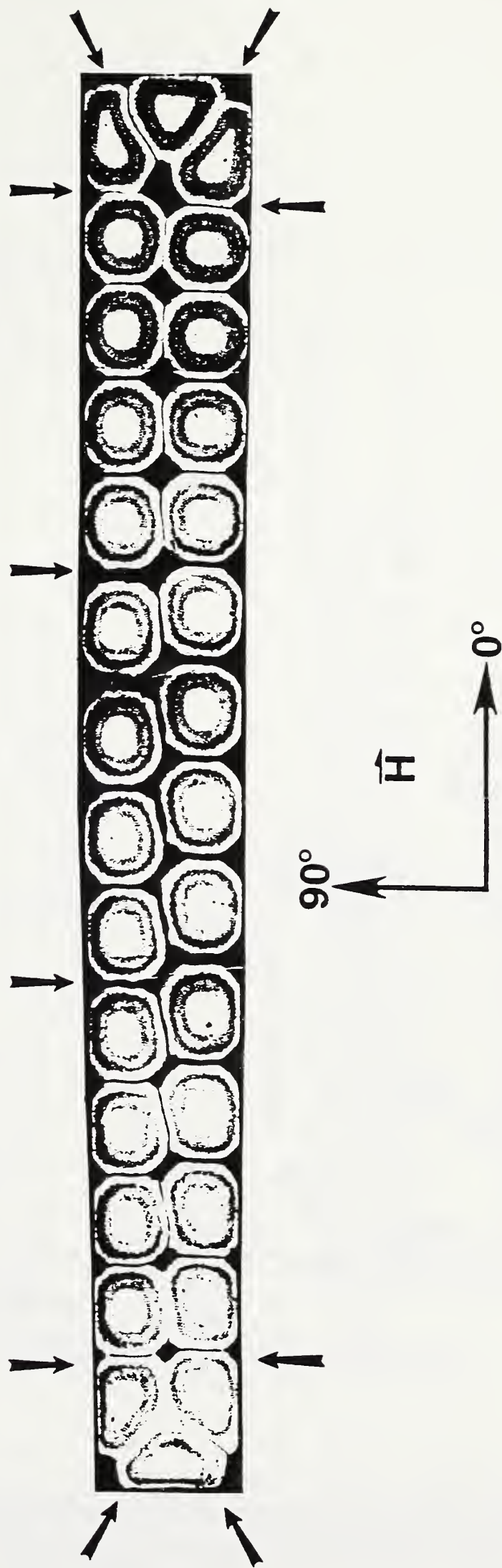
Figure 1. Cross section of cable W showing the orientation of the applied
magnetic field and the approximate locations of the voltage taps,
indicated by arrows in the figure (full cable pitch tap positions
omitted for clarity).
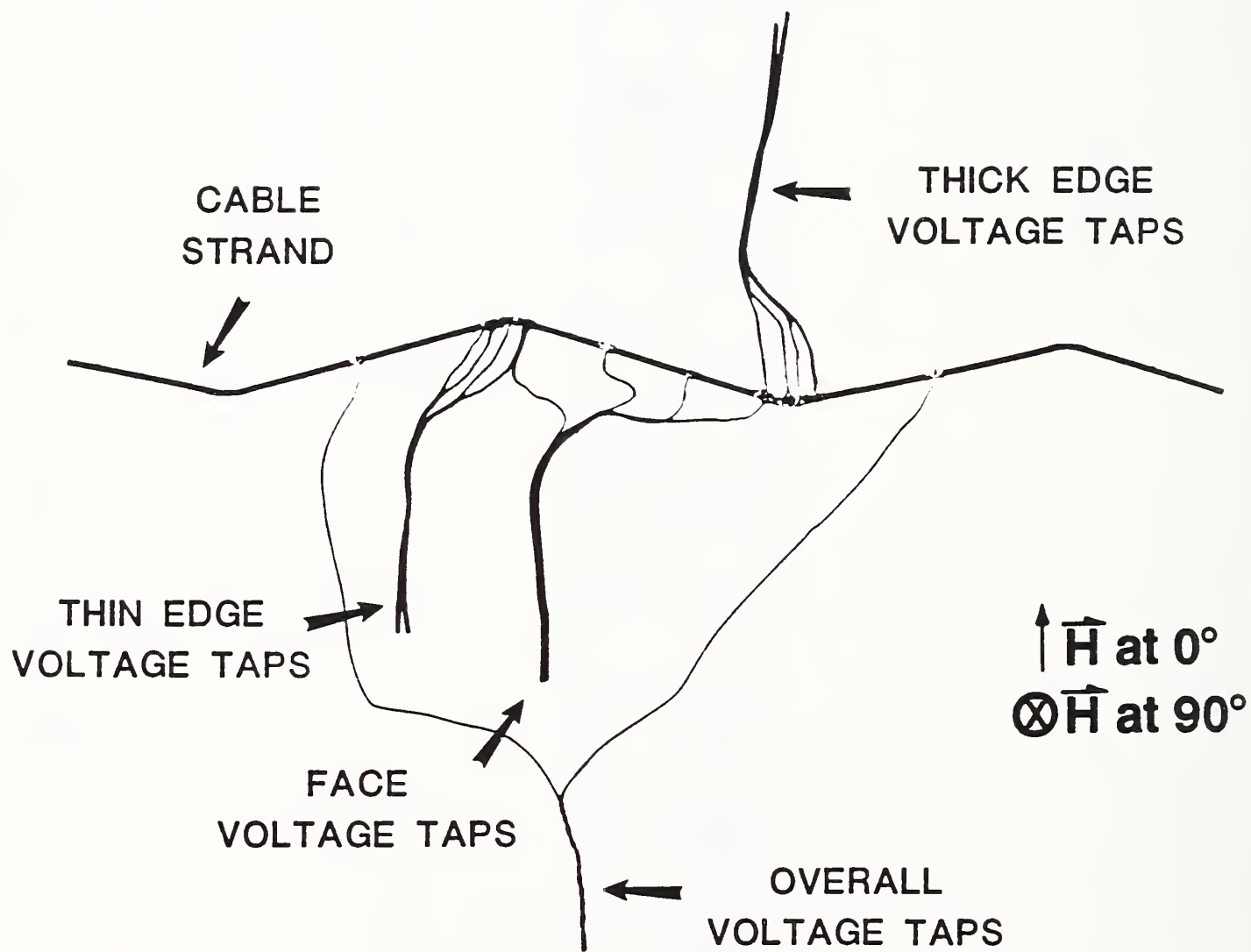
Figure 2. Instrumented portion of an extracted cable strand showing the
voltage tap placement and the orientation of the applied magnetic
field.
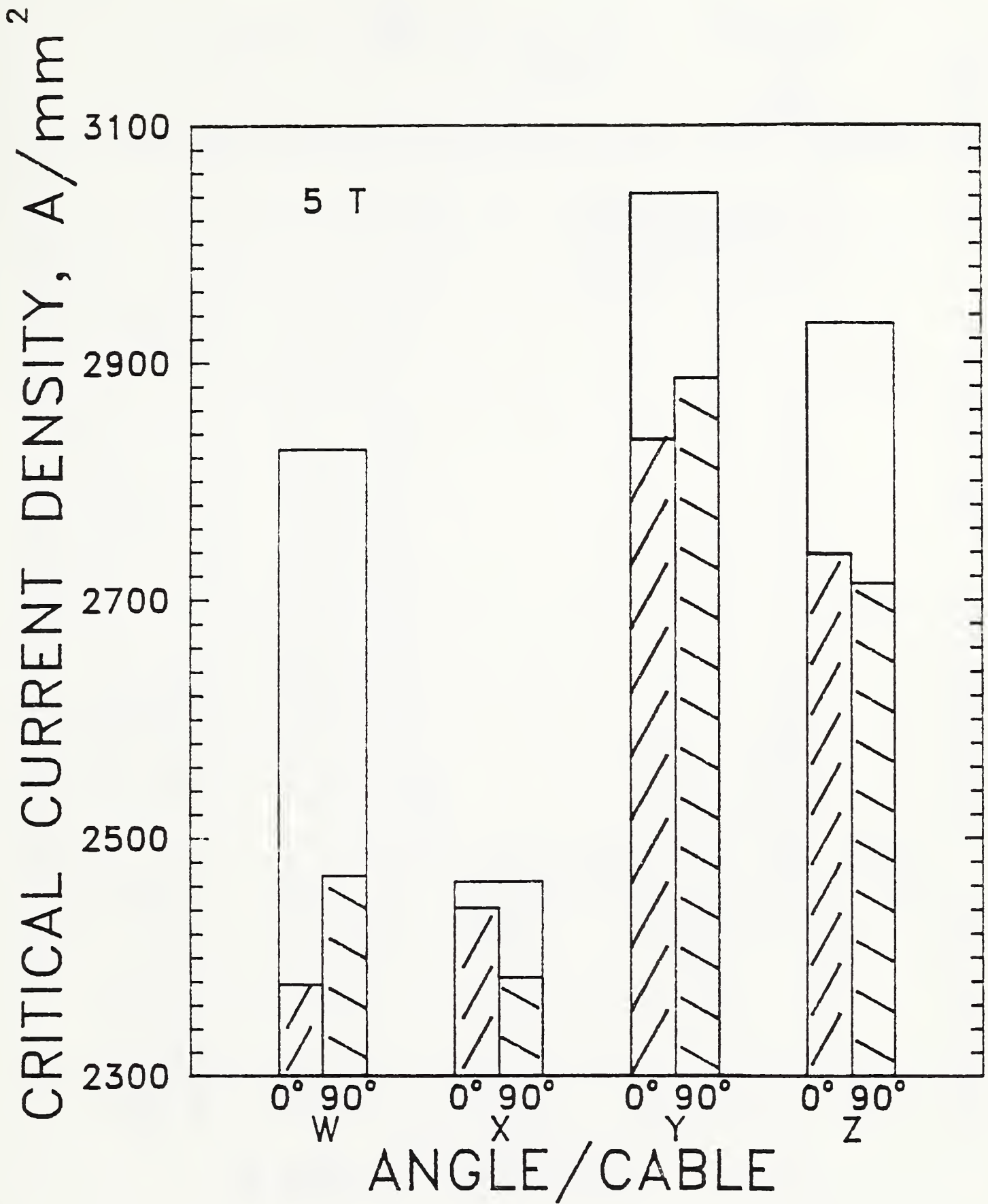
Figure 3. Critical-current density of cable strands and their respective
virgin wires for 0 and 90° at 5 T. The virgin wire J_c is
represented by the continuous line segment spanning 0 to 90° for
each cable. The strand J_c at 0 and 90° are represented by the
shaded bars for each cable.
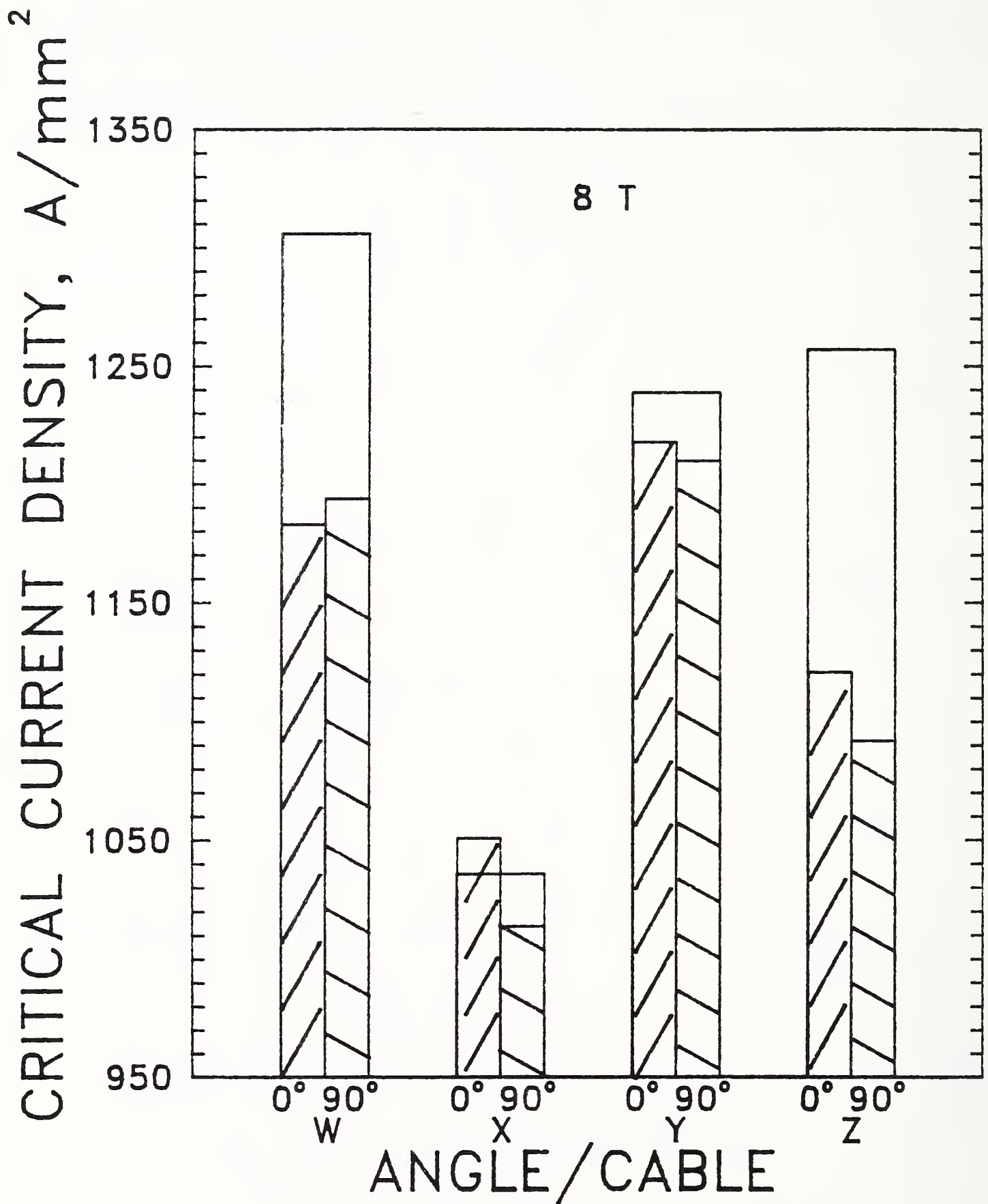
Figure 4. Critical-current density of cable strands and their respective virgin wires for 0 and 90° at 8 T. The virgin wire J_c is represented by the continuous line segment spanning 0 to 90° for each cable. The strand J_c at 0 and 90° are represented by the shaded bars for each cable.
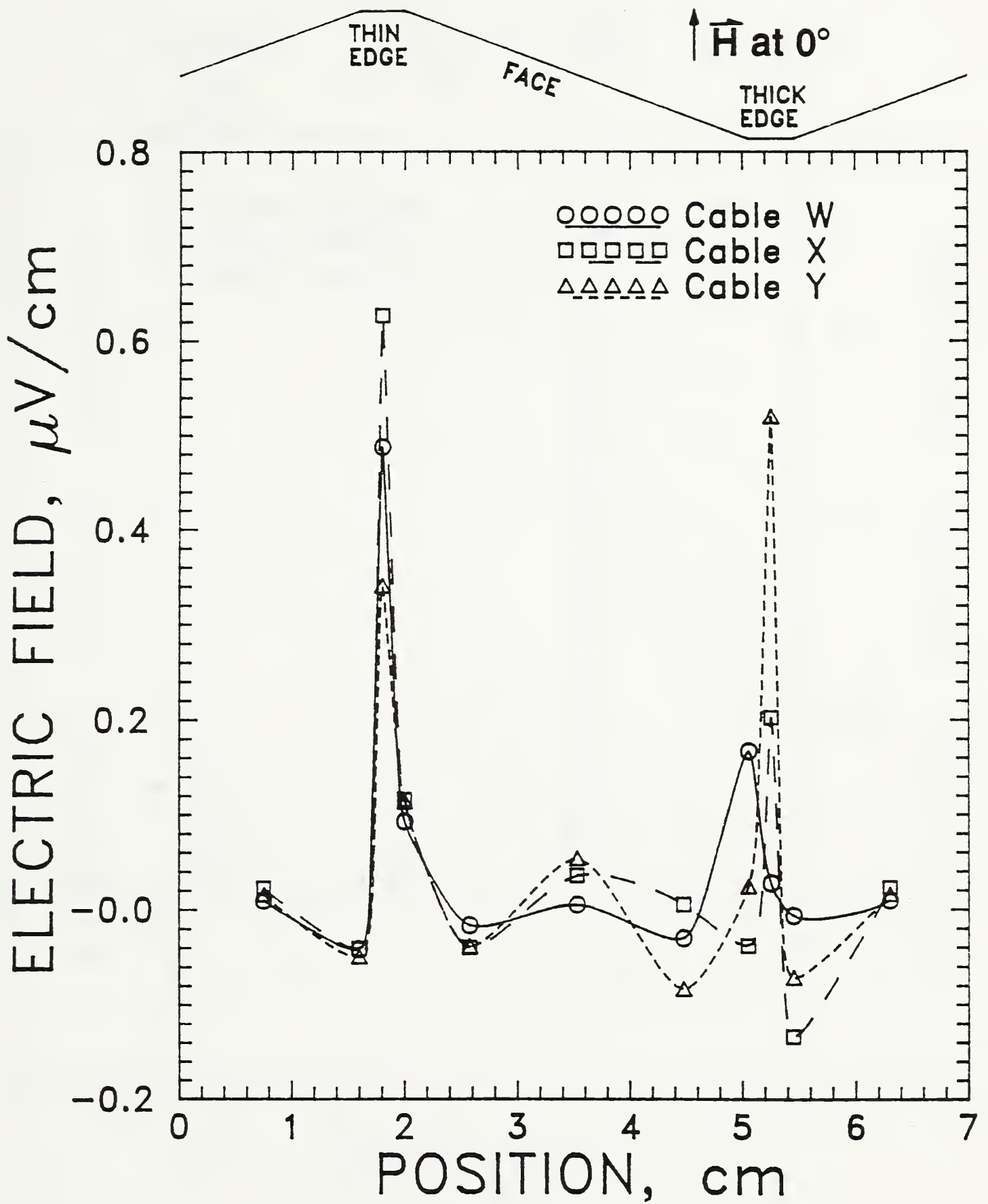
Figure 5. Electric-field profiles at 5 T and an applied magnetic field angle of 0° for cables W, X, and Y at currents of 267 A, 283 A, and 317 A, respectively, which corresponds to an overall electric field of 0.01 μV/cm.
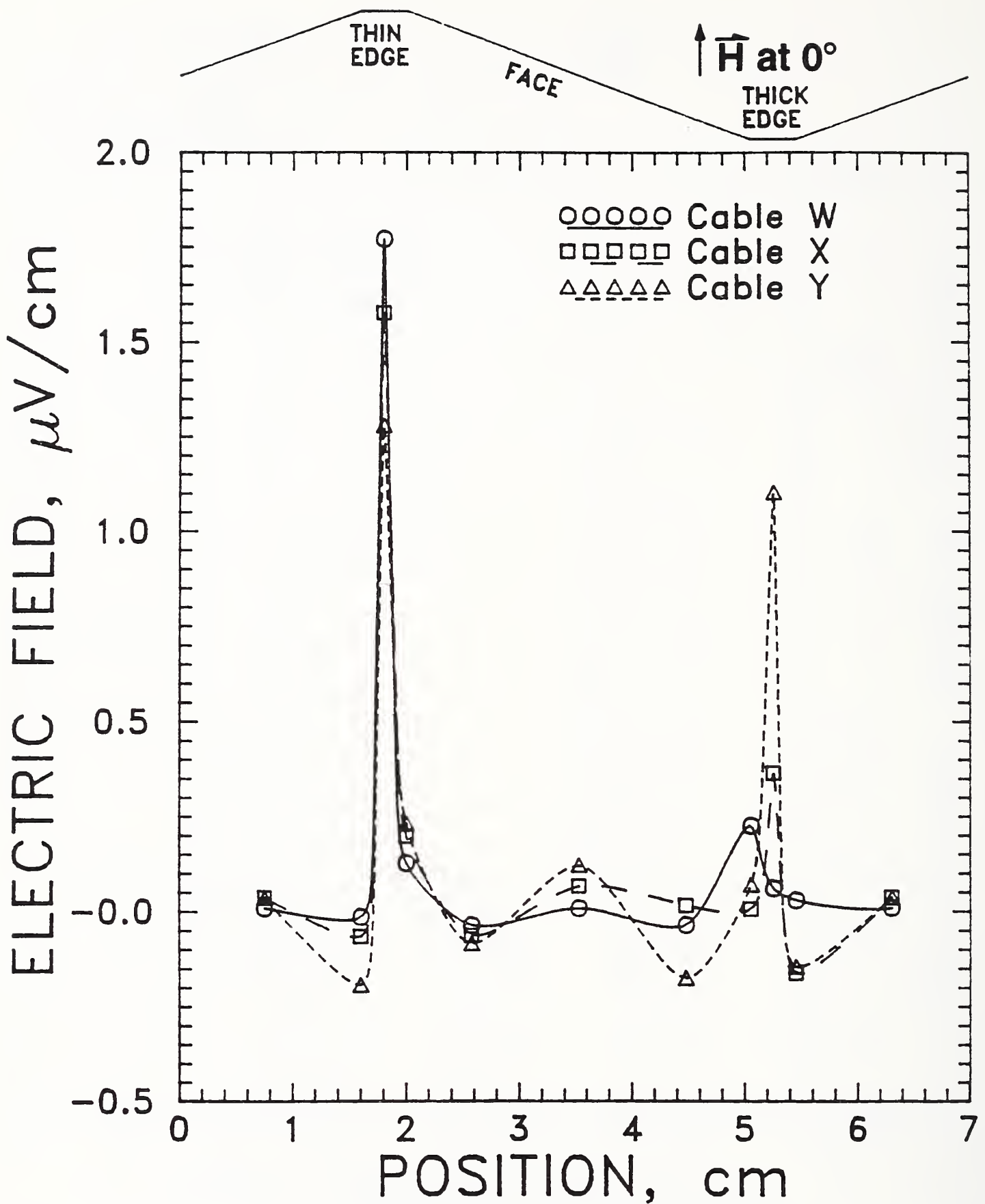
Figure 6. Electric-field profiles at 5 T and an applied magnetic field angle of 0° for cables W, X, and Y at currents of 279 A, 299 A, and 332 A, respectively, which corresponds to an overall electric field 0.05 μV/cm.
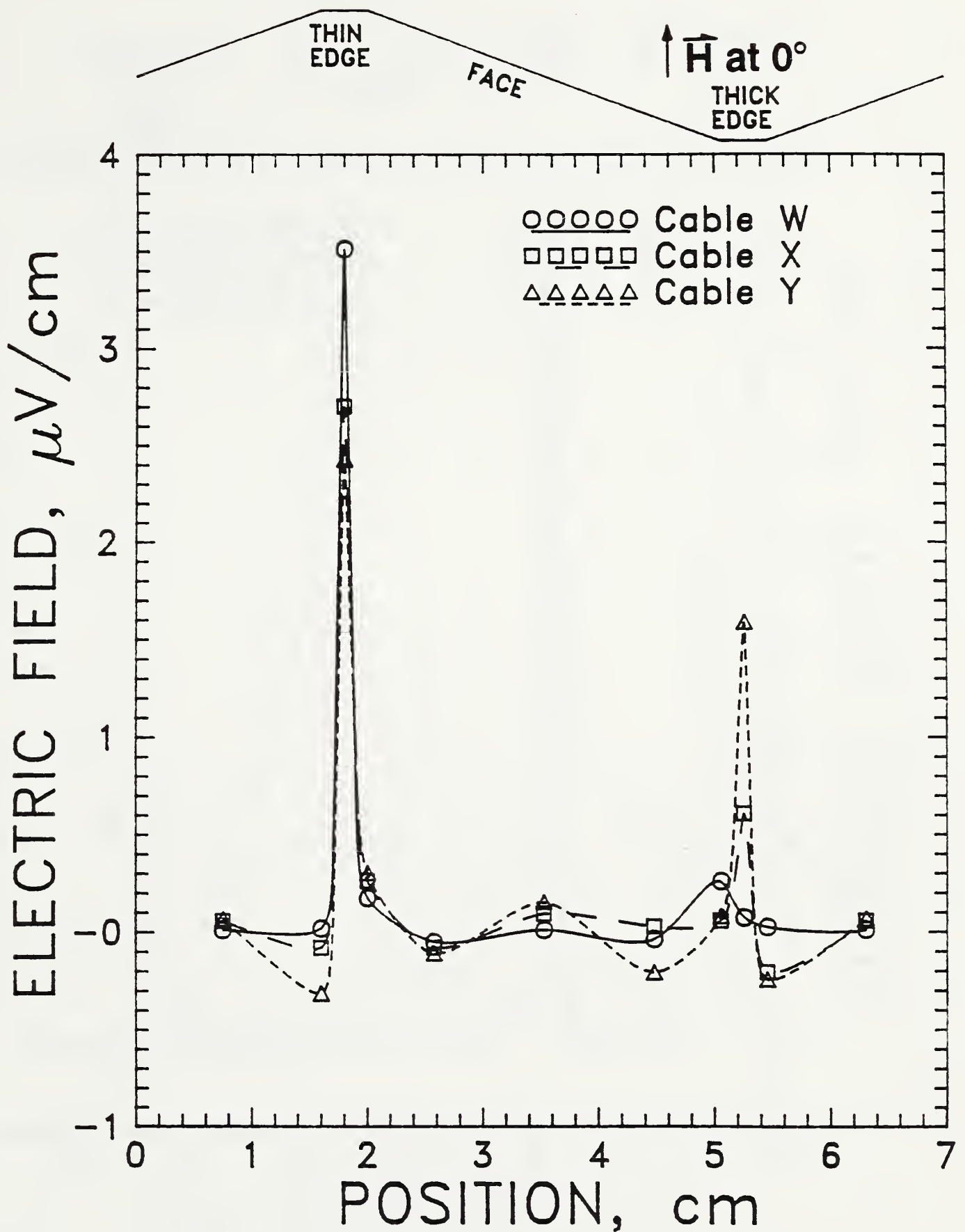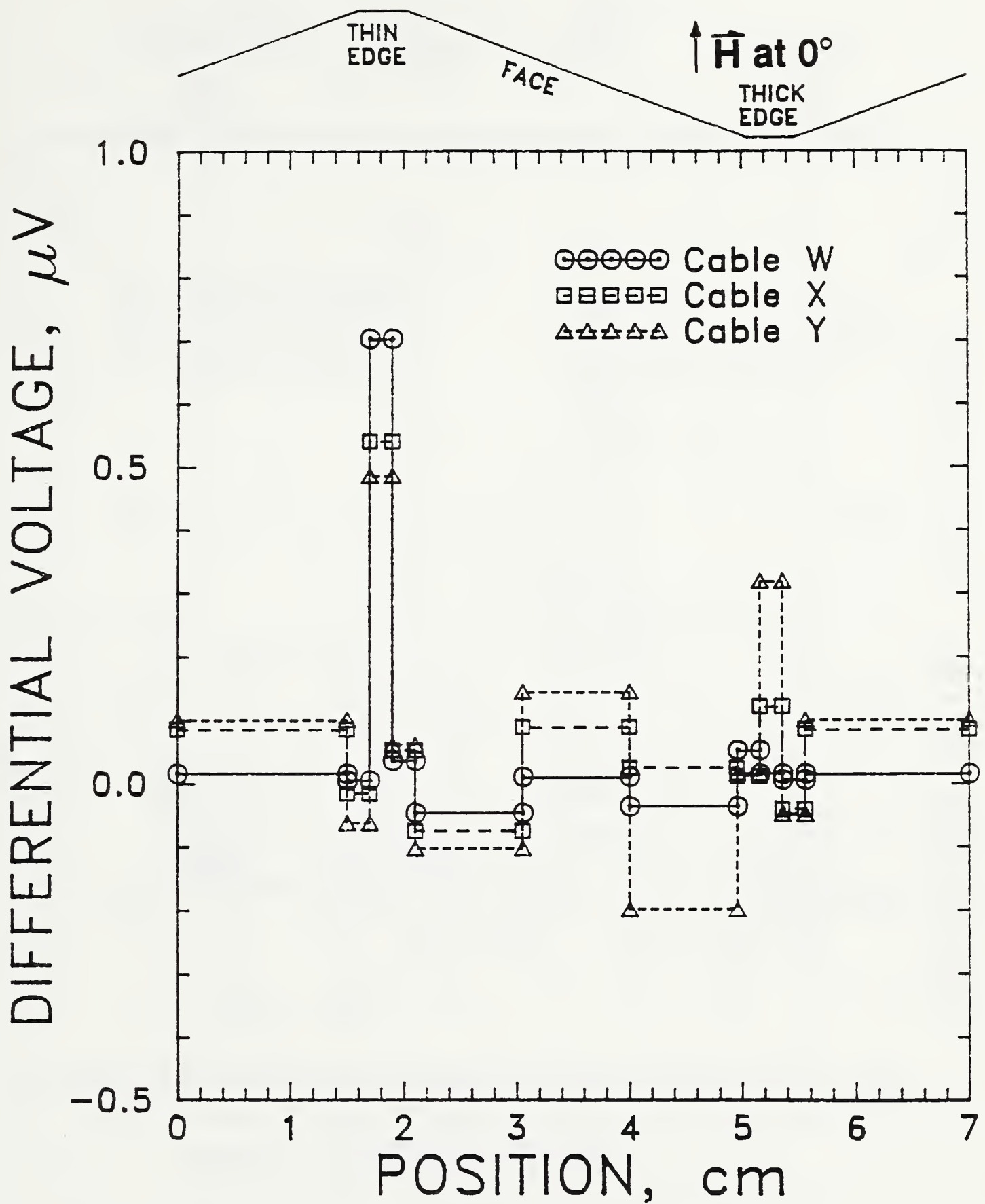
Figure 7. Electric-field profiles at 5 T and an applied magnetic field angle of 0° for cables W, X, and Y at currents of 285 A, 307 A, and 339 A, respectively, which corresponds to an overall electric field of 0.1 μV/cm.
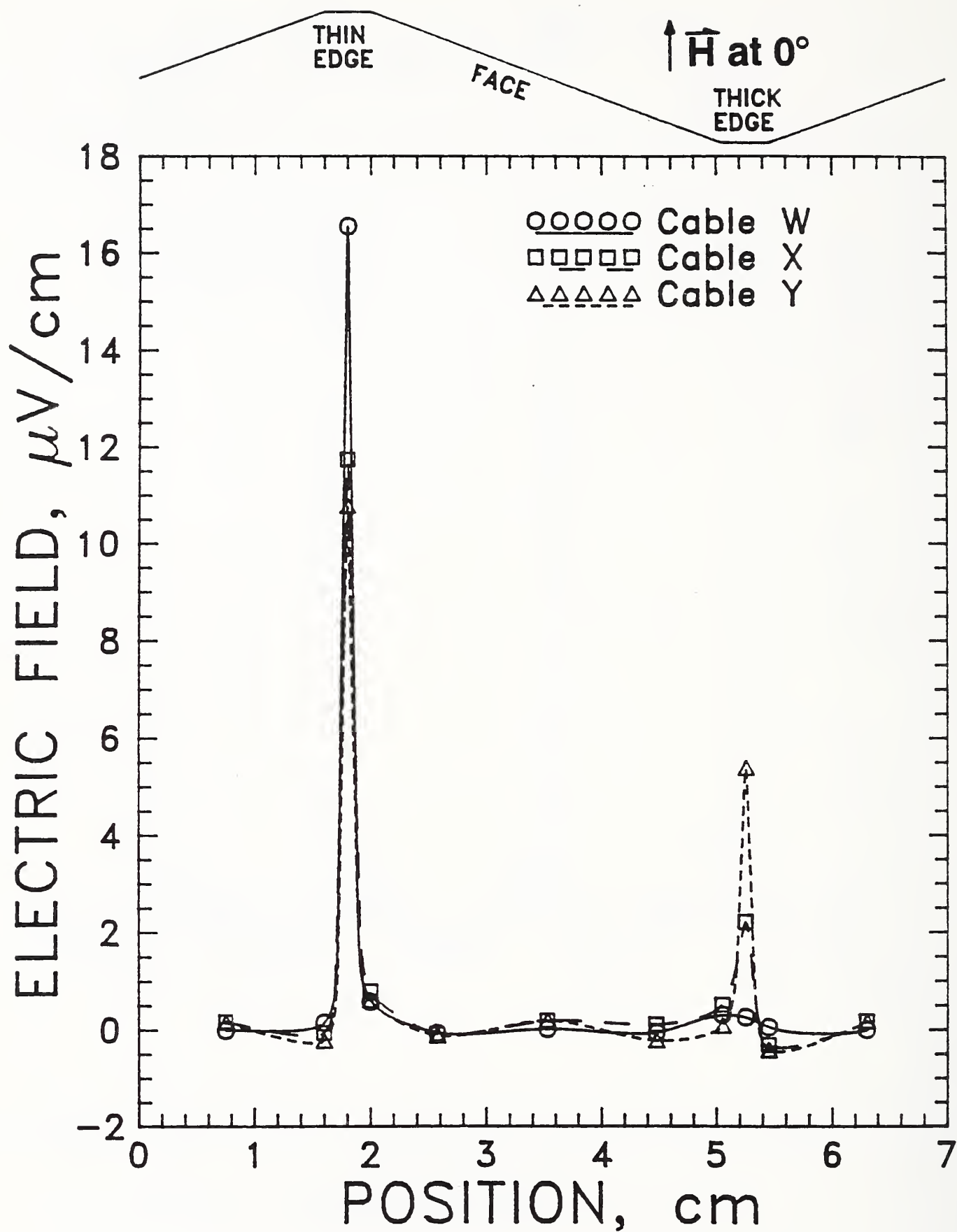
Figure 8. Electric-field profiles at 5 T and an applied magnetic field angle of 0° for cables W, X, and Y at currents of 300 A, 326 A, and 351 A, respectively, which corresponds to an overall electric field of 0.5 µV/cm.
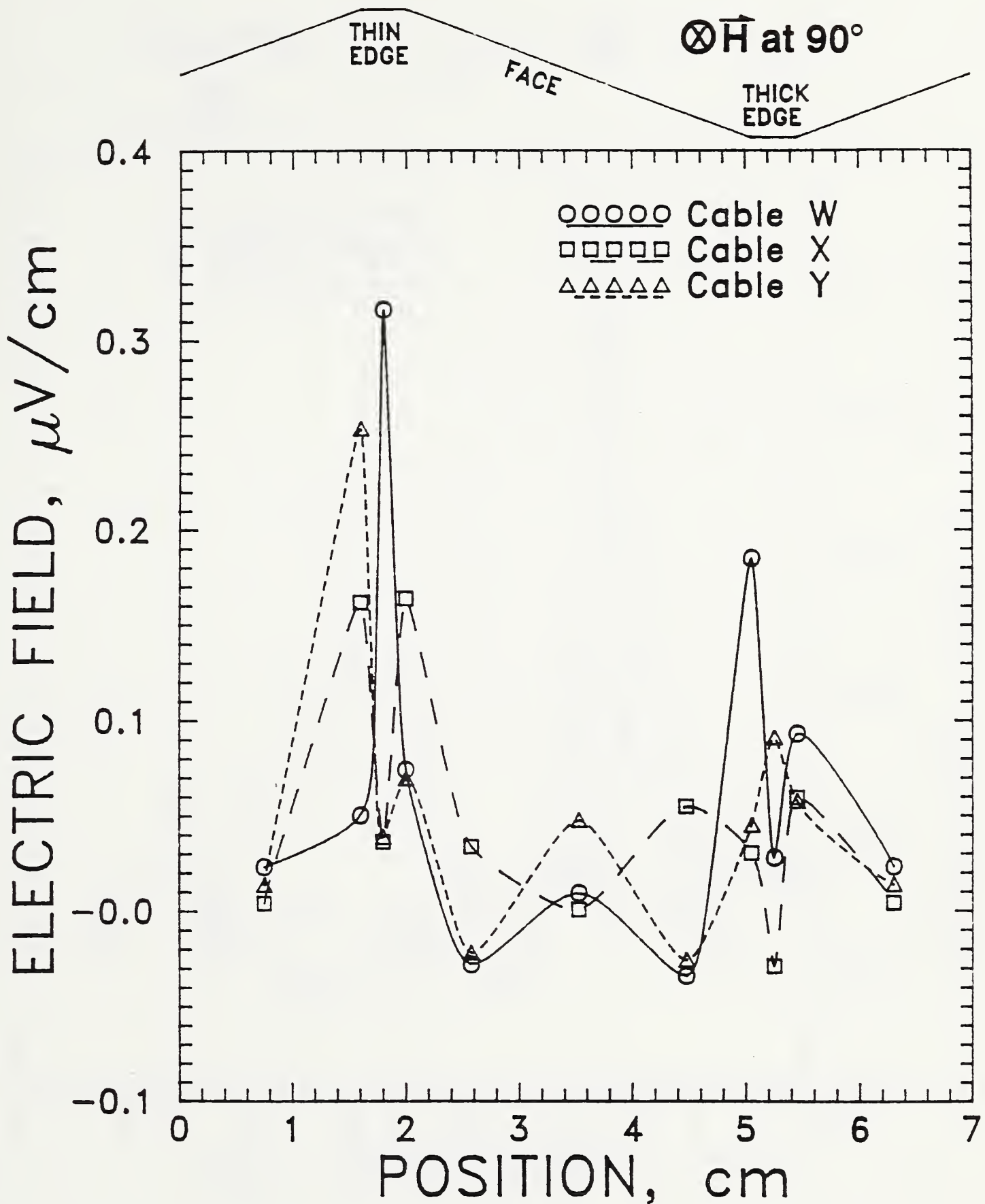
Figure 9. Electric-field profiles at 5 T and an applied magnetic field angle of 90° for cables W, X, and Y at currents of 275 A, 277 A, and 327 A, respectively, which corresponds to an overall electric field of 0.01 μV/cm.
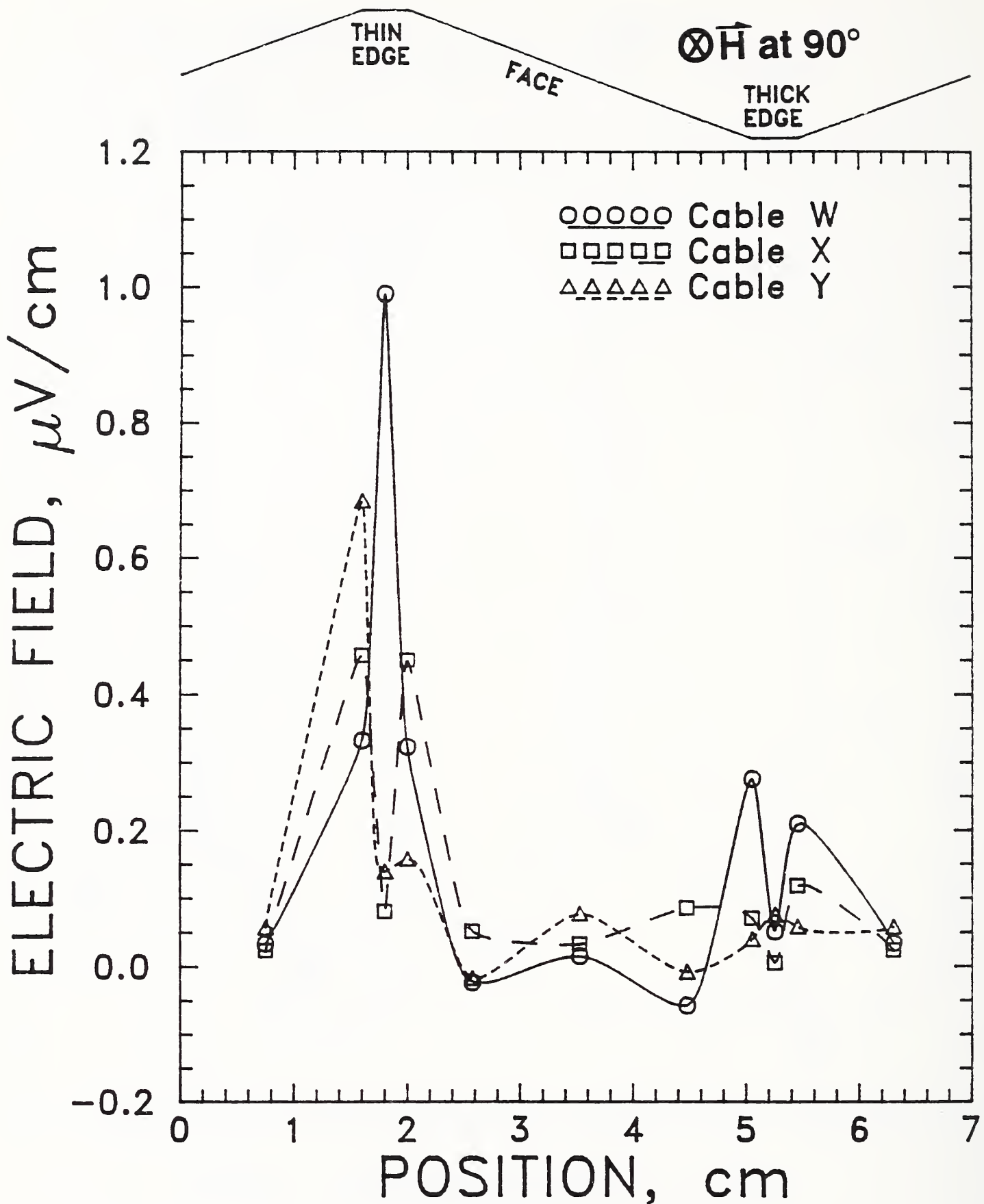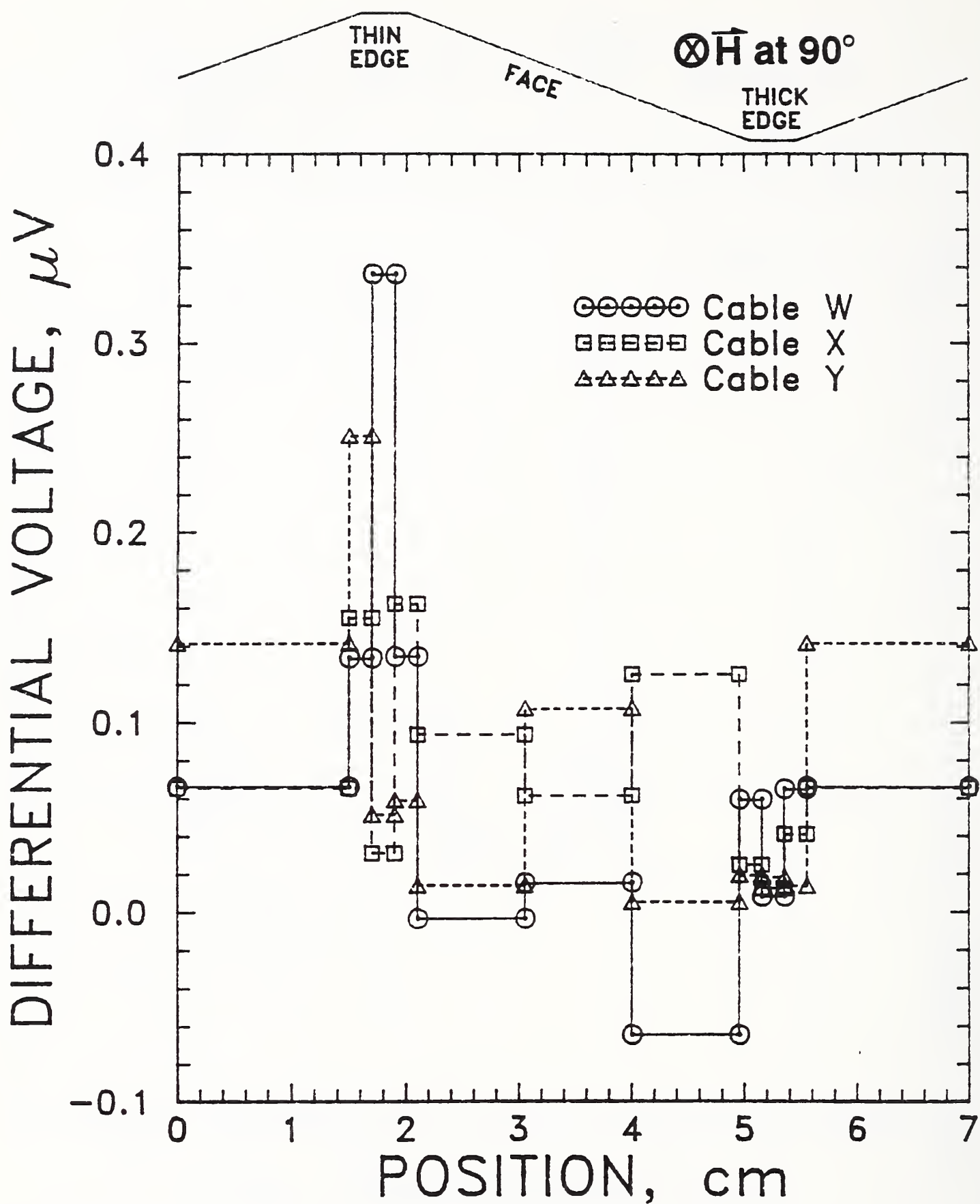
Figure 10. Electric-field profiles at 5 T and an applied magnetic field angle of 90° for cables W, X, and Y at currents of 289 A, 292 A, and 339 A, respectively, which corresponds to an overall electric field of 0.05 μV/cm.
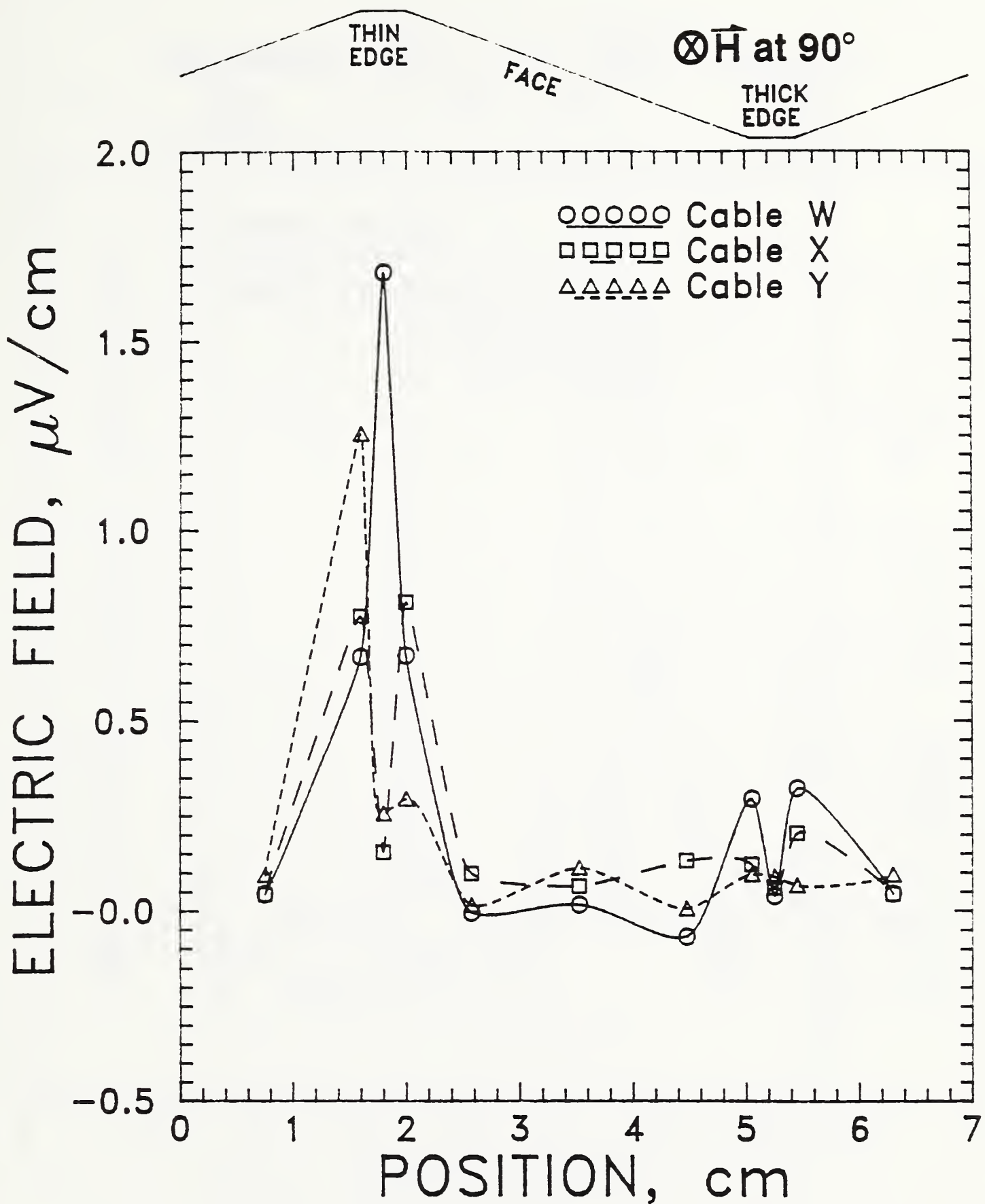
Figure 11. Electric-field profiles at 5 T and an applied magnetic field angle of 90° for cables W, X, and Y at currents of 296 A, 300 A, and 345 A, respectively, which corresponds to an overall electric field of 0.1 $\mu V/cm$.
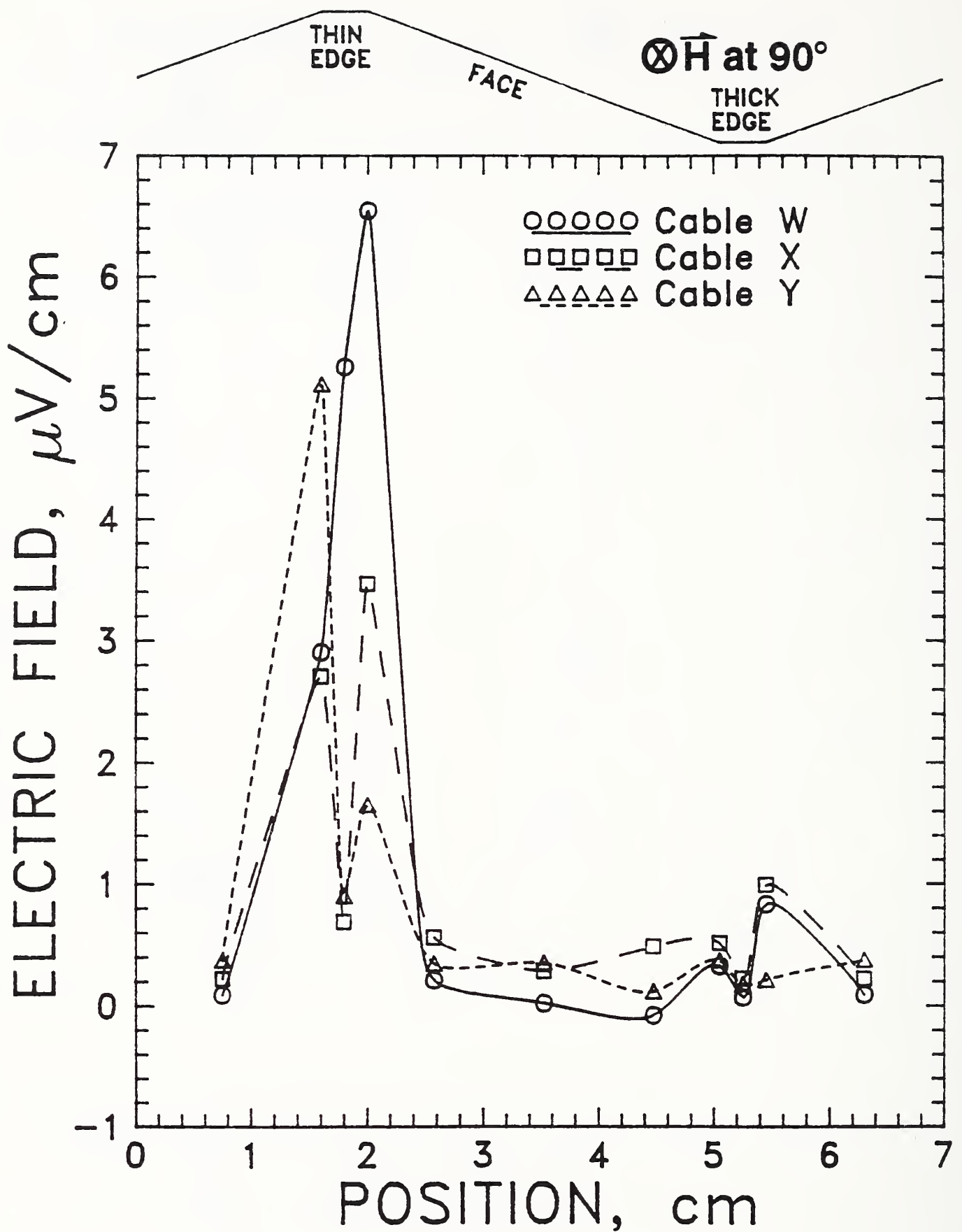
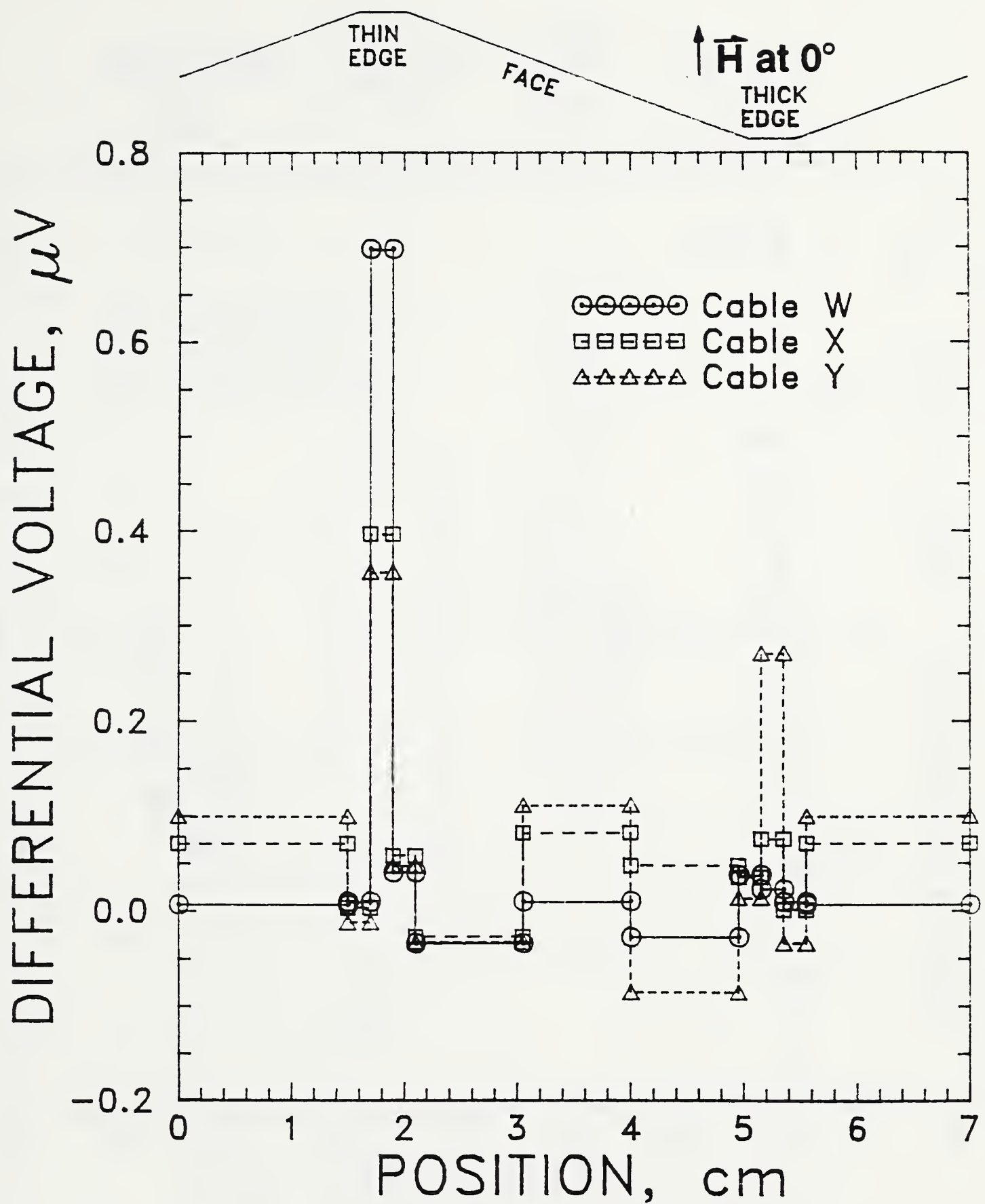Figure 12. Electric-field profiles at 5 T and an applied magnetic field angle of 90° for cables W, X, and Y at currents of 307 A, 318 A, and 358 A, respectively, which corresponds to an overall electric field of 0.5 μV/cm.
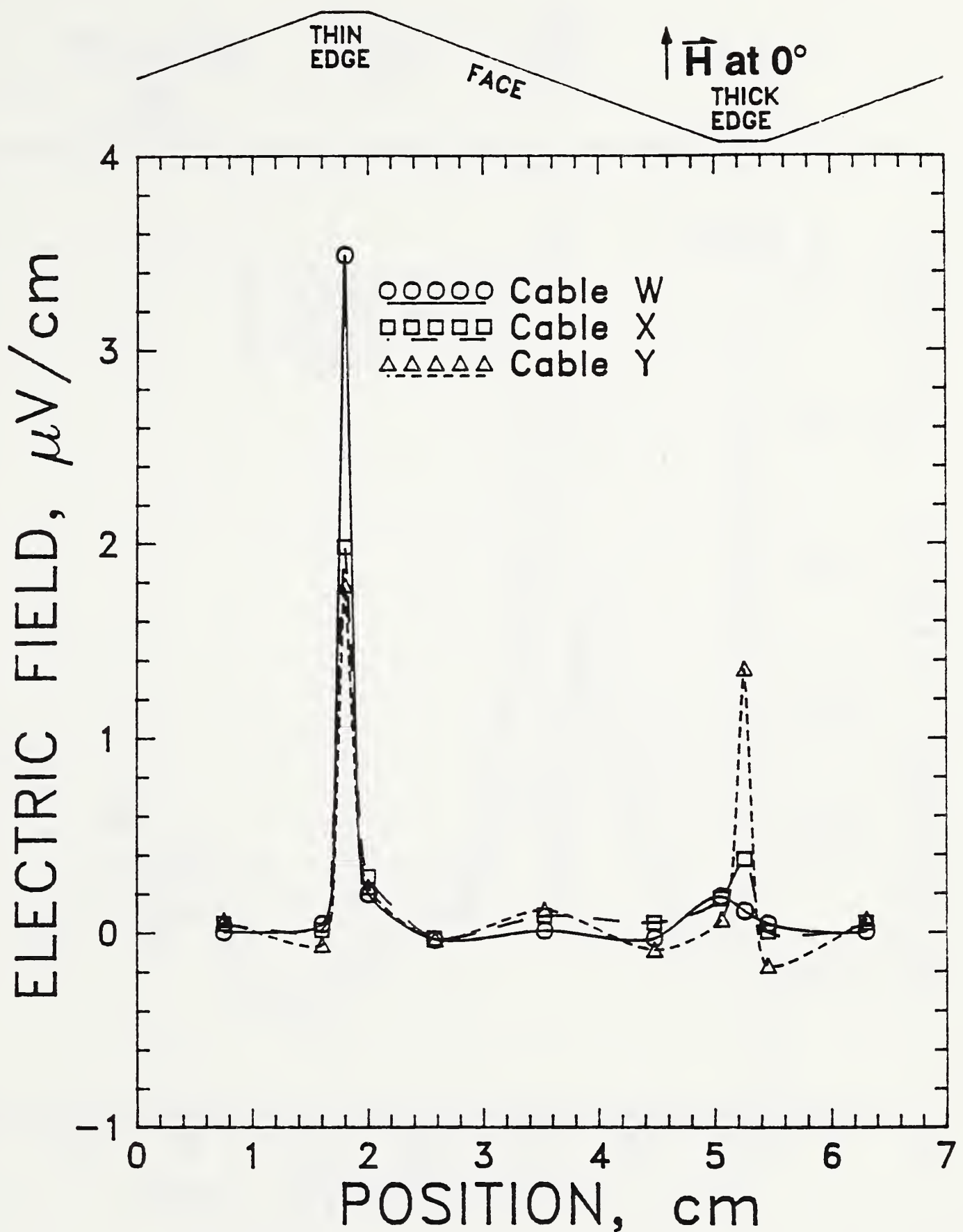
Figure 13. Electric-field profiles at 8 T and an applied magnetic field angle of 0° for cables W, X, and Y at currents of 142 A, 132 A, and 145 A, respectively, which corresponds to an overall electric field of 0.1 μV/cm.
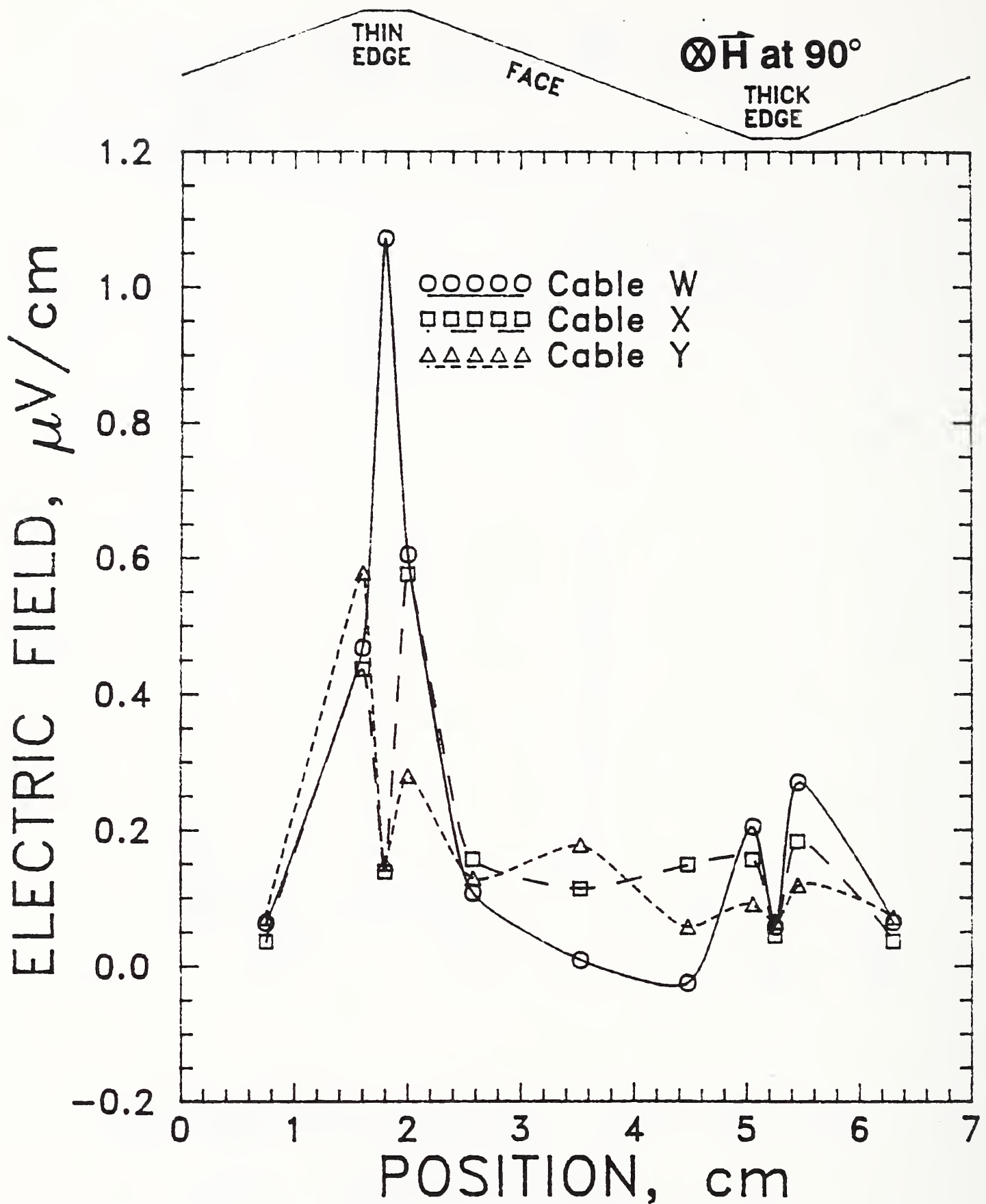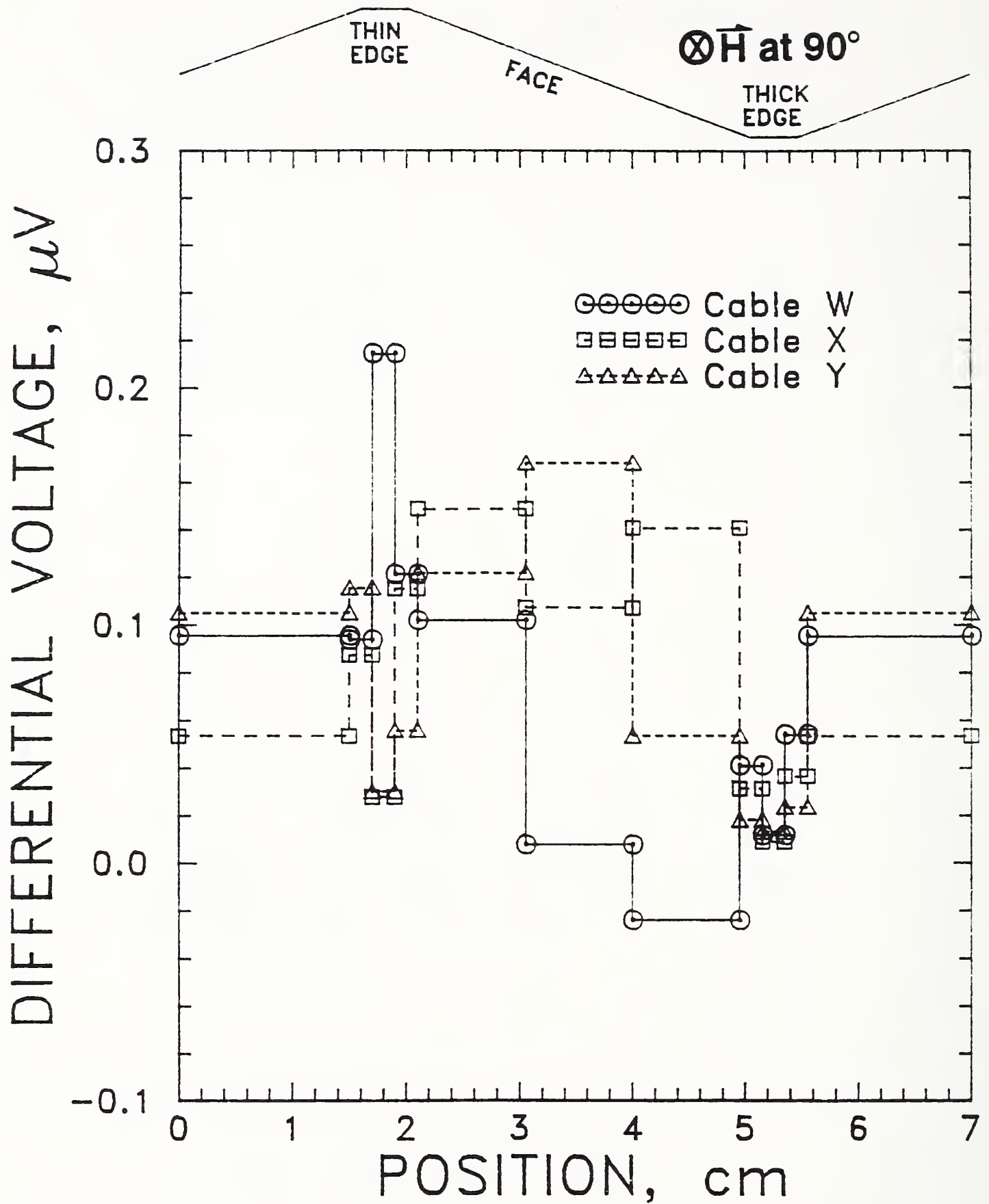
Figure 14. Electric-field profiles at 8 T and an applied magnetic field angle of 90° for cables W, X, and Y at currents of 143 A, 128 A, and 144 A, respectively, which corresponds to an overall electric field of 0.1 μV/cm.
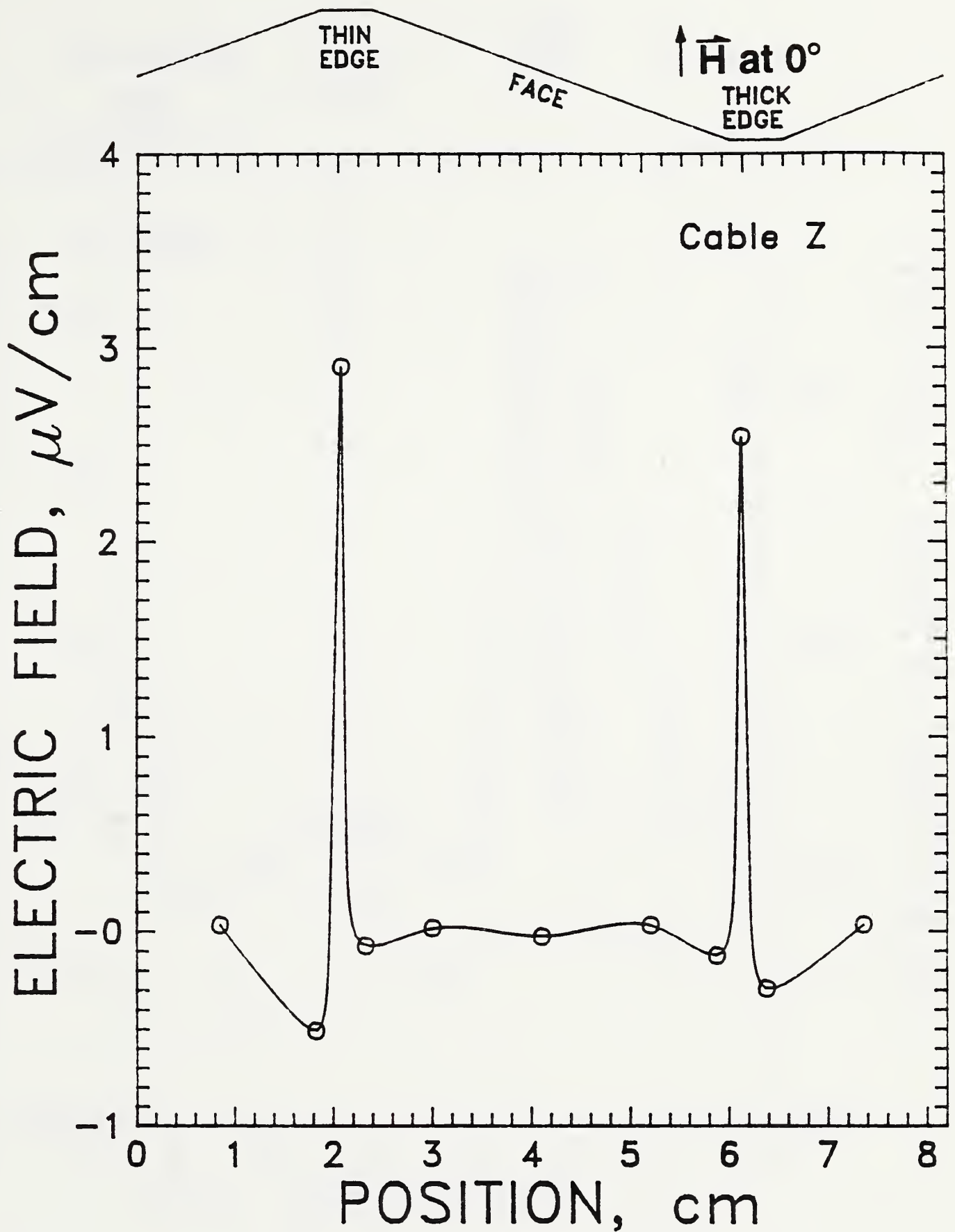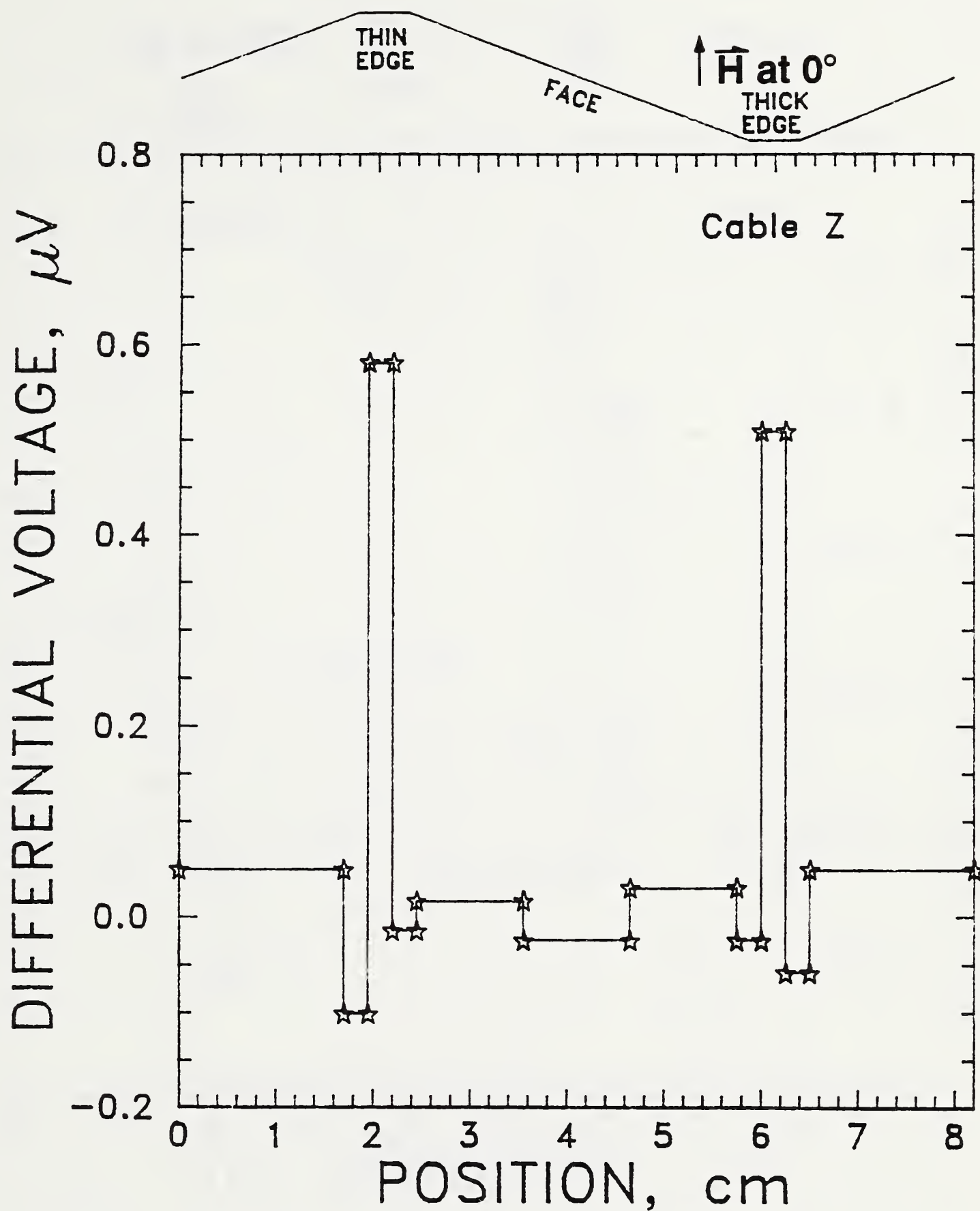
Figure 15.   Electric-field profiles at 5 T and an applied magnetic field angle of 0° for cable Z at a current of 585 A, which corresponds to an overall electric field of 0.1 μV/cm.
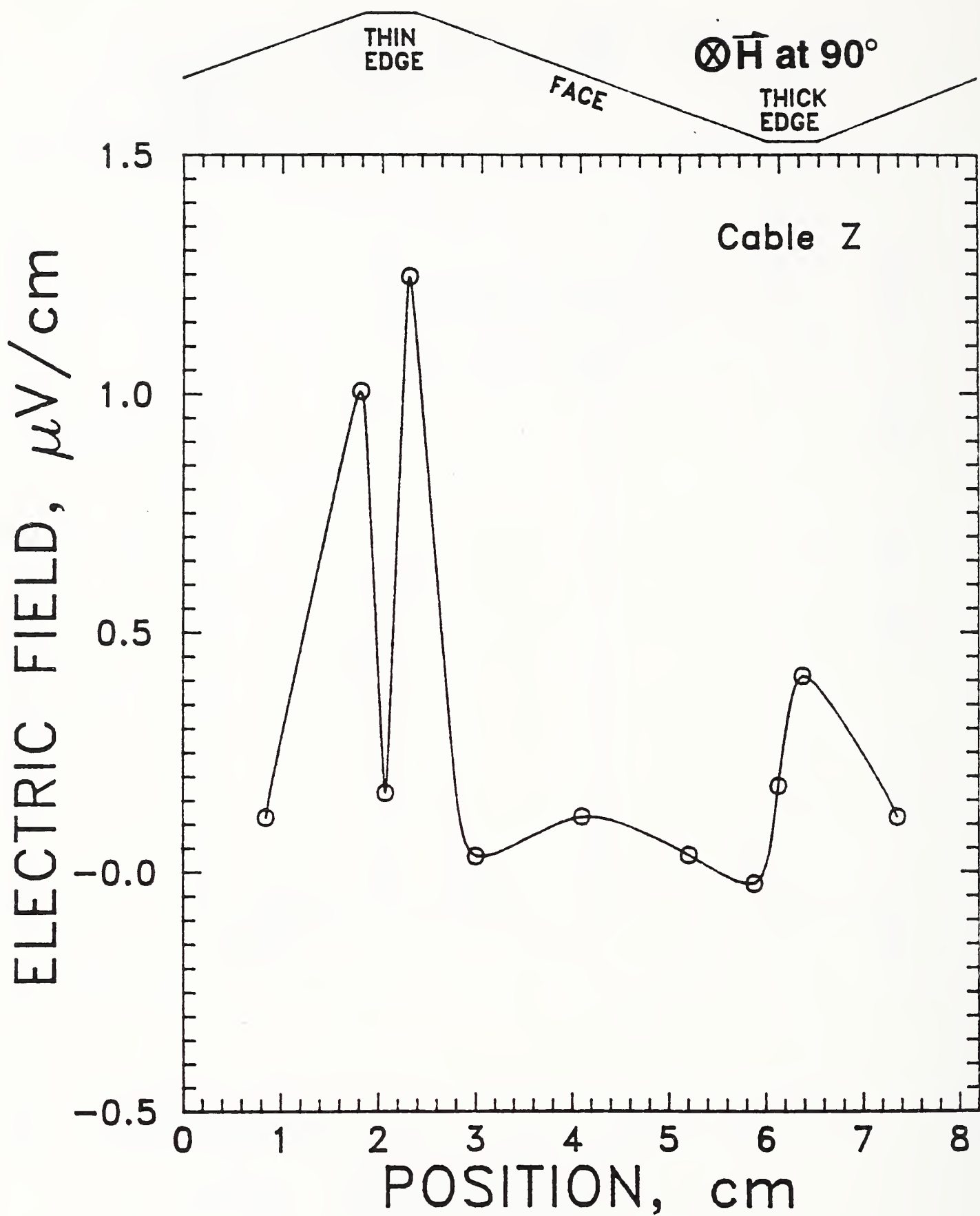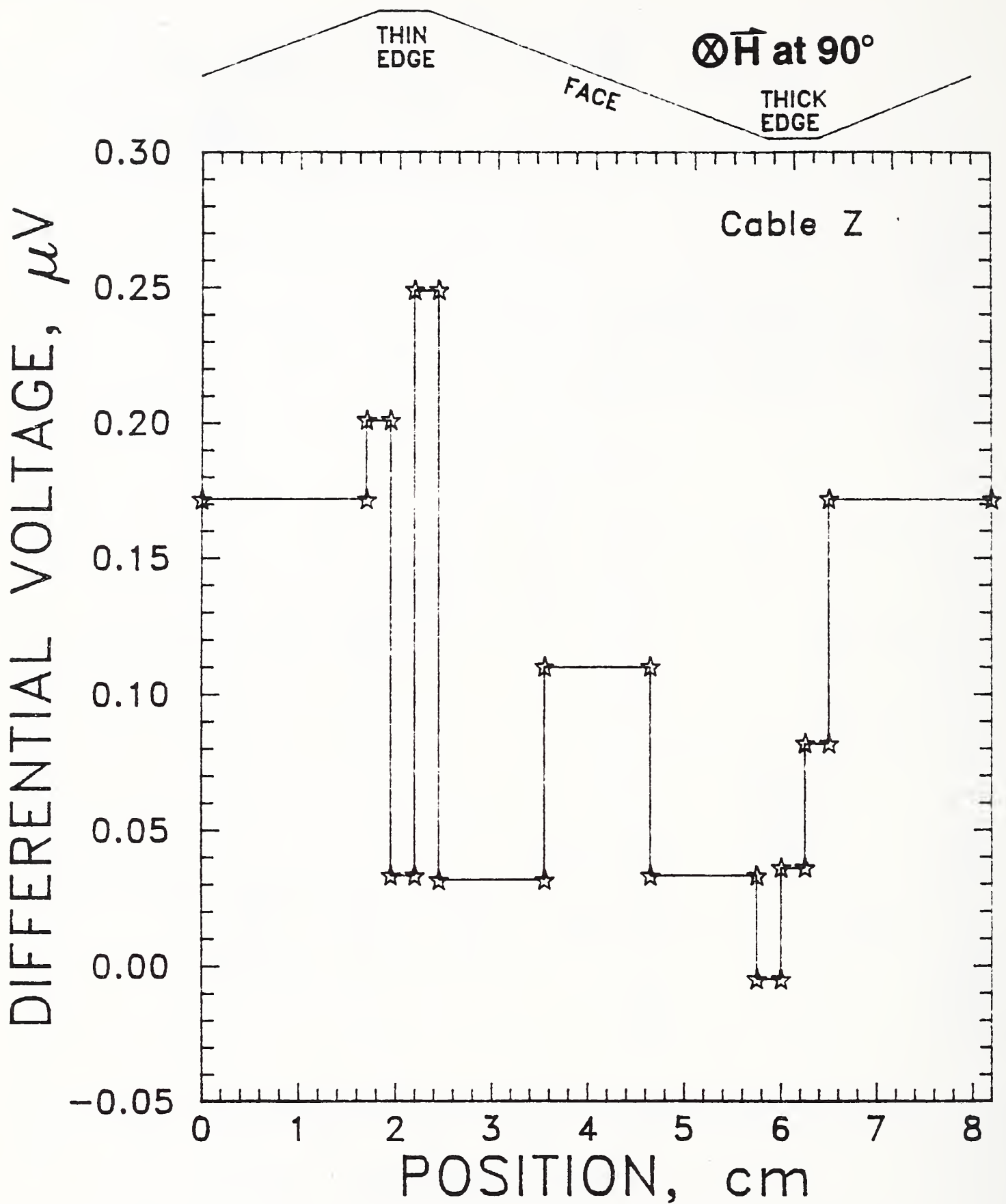
Figure 16. Electric-field profiles at 5 T and an applied magnetic field angle of 90° for cable Z at a current of 579 A, which corresponds to an overall electric field of 0.1 µV/cm.
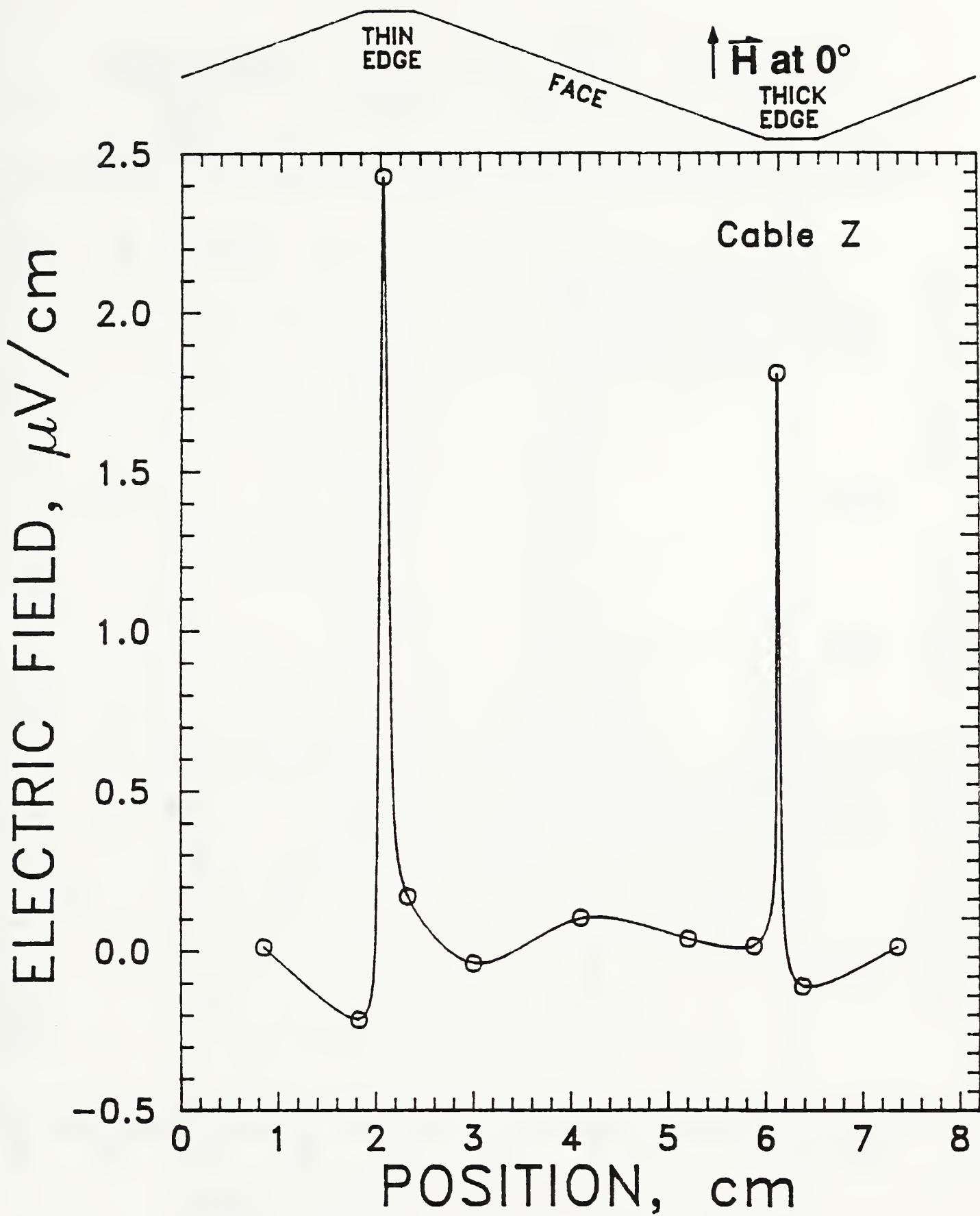
Figure 17.   Electric-field profiles at 8 T and an applied magnetic field
             angle of 0° for cable Z at a current of 239 A, which corresponds
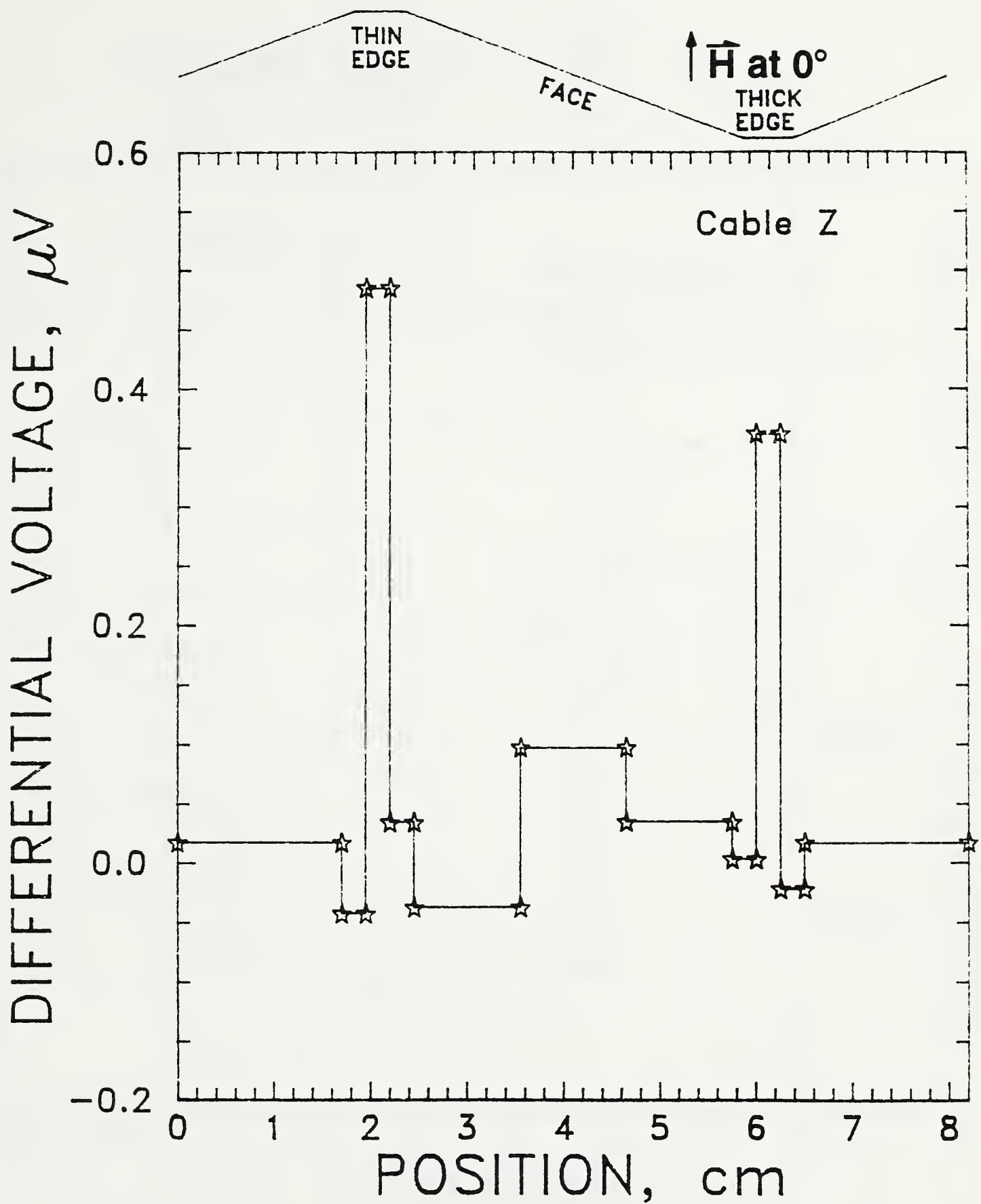   to an overall electric field of 0.1 μV/cm.
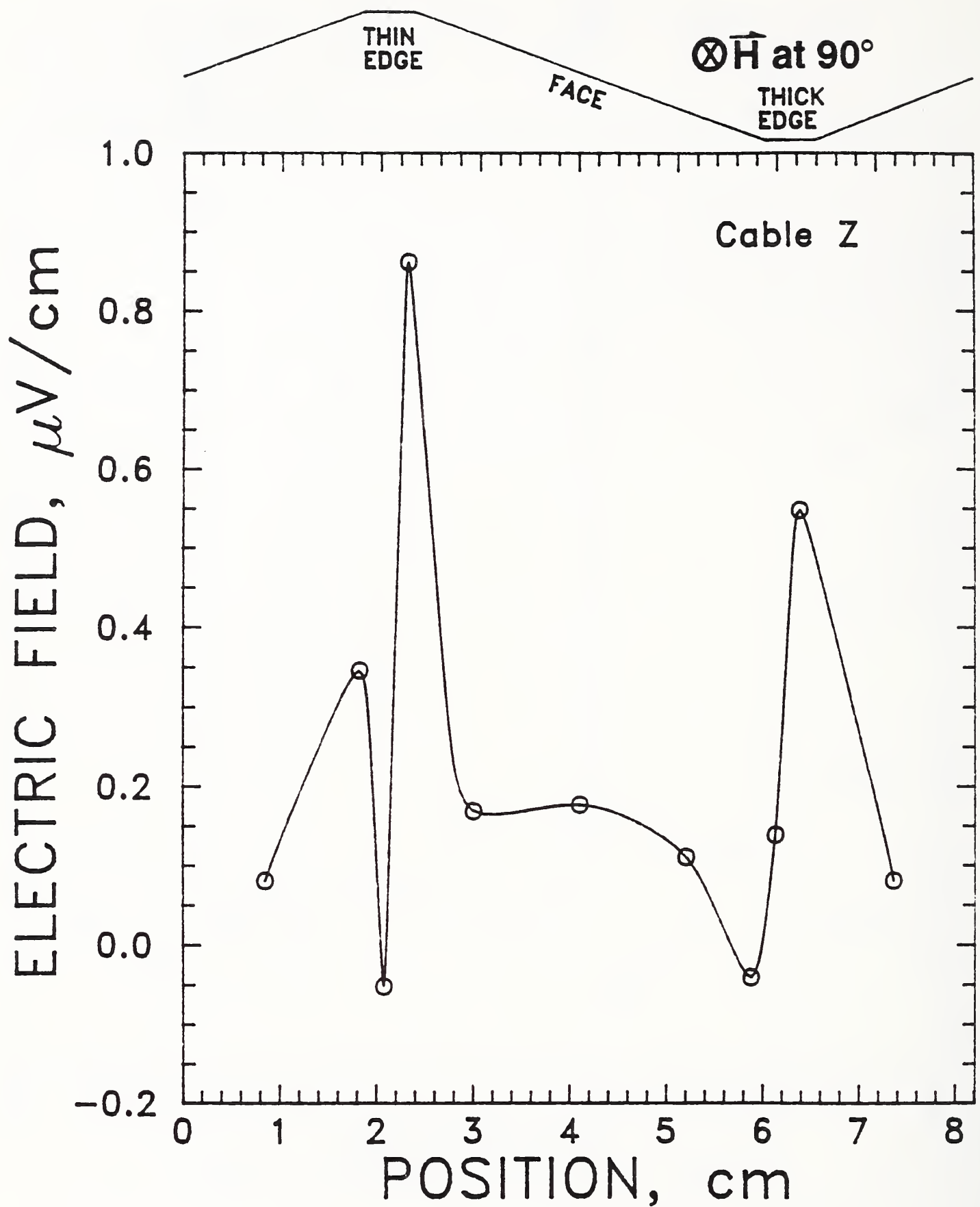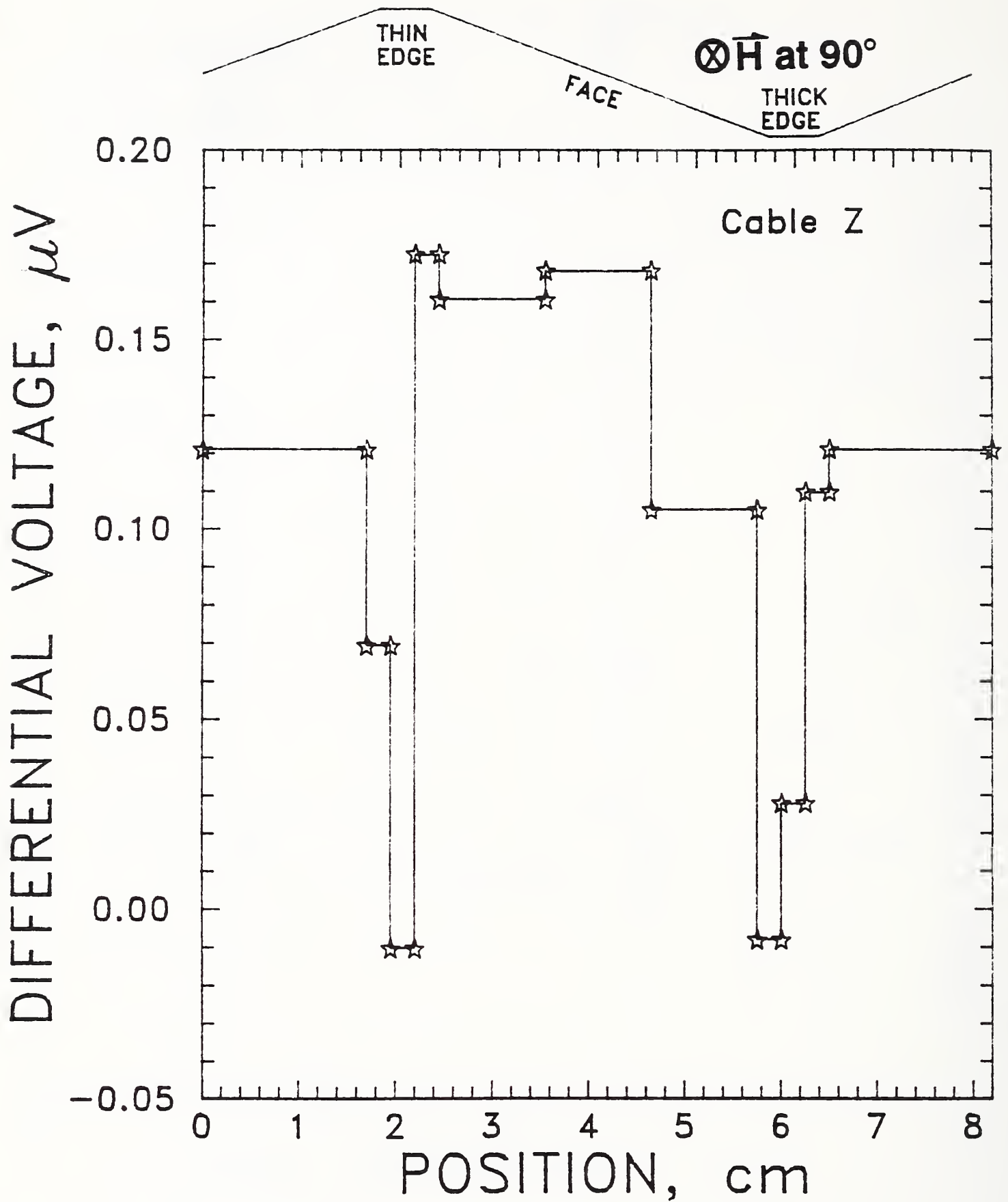
Figure 18. Electric-field profiles at 8 T and an applied magnetic field angle of 90° for cable Z at a current of 233 A, which corresponds to an overall electric field of 0.1 μV/cm.

Figure 19. Differential-voltage profiles at 5 T and an applied magnetic field angle of 0° for cables W, X, and Y at currents of 285 A, 307 A, and 339 A, respectively, which corresponds to an overall electric field of 0.1 µV/cm.

Figure 20. Differential-voltage profiles at 5 T and an applied magnetic field angle of 90° for cables W, X, and Y at currents of 296 A, 300 A, and 345 A, respectively, which corresponds to an overall electric field of 0.1 μV/cm.

Figure 21. Differential-voltage profiles at 8 T and an applied magnetic field angle of 0° for cables W, X, and Y at currents of 142 A, 132 A, and 145 A, respectively, which corresponds to an overall electric field of 0.1 μV/cm.

Figure 22. Differential-voltage profiles at 8 T and an applied magnetic field angle of 90° for cables W, X, and Y at currents of 143 A, 128 A, and 144 A, respectively, which corresponds to an overall electric field of 0.1 μV/cm.

Figure 23. Differential-voltage profiles at 5 T and an applied magnetic field angle of 0° for cable Z at a current of 585 A, which corresponds to an electric field of 0.1 μV/cm.
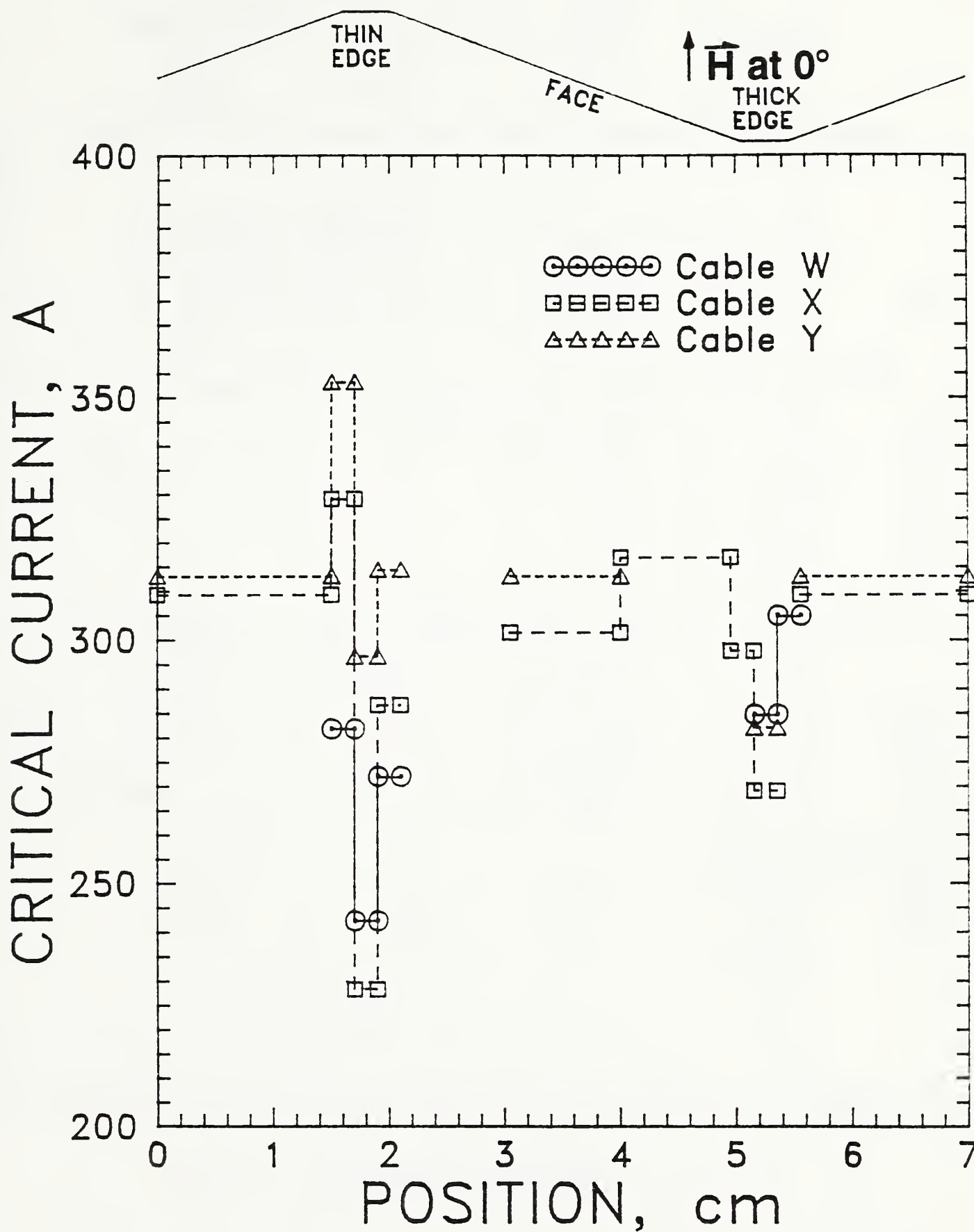
Figure 24. Differential-voltage profiles at 5 T and an applied magnetic field angle of 90° for cable Z at a current of 579 A, which corresponds to an electric field of 0.1 μV/cm.

Figure 25. Differential-voltage profiles at 8 T and an applied magnetic field angle of 0° for cable Z at a current of 239 A, which which corresponds to an electric field of 0.1 µV/cm.

Figure 26. Differential-voltage profiles at 8 T and an applied magnetic field angle of 90° for cable Z at a current of 233 A, which which corresponds to an electric field of 0.1 μV/cm.
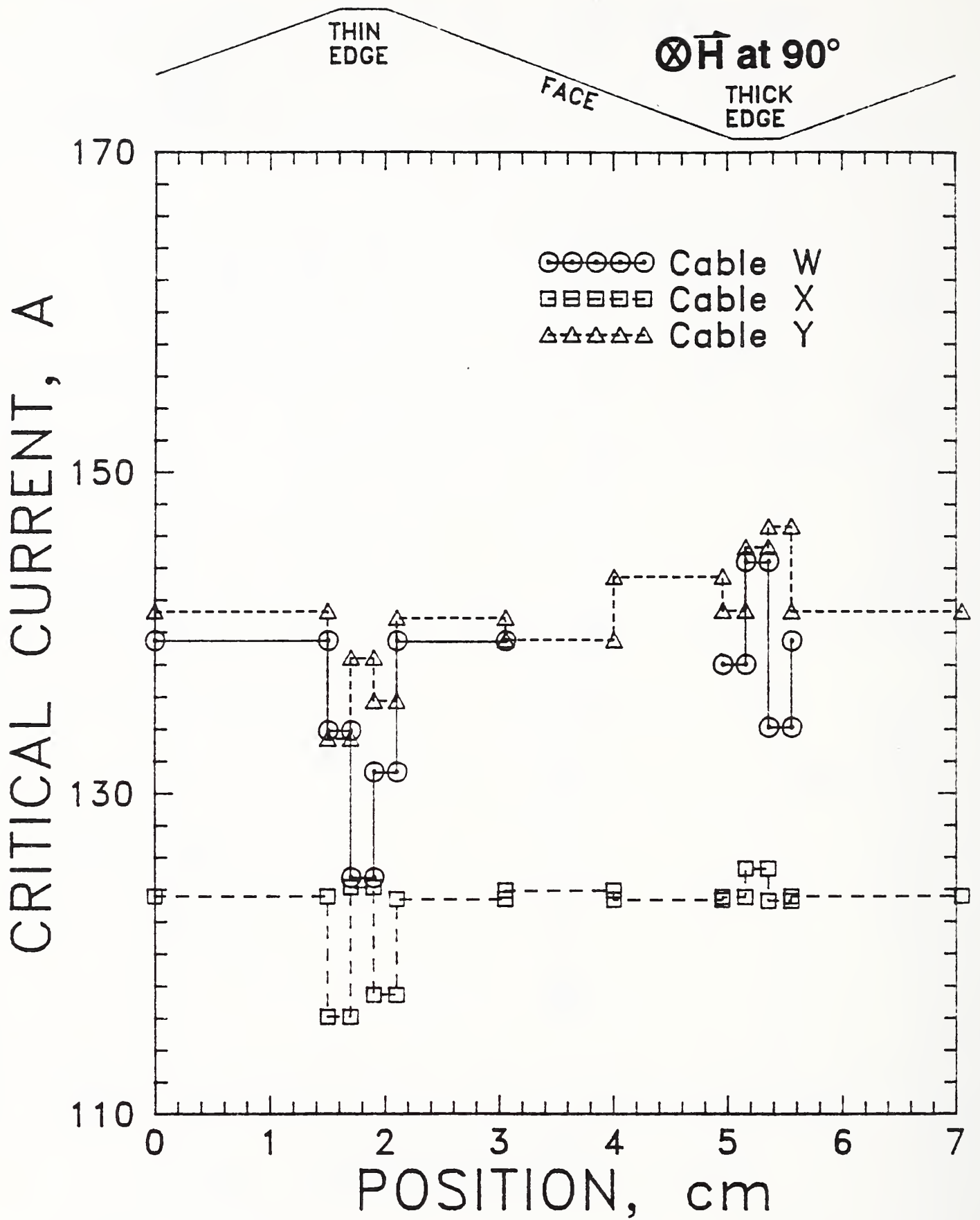
Figure 27. Critical-current profiles at 5 T and an applied magnetic field angle of 0° for cables W, X, and Y at an electric field of 0.05 μV/cm.
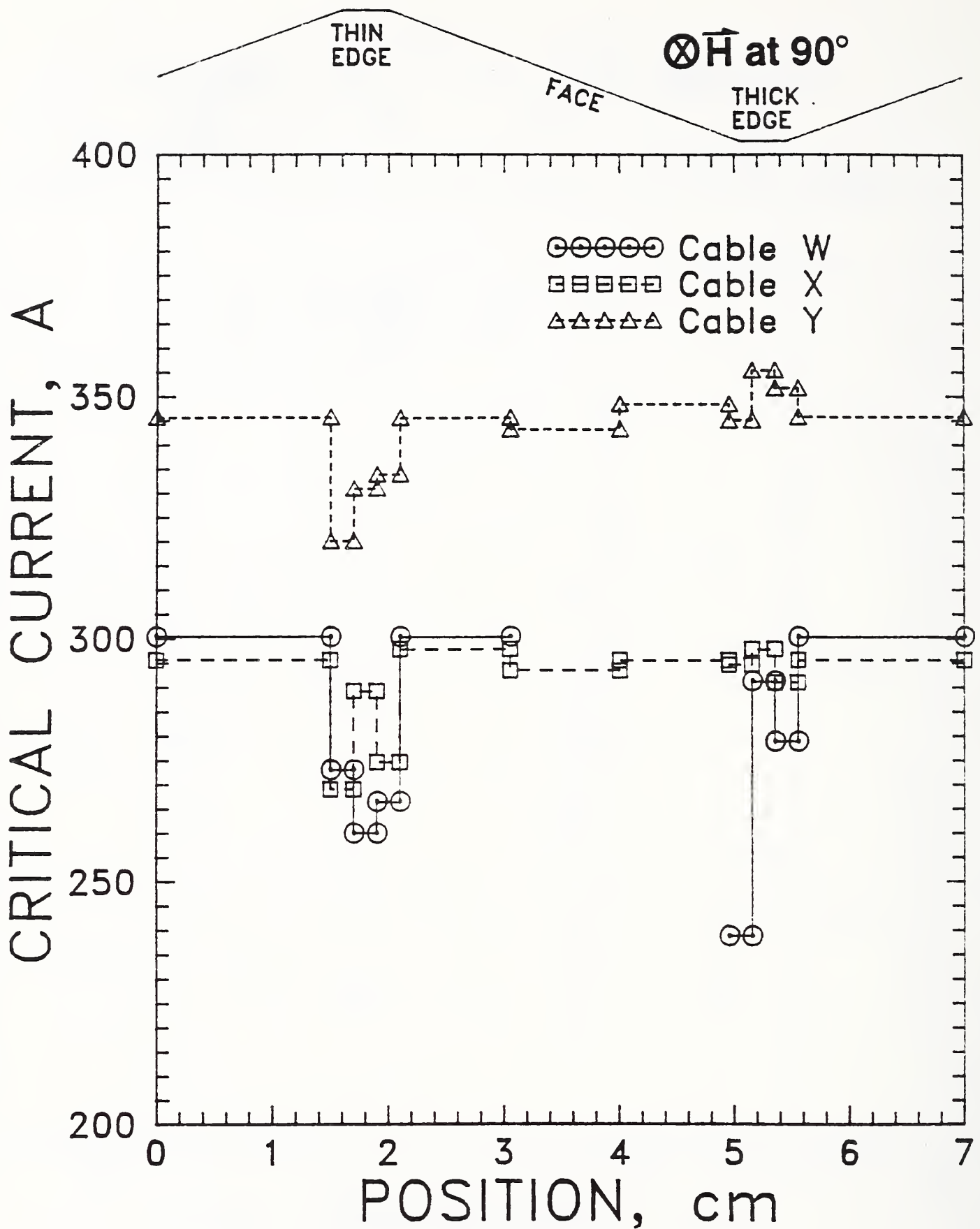
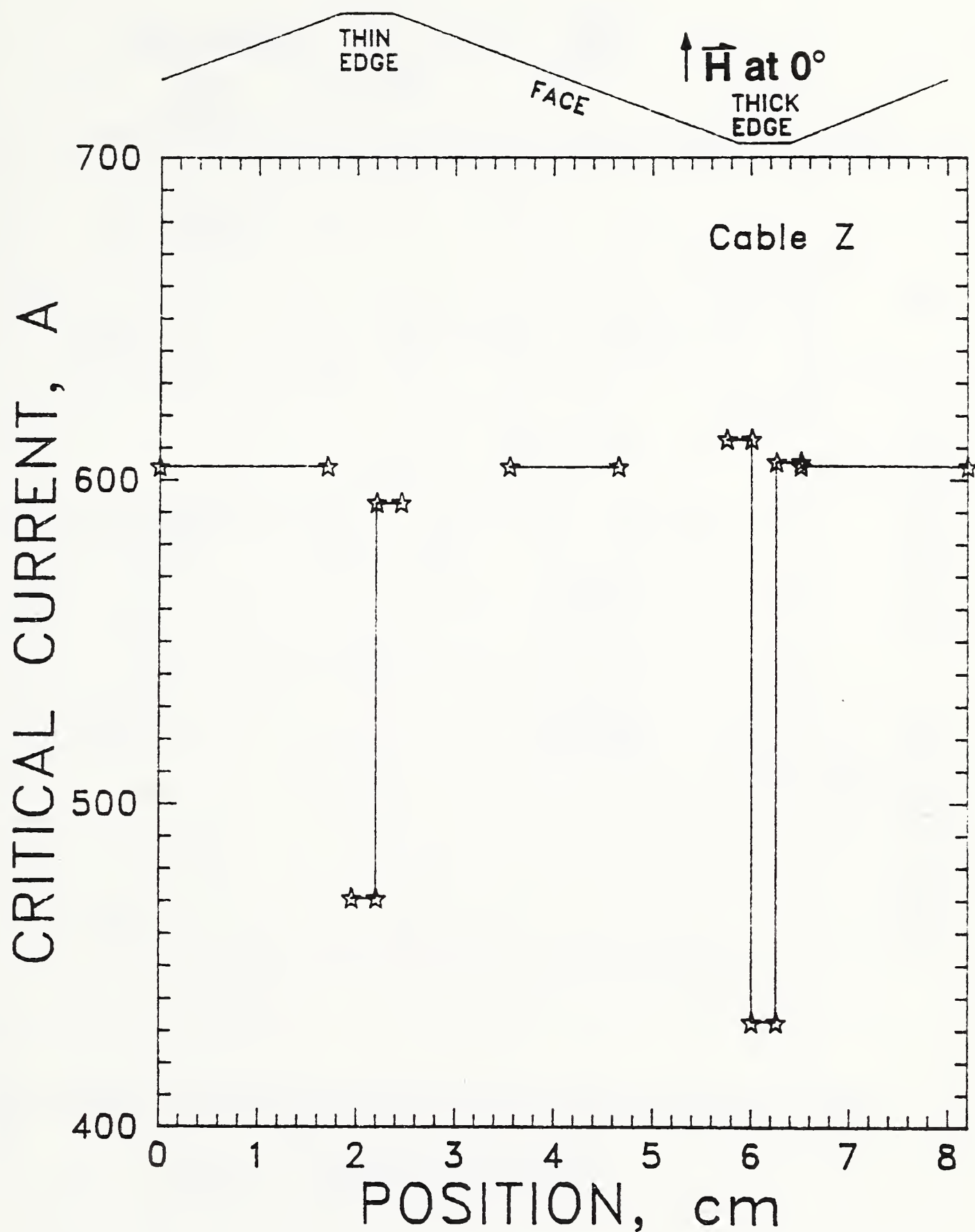Figure 28. Critical-current profiles at 5 T and an applied magnetic field angle of 90° for cables W, X, and Y at an electric field of 0.05 μV/cm.
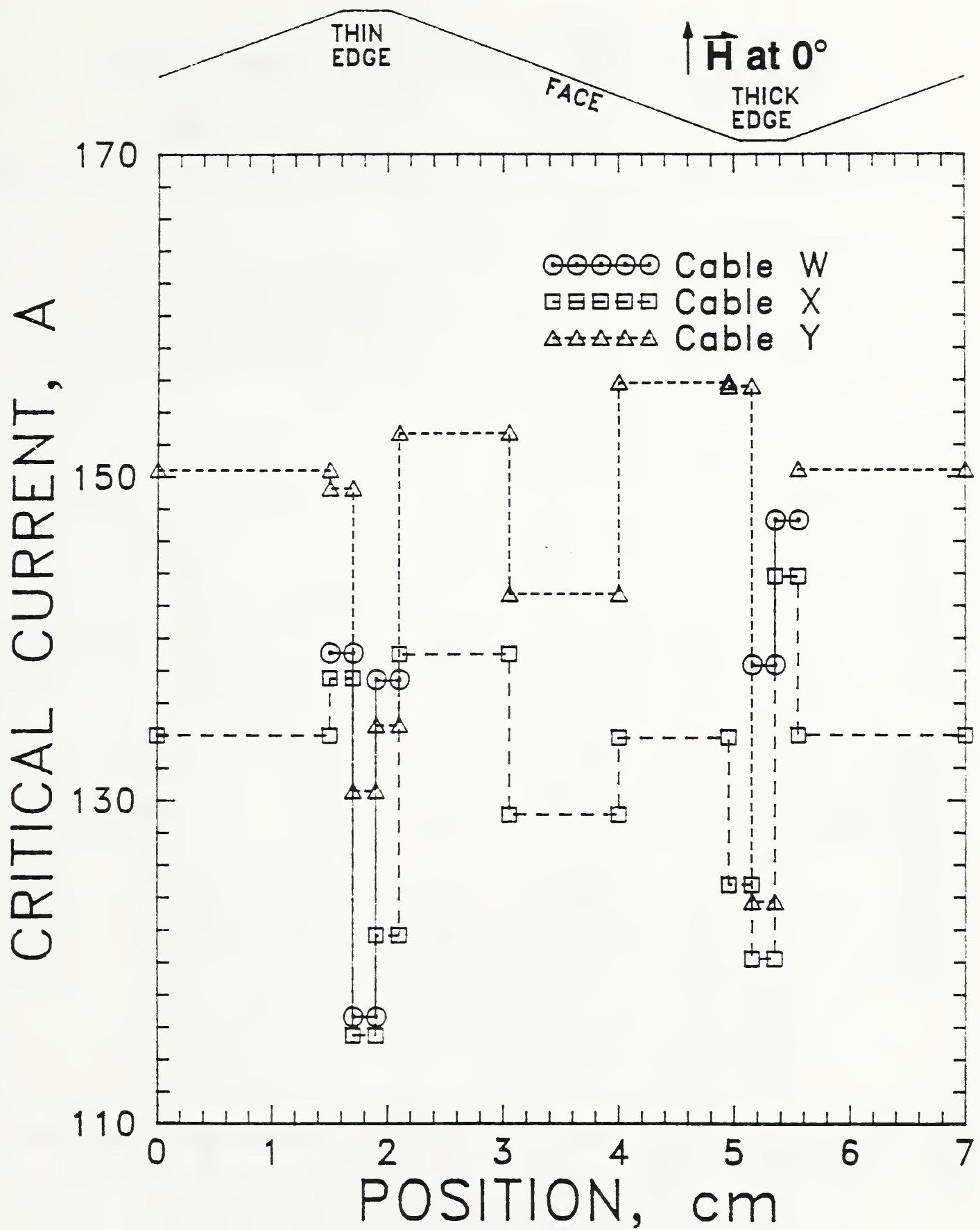
Figure 29. Critical-current profiles at 8 T and an applied magnetic field angle of 0° for cables W, X, and Y at an electric field of 0.05 μV/cm.

Figure 30. Critical-current profiles at 8 T and an applied magnetic field angle of 90° for cables W, X, and Y at an electric field of 0.05 μV/cm.
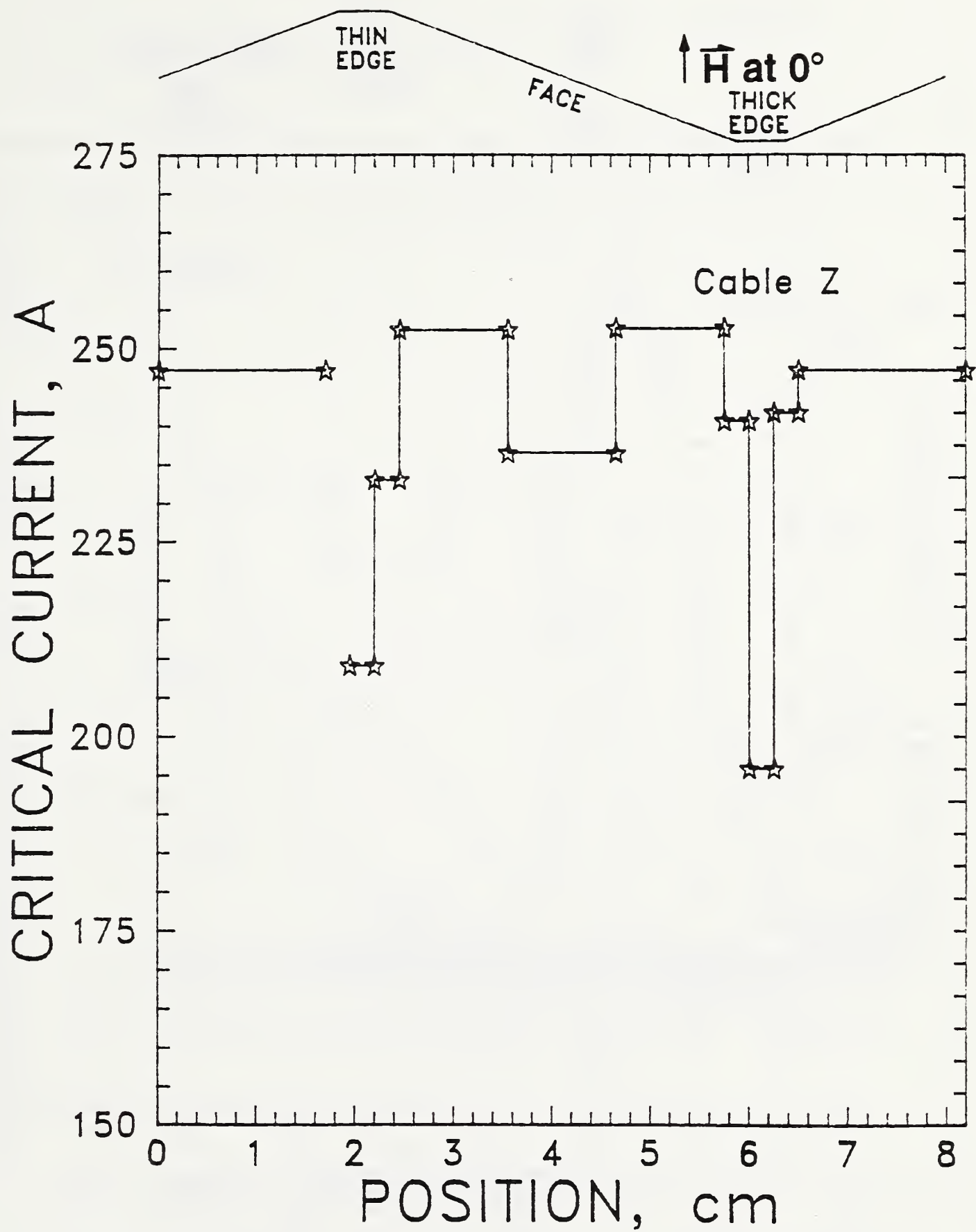
Figure 31.   Critical-current profile at 5 T and an applied magnetic field
angle of 0° for cable Z at an electric field of 0.05 µV/cm.

Figure 32. Critical-current profile at 5 T and an applied magnetic field
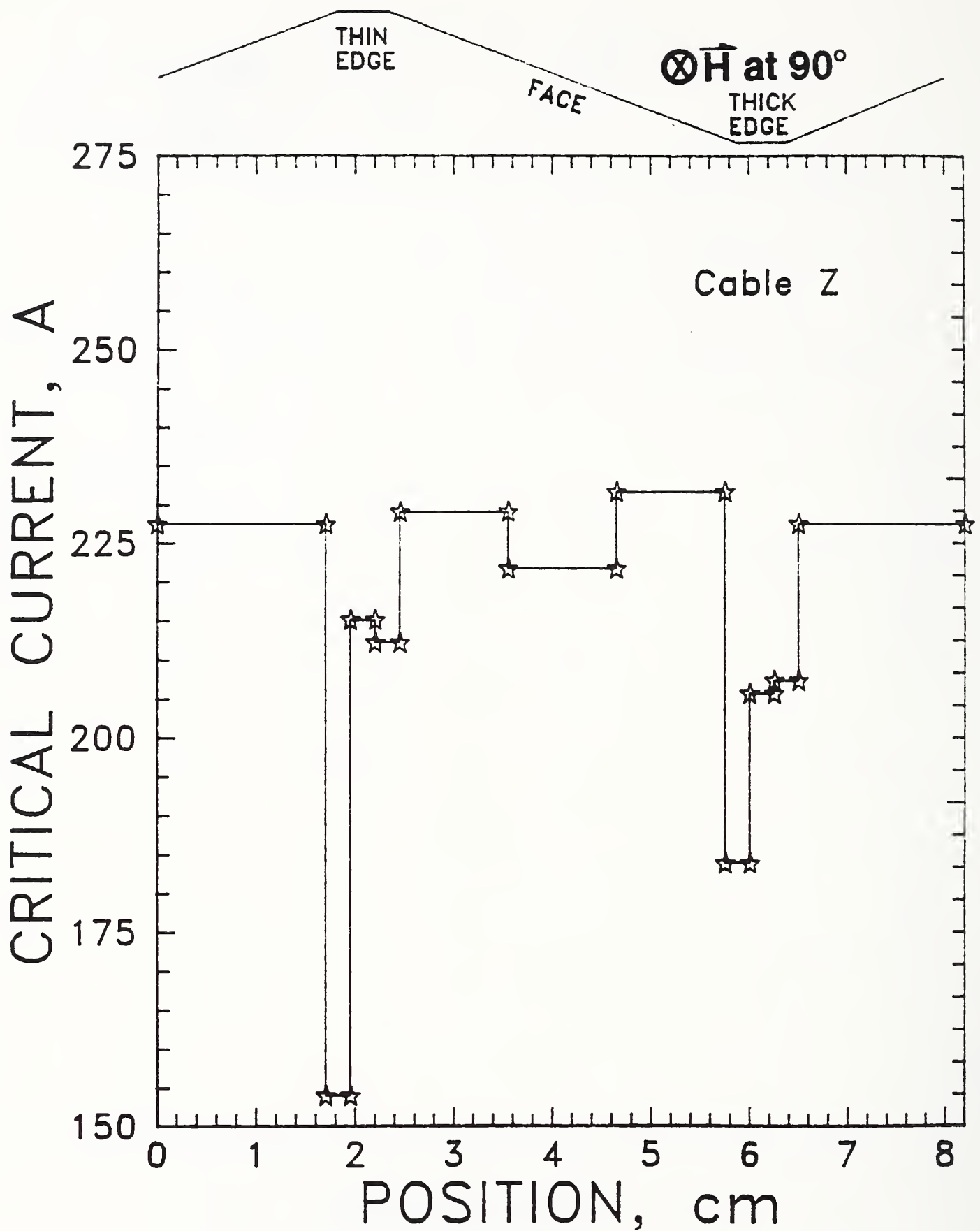angle of 90° for cable Z at an electric field of 0.05 μV/cm.

Figure 33. Critical-current profile at 8 T and an applied magnetic field angle of 0° for cable Z at an electric field of 0.05 μV/cm.

Figure 34. Critical-current profile at 8 T and an applied magnetic field angle of 90° for cable Z at an electric field of 0.05 μV/cm.
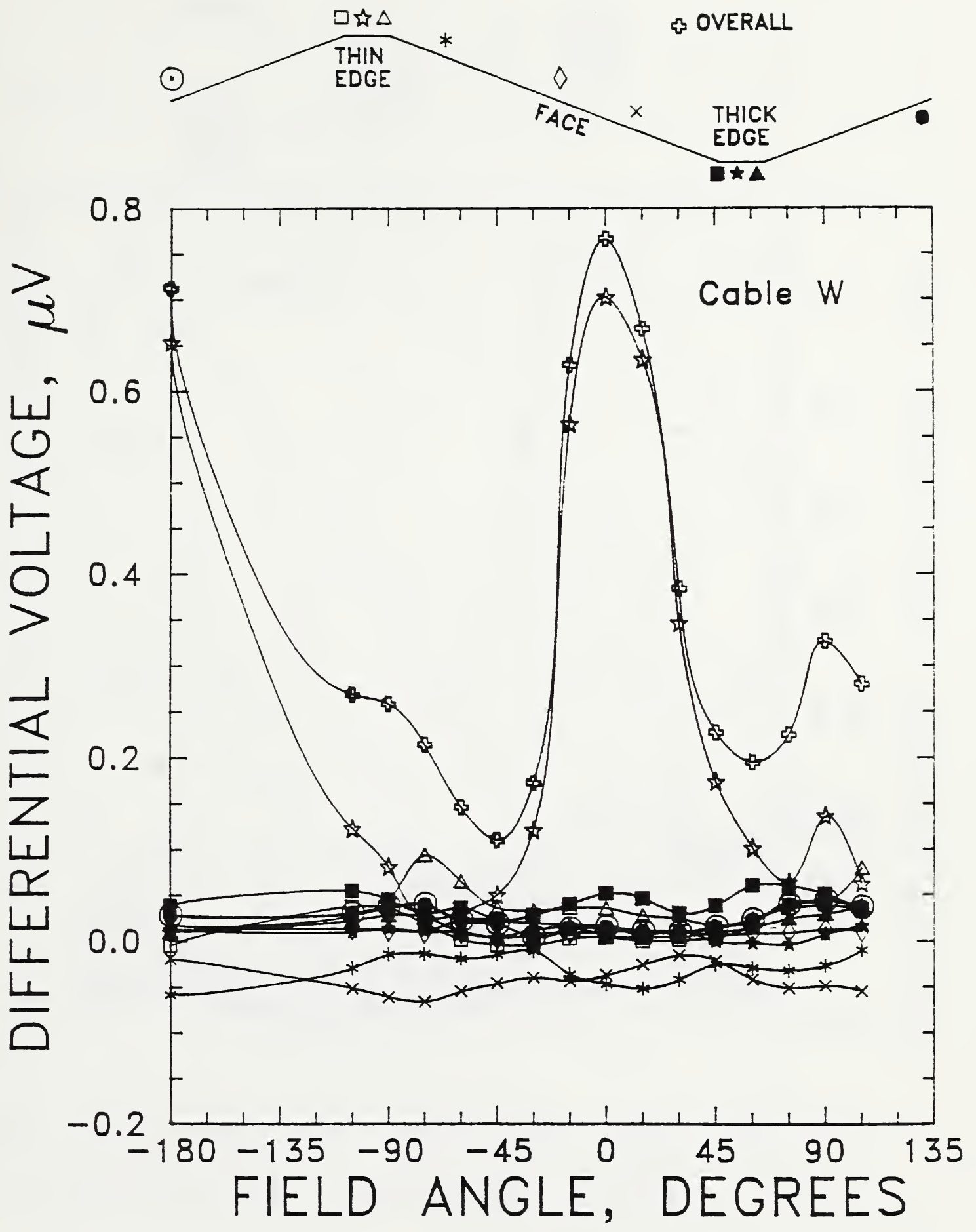
Figure 35. Differential-voltage plotted as a function of the applied field angle for all of cable W's taps at 5 T and a current of 285 A, which corresponds to an overall electric field of 0.1 μV/cm at 0°.
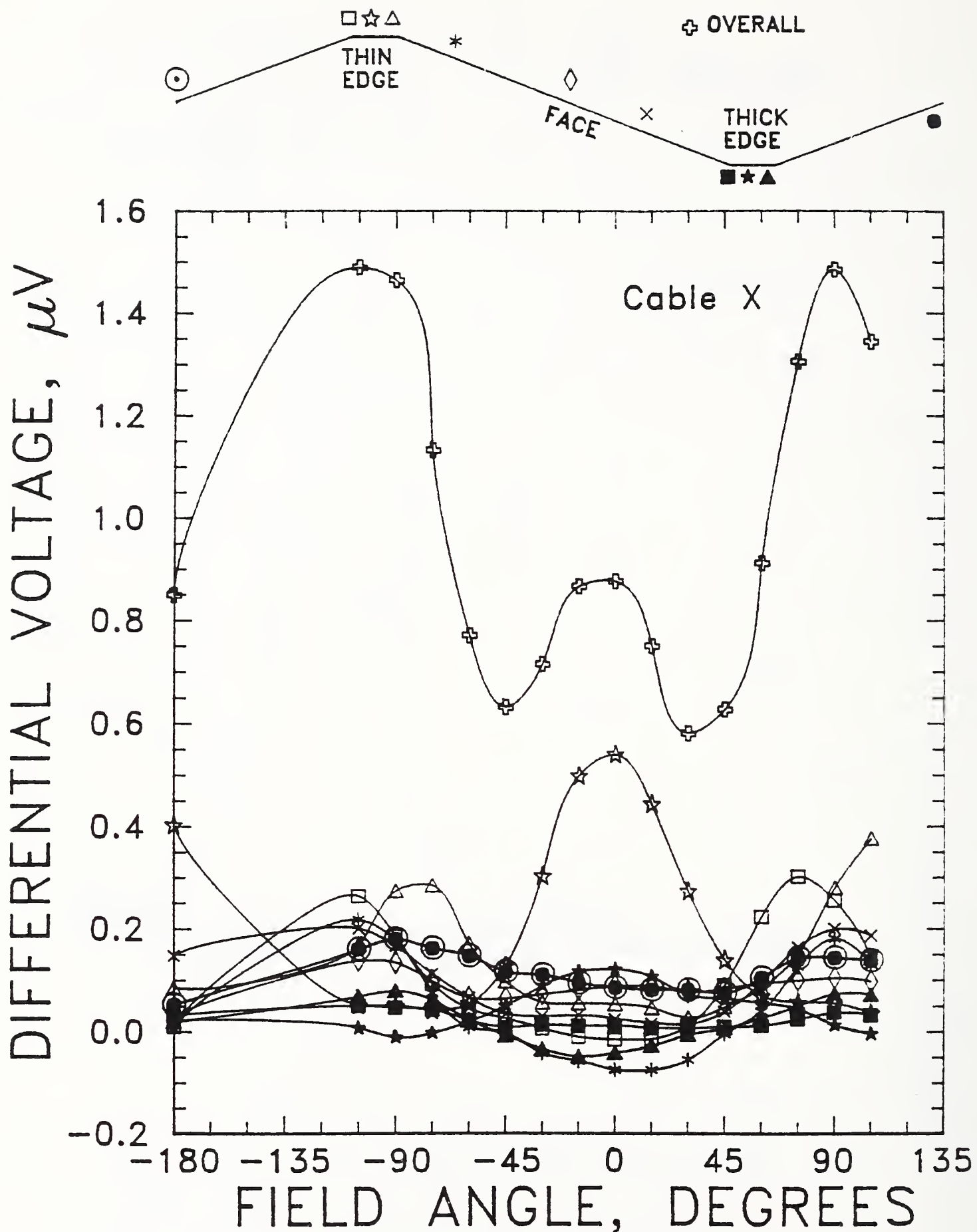
Figure 36. Differential-voltage plotted as a function of the applied field angle for all of cable X's taps at 5 T and a current of 307 A, which corresponds to an overall electric field of 0.1 μV/cm at 0°.

94

Figure 37. Differential-voltage plotted as a function of the applied field angle for all of cable Y's taps at 5 T and a current of 339 A, which corresponds to an overall electric field of 0.1 μV/cm at 0°.
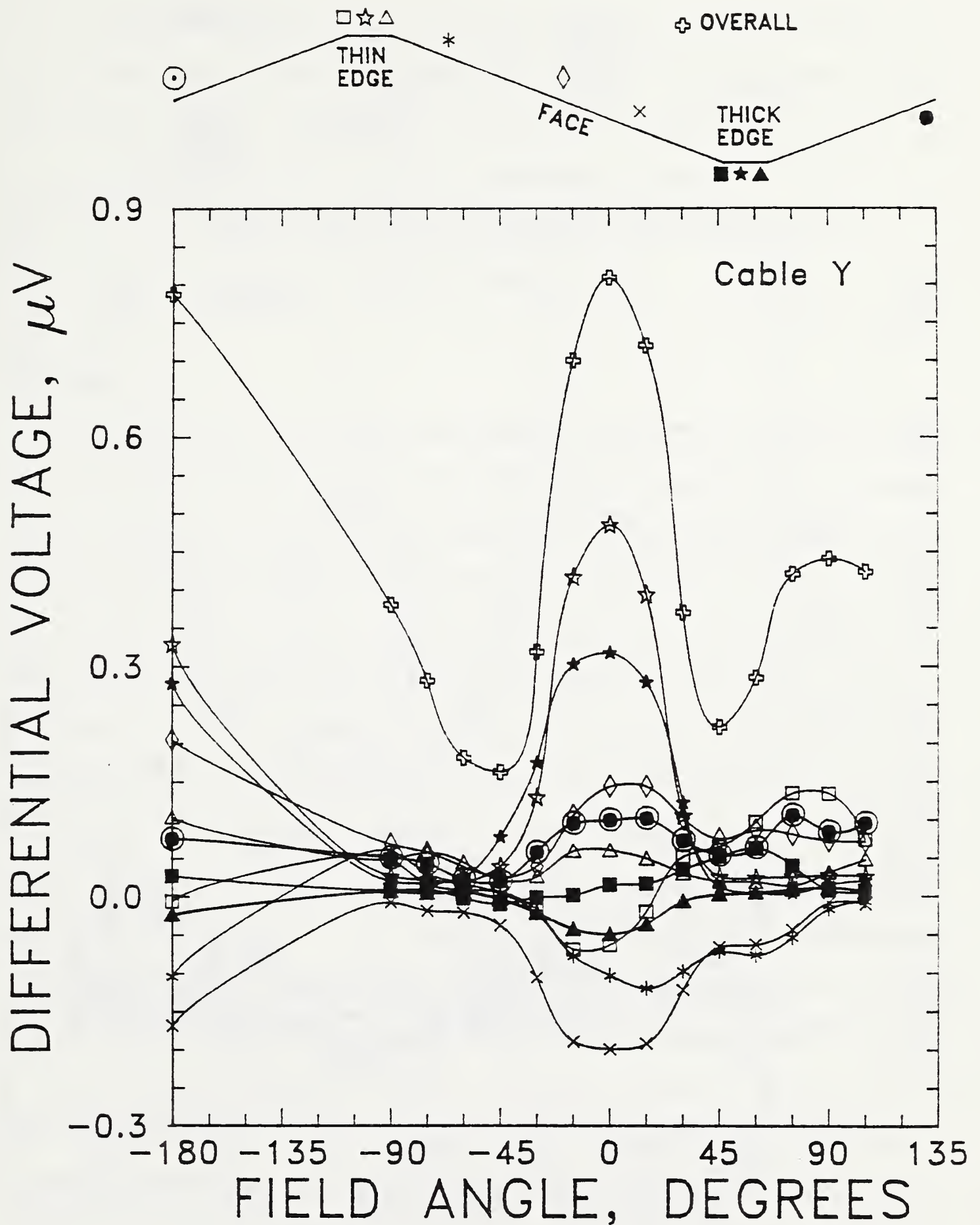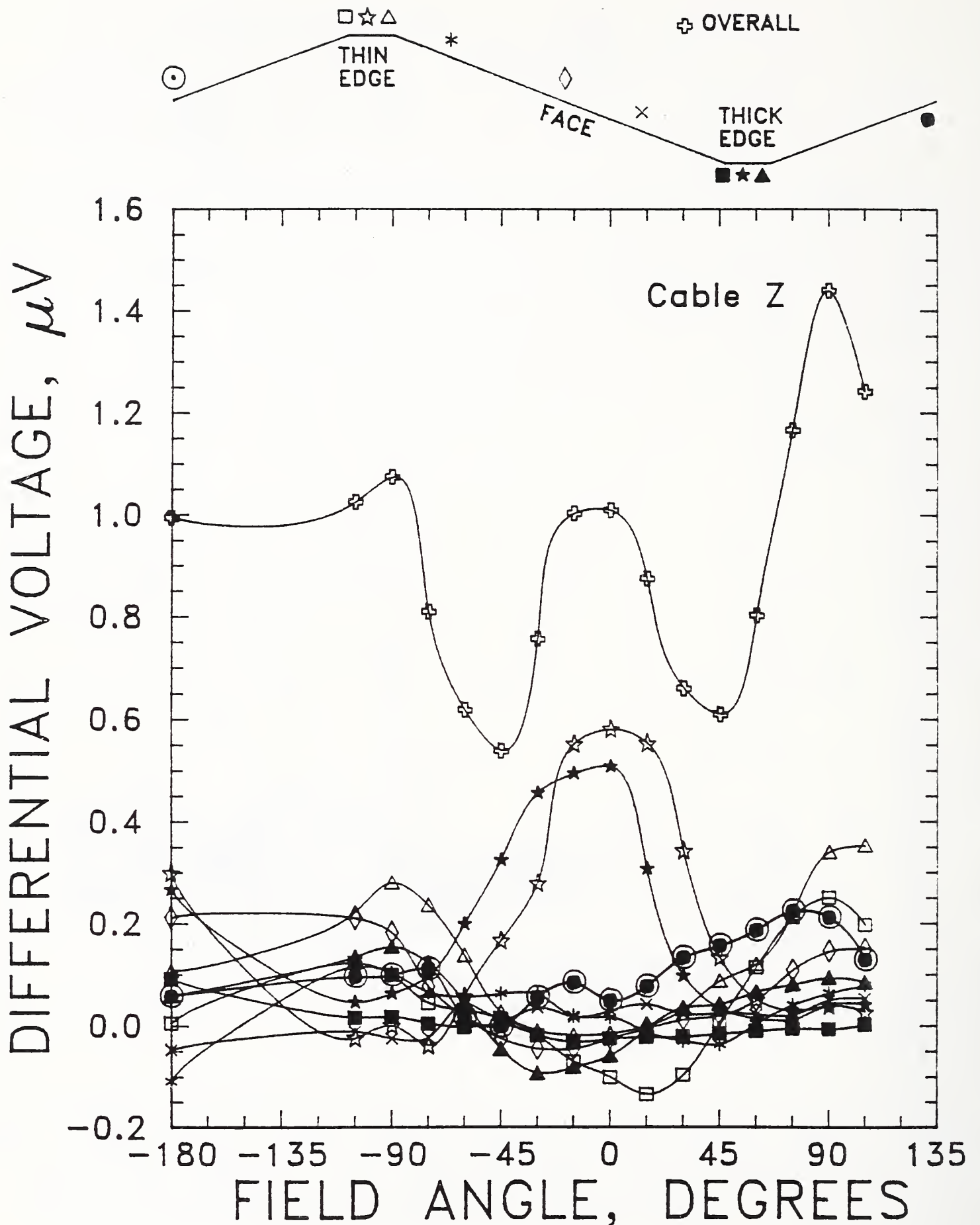
Figure 38. Differential-voltage plotted as a function of the applied field angle for all of cable Z's taps at 5 T and a current of 585 A, which corresponds to an overall electric field of 0.1 μV/cm at 0°.

THE EFFECT OF LOCAL AREA RATIO AND DIFFUSION-BARRIER MATERIAL
ON CRITICAL-CURRENT BEND DEGRADATION OF MULTIFILAMENTARY NbTi WIRES

J. W. Ekin, S. L. Bray, and N. F. Bergren

Electromagnetic Technology Division

National Institute of Standards and Technology

Boulder, Colorado 80303

Abstract

A systematic study of the effects of bending strain on the critical current of NbTi conductors has been performed. The critical-current (I_c) degradation caused by bending decreases with increasing magnetic field, suggesting that the source of degradation is not an intrinsic degradation of H_{c2}, as with the elastic axial-strain effect. The degradation of the I_c from bending strain is much greater at low electric field criteria E_c than at high (for example, 12% degradation at $E_c = 1$ μV/cm versus over 22 % at $E_c = 0.1$ μV/cm for a conductor-core-to-bend-diameter ratio of 0.43). The effect of bending on the critical current may be characterized simply by a decrease in the value of n toward the same low value for all conductors, typically 10 to 15. Here n represents the sharpness of the electric field-vs.-current relationship for the NbTi wire ($E \propto I^n$). The degradation of n suggests that irregularity of the filament's cross-sectional area, introduced by bending, may be the source of the I_c degradation. By testing a controlled series of similarly fabricated NbTi wires in which the local copper-to-superconductor area ratio (LAR) was systematically varied, we found that as the LAR increased from 0.4 to 0.7, the I_c bend degradation decreased by about 1/7. The increasing susceptibility of a superconductor to bend degradation with decreasing LAR thus places a

mechanical limit on the reduction of the LAR for controlling filament-sausaging effects. In another controlled series of NbTi wires in which the diffusion barrier material that surrounds each NbTi filament was systematically changed, the I_c bend degradation was less by about 1/4 to 1/5 for diffusion barriers made of vanadium, than for diffusion barriers made of niobium or niobium with a copper-nickel matrix.

Introduction

In the manufacture of superconducting cables for many magnet applications, compaction of the cable is necessary to achieve high filling factors and, consequently, high overall critical-current densities. However, compaction can also introduce strain concentrations in the cable strands; these may act as weak links in limiting the cable's critical current (I_c). In both rope cables and braided cables these strain concentrations occur periodically at the points where the cable strands cross one another. In flattened hollow cables (sometimes referred to as Rutherford cables) the strain is concentrated at the cable edges where each strand is subjected to severe bend strain (ϵ_b) and flattening.

Rutherford cables were developed for use in high-energy physics applications, the Fermilab Tevatron accelerator and the Superconducting Super Collider (SSC), for example. The Rutherford design allows for higher compaction then rope or braided cables with minimal strain concentration and strand deformation. Rutherford cables are typically rectangular in cross section, or trapezoidal in the case of a keystone cable, and each strand follows a path of full transposition about the cable's cross section. In

traversing from one cable face to the other, the strands must periodically

bend around the cable edges. The severity of the bend depends primarily on

the strand diameter, the cross-sectional dimensions of the cable, and its

pitch length. This paper presents measurements on a controlled series of NbTi

conductors to determine strand-design parameters that could be changed to

minimize the effect of bending on the critical current.

Localized I_c measurements of NbTi strands that were extracted from

prototype SSC cables indicate that significant I_c degradation can occur at the

edges of a Rutherford cable (See Ref 1-4). Microscopy studies of these

specimens have shown that the severity of filament damage and the resulting I_c

degradation varies among strands that are extracted from different cables. In

an extreme case, the damage is characterized by serrated yielding and breakage

of the NbTi filaments, which is accompanied by a reduction of more than 30% in

the measured I_c. This level of degradation is not typical of most cables, nor

is it typical of the specimens that were studied here. A reduction of less

than 20% in the I_c and virtually no visible filament damage is typical for

these specimens. The results presented here are a systematic study of the

effect of severe bending on the I_c of NbTi wires that are candidate strands

for SSC cables. The filament damage for the specimens tested in this study is

similar to what is commonly found in cable strands.

The measurements were conducted in two stages. First, the effect of

bending on I_c was measured in a number of different deformation geometries in

order to determine a standard test method that would yield a significant and

reproducible test of the ϵ_b effect. Once this test method was determined, it

was then used to evaluate a number of different conductors to obtain a relative measure of the effect of local area ratio diffusion-barrier material on critical-current bend degradation.

Rather than attempt to reproduce or even mimic the complex strand deformation found in Rutherford cables, a much simpler bend geometry was selected for the standard test method. There are several reasons for this approach. To begin, the cost and time required to manufacture Rutherford cables from the broad range of strand materials that were tested would be prohibitive. Furthermore, this approach would also introduce a great number of variables that would diminish the level of experimental control. Finally, the results of measurements using the simple bend geometry are more general and, therefore, they begin to address the issue of understanding the basic mechanism underlying bend degradation of I_c in NbTi superconductors.

Experimental Details

The detailed specifications of the superconducting samples are given in Table I. The conductors are similar in the sense that they are all prototype materials for SSC cables. These are round NbTi wires with a 0.648 mm diameter. The samples have different local copper-to-superconductor area ratios (LAR, the local area ratio of the cross-sectional area of the filament to that of the copper surrounding each filament going into the billet), different diffusion barrier materials locally surrounding each filament, and, in some cases, different filament configurations.

For this study, the background magnetic field is provided by a 9 T, 3.8 cm bore superconducting solenoid. A voltage-controlled 1000 A battery-powered constant-current supply is used as the sample-current source.

The basic testing geometry is that of a coil, shown in Fig. 1, where the diameter of the coil determines the severity of the bending strain, ϵ_b. The tested bend diameters range from a maximum of 31.7 mm (minimum ϵ_b) to a minimum of 0.38 mm (maximum ϵ_b). The I_c degradation for the 31.7 mm coil measurements is negligible, as substantiated by measuring the I_c of a straight sample. Consequently, the 31.7 mm coil measurements serve as a baseline for determining the bend degradation of the small diameter coil samples. The sample coils are wound on cylindrical measurement mandrels that are made from either nonmagnetic stainless steel (#316) or, in the cases of the 31.7 mm and the 3.18 mm mandrels, fiberglass-epoxy composite (G-10) tubes. A 1.28 mm stainless-steel mandrel (approximately twice the wire diameter) is the standard selected for the second stage of testing where various samples were tested at a common level of ϵ_b to determine whether there were conductor parameters that could be changed to maximize the bending strain tolerance. This standard bend diameter yields significant and repeatable degradations in the I_c of a given wire sample.

A significantly different coil geometry was also tried in an attempt to simulate the current-transfer effects that might occur in actual cable strands. In these tests the sample coil was wound around a thin rectangular plate with rounded edges. This resulted in a series of hairpin bends at the edges of the plate, separated by straight nondeformed sections of the wire

across the faces of the plate to simulate the deformation found in actual

Rutherford cable strands. This plate geometry was abandoned in favor of the

cylindrical geometry because it was difficult to control and it yielded

inconsistent bending at the plate edges.

To address the effect of the magnetic field generated by the sample coil

on the measured I_c, the I_c measurements were made with two different

orientations between the background field and the solenoidal sample field,

parallel and antiparallel. The reported I_c is the average of these two I_c

measurements. The difference between the two measurements was, in all cases,

less than 10% of their average value. The sample coils were bonded to the

mandrels with a light coating of varnish. The varnish coating is necessary

for containing the outward Lorentz force acting on the sample in the parallel

magnetic-field case.

With the exception of the 31.7 mm diameter mandrels, the sample mandrels

are held in the test fixture by the current contacts; see Fig. 1. Round

copper rod of 12.7 mm diameter is used for the current contacts. The ends of

the contacts that hold the mandrel in place are tapered to allow a gradual

transition from the smaller diameter of the sample mandrel to the larger

diameter of the current contact.

A pair of voltage-tap leads are soldered to the sample with a separation

of about 12 coil-turns. One of the voltage leads is counter-wound around the

sample coil to minimize induced voltage noise from variations in the magnetic

field. To measure the length of the sample that is spanned by the voltage

taps, first a known length of the sample wire is weighed using an analytic balance and then the actual sample coil is cut at its voltage taps and the resulting coil segment is weighed. The length of the instrumented portion of the sample coil is calculated from these weight values.

An automated, computer controlled, data acquisition and analysis system that was developed at NIST was used in this study. This system measures the voltage-current (V-I) relationship at discrete points along the V-I curve by holding the current constant, at preselected levels, and monitoring the resulting voltage. This technique allows averaging of the voltage data at each current level and, therefore, reduces the uncertainty associated with the voltage signal noise. Furthermore, the system uses an optimization process that automatically adjusts the locations of the discrete data points along the nonlinear V-I curve using voltage feedback. This process was designed to enhance the precision and accuracy of the I_c measurement while minimizing the data-acquisition time. The overall accuracy of the I_c measurement is within ±3%, the precision within ±0.5%.

Results

The effect of severe bending on the electrical characteristics of NbTi wires is shown in Figures 2 and 3 where the logarithm of the current (LOG I) is plotted against the logarithm of the electric field (LOG E) for several different bend diameters. The data presented in Fig. 2 is for sample A of Table 1 and the data in Fig. 3 is for sample B.

In Fig. 2 each curve is labeled with the sample coil's mandrel bend diameter with the exception of the curve that is labeled "STRAIGHT." A straight specimen of sample A was measured to determine what degradation, if any, is present in the 31.7 mm coil samples that serve as a baseline for comparison of the small-diameter-coil measurements. The close agreement between the "straight" curve and the "31.7 mm" curve, in their overlap region, indicates that the 31.7 mm coil data adequately represent the nondegraded state of the conductor.

Several effects of bending are evident in both of these plots. First, bend degradation is much more severe at low electric-field criteria (E_c) than at high E_c. In other words, the slope of the log E-log I curves vary with ϵ_b. For these logarithmic plots, the slope of the E-I curve is equal to the characteristic value n, where n is given by the approximate relationship between the electric field and the current $E \propto I^n$. Thus, the effect of bending is characterized by a decrease in the value of n.

Figures 2 and 3 show that the overall magnitude of the bend effect is nontrivial; it amounts, for example, to over 29% at $E_c = 1$ μV/cm for Sample A at the most severe ϵ_b (bend diameter = 0.38 mm) and increasing to 35% at $E_c =$ 0.1 μV/cm.

In Figures 4 and 5, the normalized critical currents of various specimens of samples A and B are plotted against the reciprocal of the normalized bend diameters of the specimens. The data shown in Fig. 4 were taken at 5 T while the data in Fig. 5 were taken at 7 T. The critical currents are normalized

with respect to the I_c of a 31.7 mm coil specimen of each of the sample wires, A and B. The samples have a core region formed by the NbTi filaments. The bend diameter of each specimen is normalized with respect to the diameter of this NbTi core region. This method of bend-diameter normalization is motivated by the fact that the level of axial strain applied to the NbTi filaments, as a result of bending the conductor, depends on the distance between the filaments and the wire's center, or its neutral axis. Consequently, the reciprocal of the normalized bend diameter is a measure of the maximum axial strain in the outermost NbTi filaments of a specimen. Both of these plots show a substantial degradation in the measured I_c with decreasing bend diameter. The degradation for sample A is significantly greater than for sample B at both 5 T and 7 T, and the degradation for both samples decreases as the magnetic field is increased.

In Fig. 6, n is plotted as a function of the normalized reciprocal of the bend diameter for Samples A and B at three magnetic fields. At the largest bend diameters, n is considerably higher for sample A; however, at the smallest bend diameters, n is reduced to a comparable level for both samples. The conspicuous feature of this plot is that both samples show a degradation in n that seems to approach a comparable limiting value. The degradation of n suggests that irregularity in the filament cross-sectional area introduced by bending may be the source of the I_c degradation.[7]

As part of the second stage of testing, the results of a systematic comparison of three samples (C, D, and E) are presented in Fig. 7. As indicated by the specifications of Table 1, these three conductors are

comparable to one another with one exception, their local area ratios. The

local area ratios are 0.70:1, 0.55:1, and 0.40:1, respectively, for samples C,

D, and E. The normalized I_c at the standard bend diameter (1.28 mm) is

plotted as a function of the applied magnetic field for each of the three

conductors. The data indicate a correlation between the LAR of the sample and

the level of I_c degradation that results from bending. As the LAR of these

conductors increases, their sensitivity to bending decreases. All of these

samples show a decreasing level of I_c degradation with increasing magnetic

field. This indicates that the source of the degradation is not an intrinsic

degradation of H_{c2}, as with the elastic strain effect.[5]

Figure 8 is a similar plot for three samples that have the same local

area ratios (0.55:1), but different diffusion barrier materials locally

surrounding each filament (samples F, G, and D). These data indicate that the

diffusion barrier material may be at least as important as the LAR in

determining the sensitivity of a conductor to ϵ_b. The vanadium diffusion-

barrier material correlated with the least I_c degradation from bending.

Differences in the shear strength of the filament-matrix-filament interface

for these different diffusion barrier materials may account for this

dependence.

Figure 9 is a plot of the normalized I_c at the standard bend diameter as

a function of the LAR at several magnetic fields. The difference between the

I_c degradation for the maximum and minimum local area ratios is about 1/7 the

total I_c degradation. Once again, the tendency for the degradation to

increase with decreasing LAR is evident.

Discussion

Two possible sources of the degradation in I_c are residual elastic strain in the NbTi filaments[3,5,6] and local reductions in their cross-sectional areas.[7-9] The data presented in Figs. 7, 8, and 9, where the I_c degradation decreases with increasing magnetic field, refute the former explanation of the I_c degradation. The elastic-strain effect results in an intrinsic degradation of H_{c2}, which, in turn, results in greatly increasing I_c degradation at fields approaching H_{c2}. This is just the opposite of what is observed. The data presented in Fig. 6, where the n value is shown to decrease with increasing ϵ_b, supports the latter explanation, that I_c and n degrade from an increase of the filaments' cross-sectional irregularity with bending.

The correlation between the LAR and I_c degradation that is shown in Fig. 9 indicates that in order to increase a conductor's tolerance to bending its LAR should be large. However, if the LAR is made to large, the increase in the wires' tolerance to bending may be negated by a decrease in its tolerance to drawing. A large LAR is conducive to the development of filament irregularities, or sausaging, during drawing, which, in turn, results in degradation of I_c and n. Consequently, the optimum LAR may be a compromise between the wire's tolerance to bending and its tolerance to drawing.

A large LAR apparently reduces the strain that is transmitted to the filaments as a result of bending. A speculative explanation for this behavior is that the low yield stress and resulting compliance of the copper matrix material, between the filaments, in a large LAR conductor facilitates independent motion of the filaments. Furthermore, different diffusion-barrier

materials may affect the filament-to-filament shear strength of the composite. This increased independence of motion may allow the filament bundle to flatten during bending, with the outer filaments moving toward the wire's neutral axis, thereby reducing the axial strain of individual filaments introduced by bending.

Conclusions

Severe bending strain can cause a large reduction in the I_c of multifilamentary NbTi wires. This degradation is not associated with an intrinsic H_{c2} effect, as evidenced by a reduction in degradation with increasing magnetic field. Bending strain results, however, in a significant degradation in the n values of these conductors. This suggests that the degradation is associated with filament cross-sectional area irregularity introduced by bending.

By using a series of samples where the local area ratio (LAR) of copper to superconductor is systematically varied, it is shown that the wire's tolerance to bending can be increased by increasing its LAR. However, conductors that have a large LAR are more susceptible to the development of filament irregularities, or sausaging, during drawing. A compromise between these two conflicting effects (sausaging and bending degradation) is required in order to optimize the I_c of these conductors.

For the conductors tested in this study, bending degradation of I_c is also correlated with the diffusion-barrier material locally surrounding each filament. The effect is at least as great as that of the LAR. Of the

diffusion-barrier materials that were tested, the vanadium barrier material resulted in less sensitivity to bending strain than niobium barriers or niobium barriers with a copper-nickel matrix.

This systematic study of bending degradation in NbTi superconductors has thus shown that the critical-current degradation from bending can be reduced through an appropriate choice of conductor-design factors, including local area ratio and diffusion-barrier material. The overriding factor in the cables' I_c degradation is nevertheless the care used in cabling; no amount of bending tolerance engineered into the conductor design can compensate for the damage that can be introduced during cabling.

Acknowledgements

References

1. J. W. Ekin, L. F. Goodrich, J. Moreland, E. S. Pittman, and A. F. Clark, "Electromechanical Properties of Superconductors for High Energy Physics Applications," National Bureau of Standards Internal Report No. NBSIR 86-3061, December 1986.

2. L. F. Goodrich, E. S. Pittman, J. W. Ekin, and R. M. Scanlan, "Studies of NbTi Strands Extracted from Coreless Rutherford Cables," IEEE Trans. Magn., MAG-23, 1642 (1987).

3. J. W. Ekin, "Relationships Between Critical Current and Stress in NbTi," IEEE Trans. Magn. MAG-23, 1634 (1987).

4. L. F. Goodrich and S. L. Bray, "Current Capacity Degradation in Superconducting Cable Strands," IEEE Trans. Magn. (1989), to be published.

5. J. W. Ekin, F. R. Fickett, and A. F. Clark, "Effect of Stress on the Critical Current of NbTi Multifilamentary Composite Wire," Proc. Int'l. Cryog. Mat. Conf. (August 1975), Adv. Cryo. Eng. 22, 449 (1977).

6. S. L. Bray and J. W. Ekin, "Effect of Room Temperature Stress on the Critical Current of NbTi," to be published in Jour. Appl. Phys. (1989).

7. J. W. Ekin, Quarterly Progress Report No. SR-724-13-82, National Bureau of Standards (1982) and Quarterly Progress Report No. SR-724-26-82, National Bureau of Standards (1982). J. W. Ekin, "Irregularity in Nb-Ti Filament Area and Electric Field versus Current Characteristics," Cryogenics 27, 603 (1987).

8. M. Garber, M. Suenaga, W. B. Sampson, and R. L. Sabatini, Adv. Cryog. Eng. 32, 707 (1986).

15

9. W. H. Warner and D. C. Larbalestier, <u>Proc. Int'l. Symp. on Flux Pinning and Electromagnetic Properties in Superconductors</u> (Ed. T. Matsushita, K. Yamafuji, and F. Irie) p. 156, Matsukuma Press, Japan (1986).

Table 1. Sample Characteristics

Samples ->	A	B	C	D	E	F	G
Strand diameter (mm)	0.648	0.648	0.648	0.648	0.648	0.648	0.648
Filament diameter (μm)	16	5	6	6	6	6	6
Number of filaments	648	6006	4000	4000	4000	4000	4000
Cu-to-superconductor volume ratio	1.77	1.84	1.67	1.70	1.63	1.63	CuNi matrix
Cu-to-superconductor local area ratio	0.52	0.65	0.70	0.55	0.40	0.55	0.55
Twist pitch (mm)	12.7	12.7	12.7	12.7	12.7	12.7	12.7
Superconductor area (mm²)	0.119	0.125	0.124	0.122	0.125	0.125	–
Diffusion barrier	none	Nb	Nb	Nb	Nb	V	Nb
Matrix	copper	copper	copper	copper	copper	copper	CuNi
Billet	10" sgl. stack	10" dbl. stack	8" sgl. stack	8" sgl. stack	8" sgl. stack	8" sgl. stack	8" sgl. stack
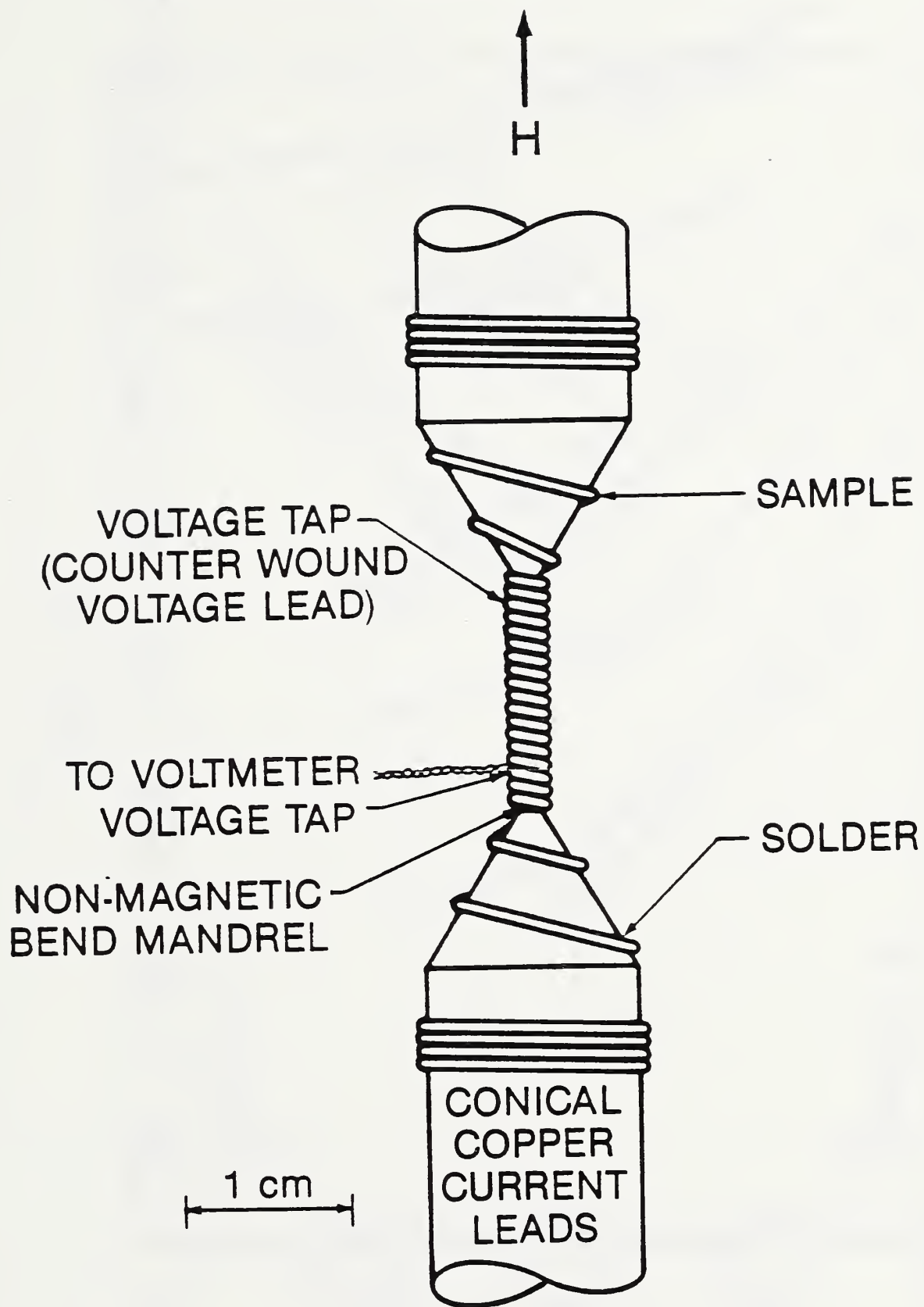
Fig. 1.   Long bend test coil configuration.
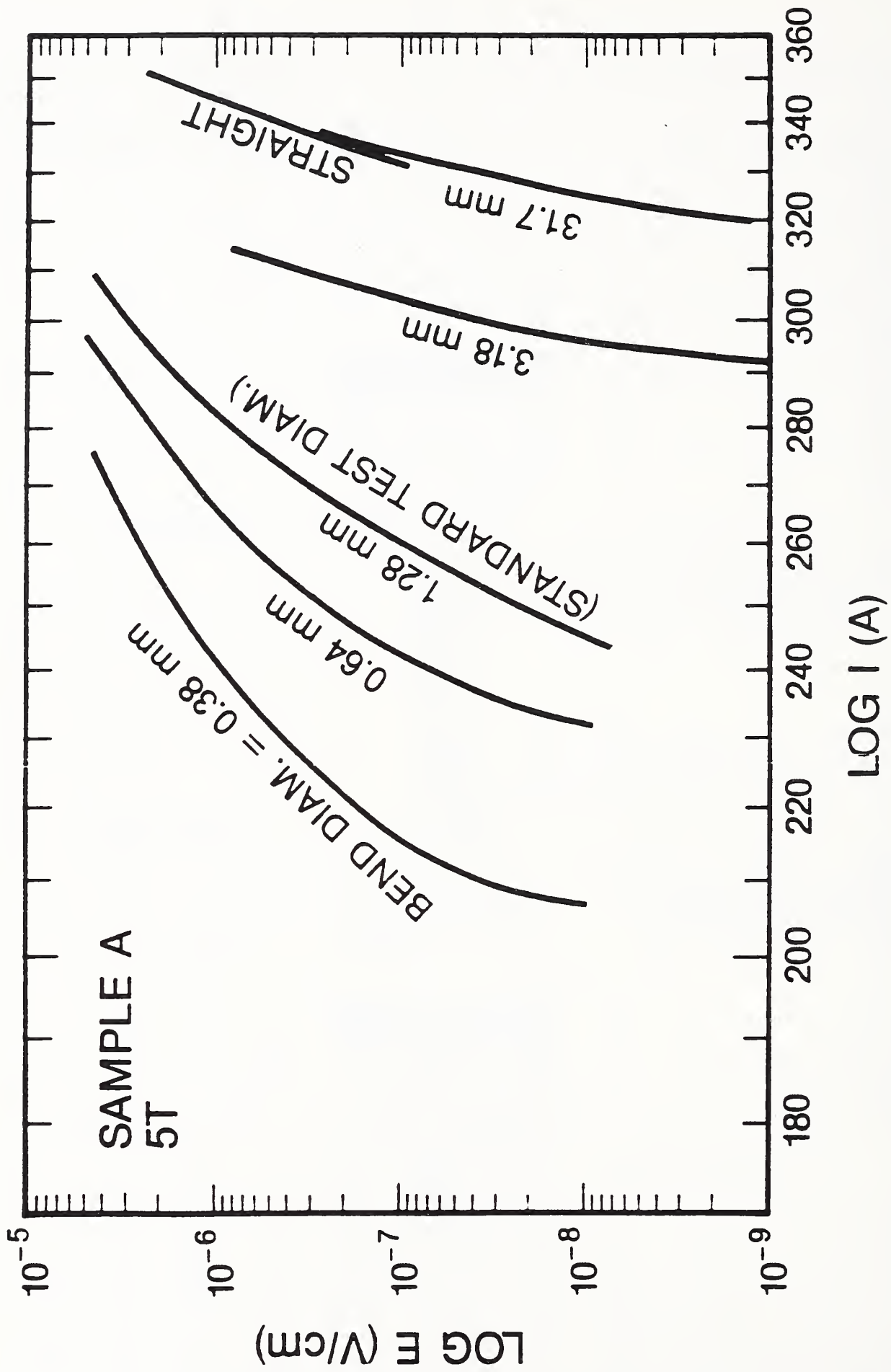
Fig. 2. Logarithmic plot of the electric field (E)-vs.-current (I) characteristic of different coils of Sample A bent around mandrels with progressively smaller diameters, showing the large degradation of n at severe bending strain.
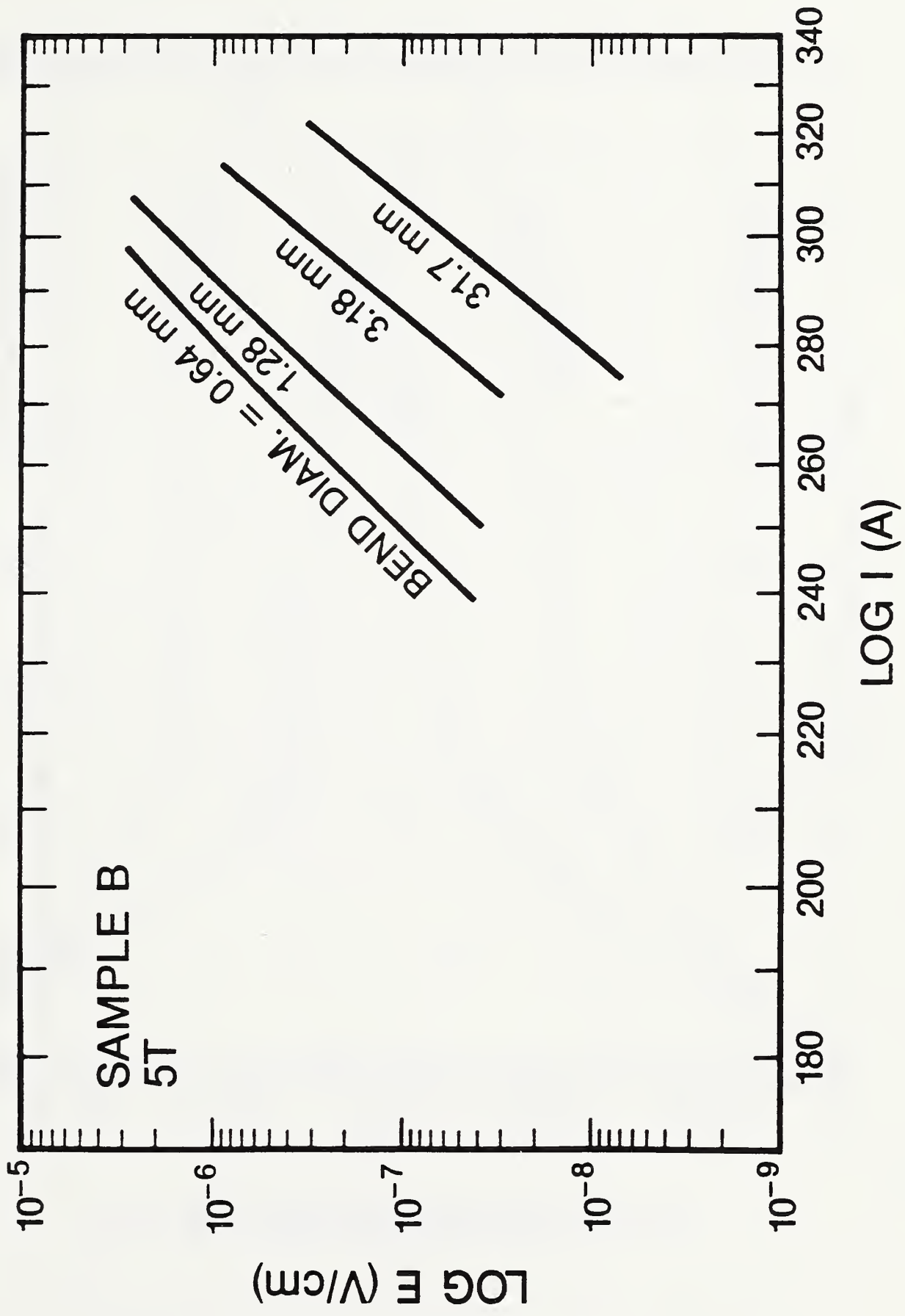
114

Fig. 3. Log E-vs.-log I characteristic of different coils of Sample B bent around mandrels with progressively smaller diameters, showing less degradation of n in a wire where n is initially low.
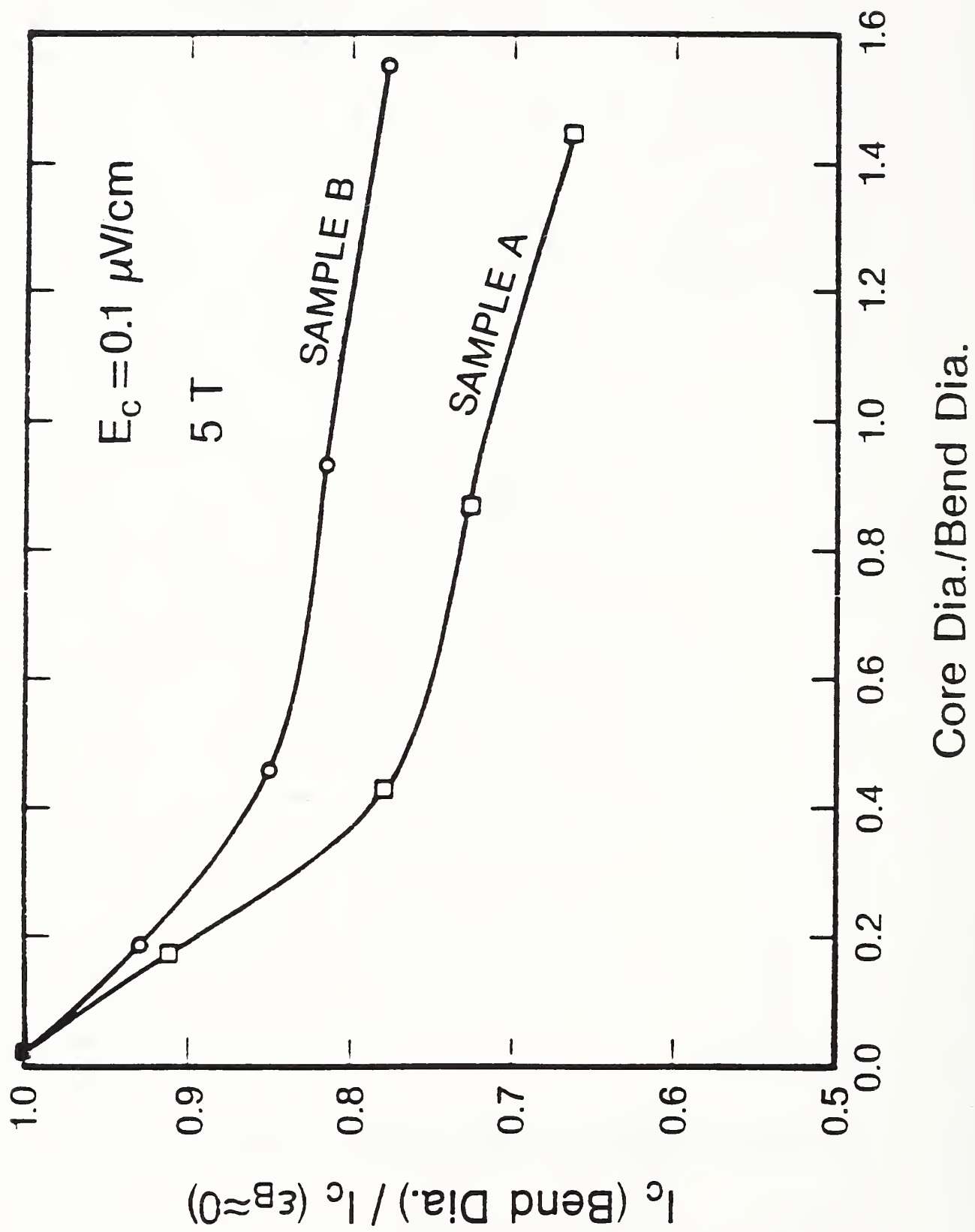
Fig. 4. Relative degradation of I_c of Samples A and B as a function of bending strain at 5 T.
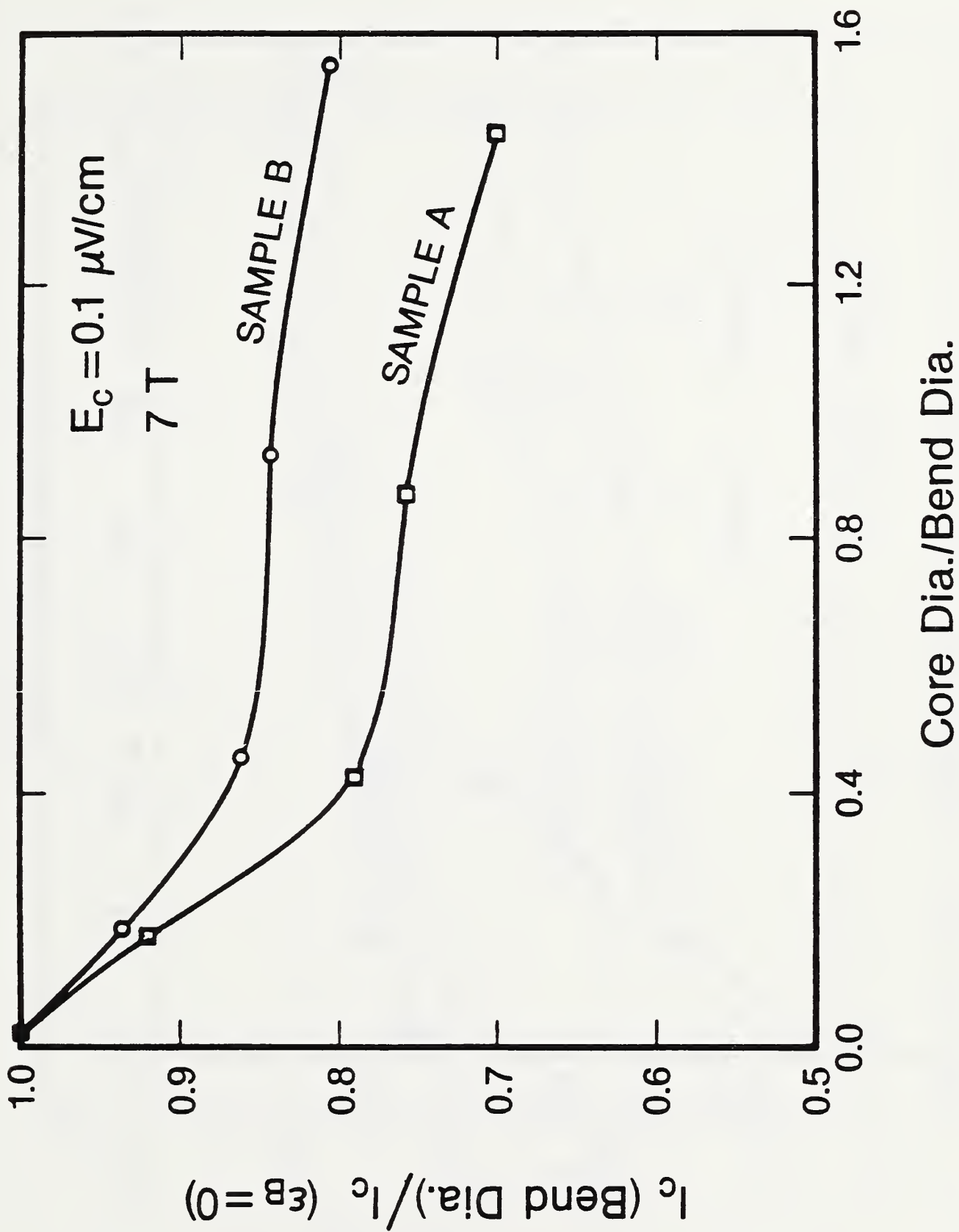
Fig. 5.   Relative degradation of I_c of Samples A and B at 7 T, showing a
decrease in degradation at higher magnetic field (compare with
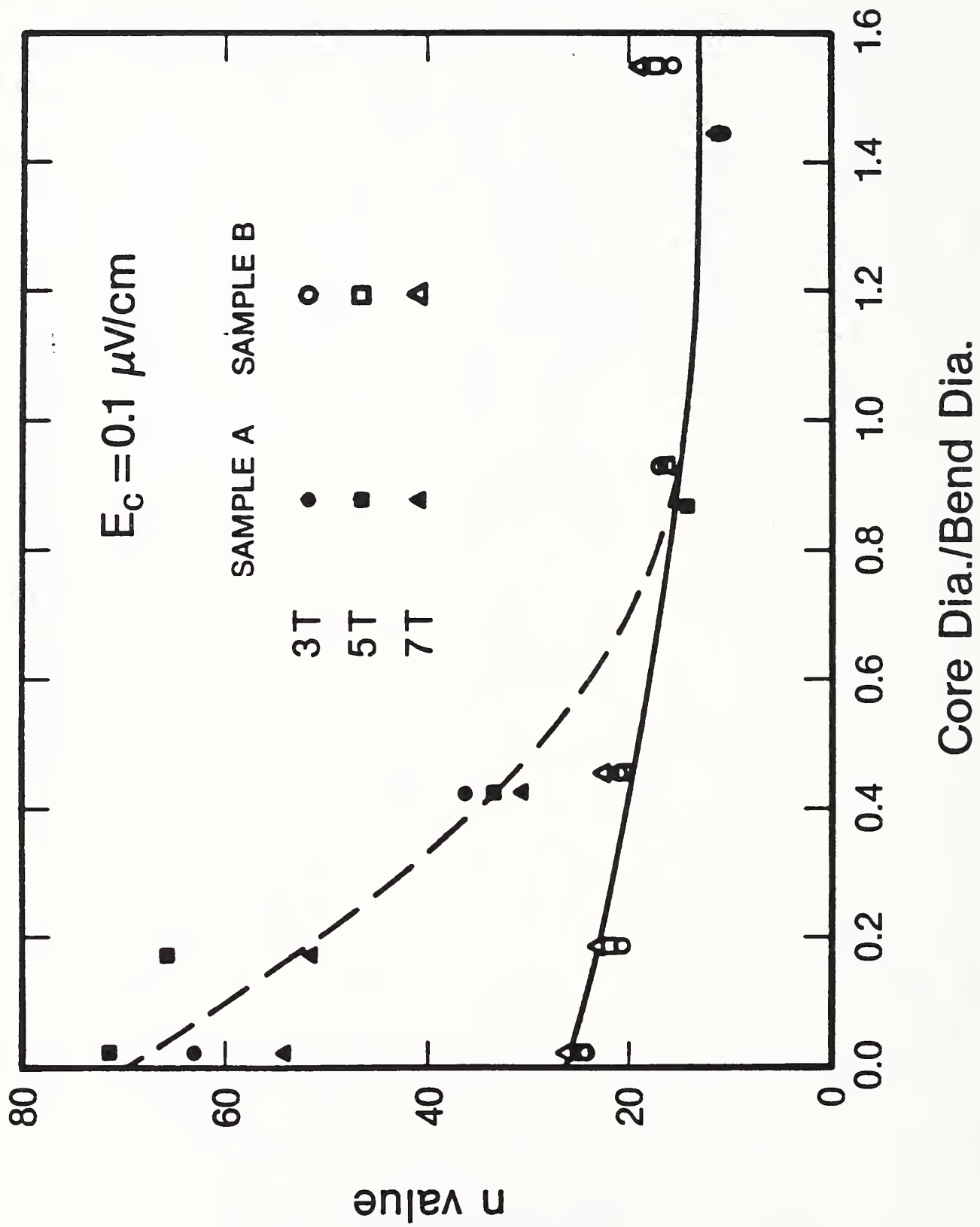Fig. 4).

Fig. 6.   Bending strain degradation of n of Samples A and B, showing the approach to the same degraded value of n at severe bending strain.
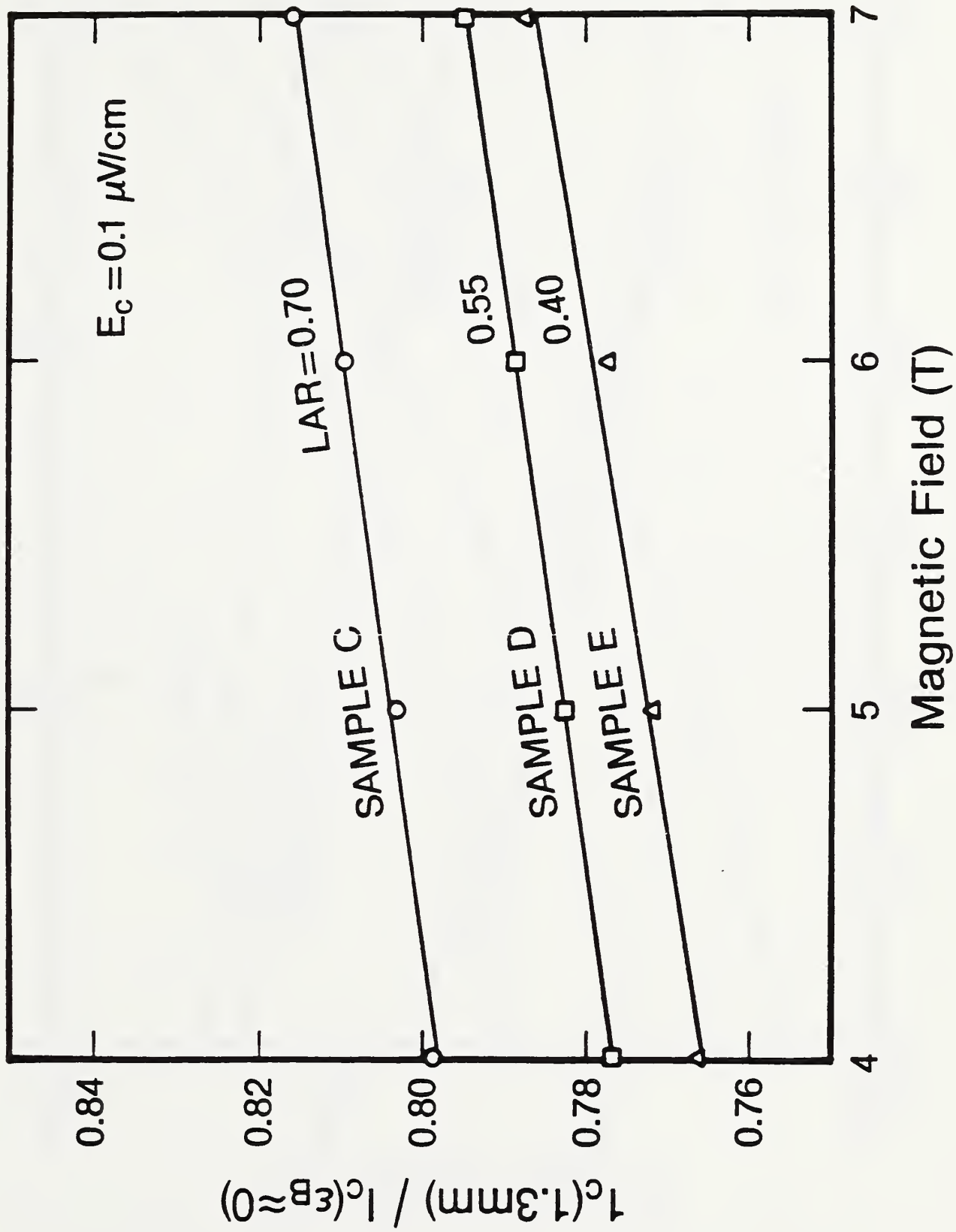
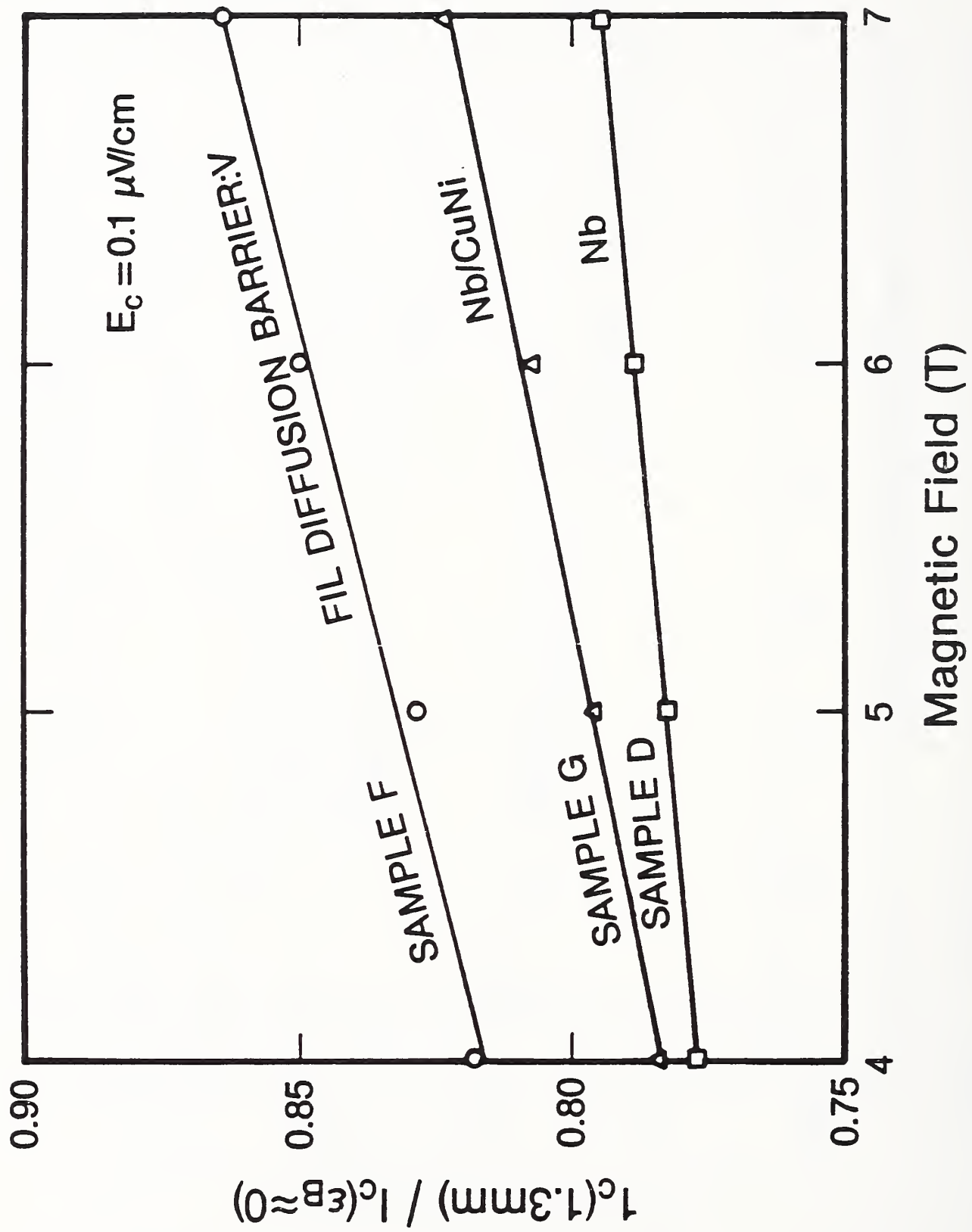Fig. 7. Effect of local area ratio (LAR) on bending degradation of I_c.

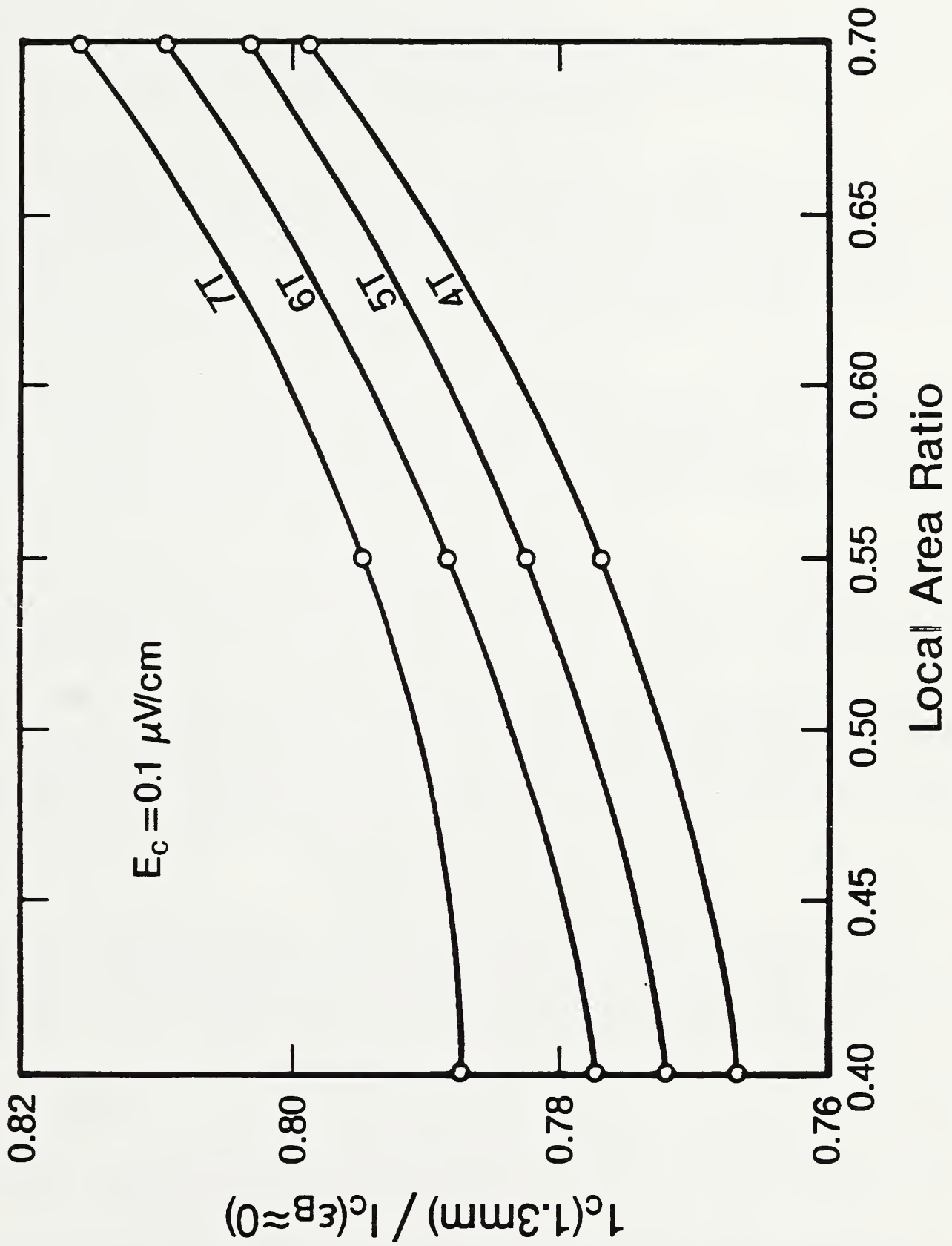Fig. 8. Effect of diffusion-barrier material on bending degradation of I_c.

Fig. 9. Dependence of bending degradation of I_c on local area ratio, at constant magnetic field.

121

Measurement of Saturation Magnetization and Intrinsic Coercivity of High-Permeability Steel for the SSC

R. B. Goldfarb
Electromagnetic Technology Division
National Institute of Standards and Technology
Boulder, Colorado 80303

Accelerators such as the proposed Superconducting Super Collider (SSC) and the Tevatron at Fermilab use high-permeability steel for the return flux path of their superconducting magnets. It is the same type of steel that is commonly used for electrical transformers. In addition to high permeability (μ), desirable magnetic properties include large saturation magnetization (M_s) and small intrinsic coercivity (H_c).

It is useful to define M_s and H_c with reference to an idealized curve of magnetization (M) vs. magnetic field strength (H). Figure 1 represents a hysteresis loop for a sample with zero demagnetization factor, such as a long, thin needle. The parameters are indicated. If required, magnetic flux density (B) may be derived as

$$B = \mu_0(H+M) \qquad (1)$$

(SI units, where μ_0 is the permeability of free space) and plotted as a function of H [1,2].

In actual measurements with instruments such as a vibrating-sample magnetometer, a sample geometry with finite demagnetization factor is used [3,4]. Magnetic field (H) in the above equations and plot refers to the <u>internal</u> field (H_{int}), equal to the applied field (H_{ext}) corrected for the proper geometric demagnetization factor (D) [5],

$$H_{int} = H_{ext} - DM. \qquad (2)$$

As a result of a sample's demagnetization factor, its plot of M vs. H_{ext} is "sheared" along the H-axis [6]. Generally, to deduce parameters characteristic of the <u>material</u> of which the sample is made, the data have to be replotted as M vs. H_{int}. Several points should be noted, however.

1. H_c is independent of demagnetization factor; when M is zero, H_{int} is identical to H_{ext}.

2. M_s is independent of demagnetization factor. At high fields, DM is only a small correction to H_{ext} in Eq. 2.

3. It is difficult to extract the exact value of μ from magnetometer data when μ is large. The most successful methods use samples with exactly known demagnetization factors, such as spheres, or with zero demagnetization factors, such as toroids with azimuthal fields [7].

In this brief note, I report on the measurement of M_s and H_c for several steels suitable for accelerator applications. We used a conventional vibrating-sample magnetometer [8]. A high-field superconducting solenoid was used for the M_s determination and a low-field copper-coil Helmholtz transverse pair was used for the H_c measurements.

The samples consisted of rectangular prisms, about 1.5 mm thick, 6 mm wide, and 12 mm long. All magnetic measurements were made with the field in the longest axis. This minimized the demagnetization factor. Brief sample descriptions are given in Table I.

Magnetization was measured in liquid helium (4 K) for maximum applied fields of ±5.6 MA/m (±70 kOe, or ±7 T in free space). There were no significant differences between the samples; they all saturated at $M_s \simeq 1.75$ MA/m (1750 emu/cm^3, or $4\pi M_s \simeq 22$ kG). A typical hysteresis loop is shown in Fig. 2. The field was cycled from zero to +7 T to -7 T to +7 T. There was no measurable hysteresis on this coarse scale.

Intrinsic coercivity was determined from the field required for zero magnetization. Measurements were made at room temperature (296 K) and in liquid nitrogen (76 K). Maximum applied fields were ±800 kA/m (±10 Oe, or ±1 mT in free space). The samples were initially demagnetized [9].

The field was increased to 1 mT while magnetization was recorded. At 1 mT, the samples were briefly exposed to field of 0.1 T in an attempt to approach saturation. (A larger field would have been preferable, but was not available. Generally, H_c is a weak function of the maximum applied field.) Thereupon data were recorded as the field was reduced to -1 mT. At -1 mT, the sample was exposed to a field of -0.1 T. The cycle continued to 1 mT. A typical trace is shown in Fig. 3. Note that the loop is sheared in the sense discussed above.

Table II summarizes the results for the five samples. Values of H_c ranged from 110 A/m (1.4 Oe) for cold-rolled samples to 170 A/m (2.1 Oe) for hot-rolled samples. The results were independent of whether the field was parallel or perpendicular to the rolling direction. Liquid-nitrogen H_c was slightly larger than room-temperature H_c. At liquid-helium temperature, H_c is expected to be slightly higher still.

In summary, there appear to be no significant differences in these steel samples with regard to saturation magnetization and intrinsic coercivity.

REFERENCES

[1] "Intrinsic coercivity" is the H at which M goes to zero. The terms "coercive force" and "coercivity" refer to the value of H at which B goes to zero. The symbol H_c is commonly used for both meanings.

[2] Permeability μ is defined as dB/dH. A related quantity, susceptibility χ, is dM/dH. In SI units, $\mu = 1+\chi$.

[3] R. M. Bozorth and D. M. Chapin, J. Appl. Phys. <u>13</u>, 320 (1942).

[4] T. L. Templeton and A. S. Arrott, IEEE Trans. Magn. <u>MAG-23</u>, 2650 (1987).

[5] R. B. Goldfarb, Cryogenics <u>27</u>, 621 (1986).

[6] If a sample has a large M but unknown D, the value of D can be estimated as that required to "unshear" the hysteresis loop, using Eq. 2. For example, see: J. C. Mallinson, <u>The Foundations of Magnetic Recording</u>, (Academic Press, San Diego, 1987) p.23.

[7] R. B. Goldfarb and H. E. Bussey, Rev. Sci. Instrum. <u>58</u>, 624 (1987).

[8] S. Foner, Rev. Sci. Instrum. <u>30</u>, 548 (1959).

[9] The ac demagnetization process consists of exposing the sample to an alternating field that is decreasing in amplitude. In practice, a simple wire-wound solenoid is energized with a variable transformer ("Variac") at line frequency. The purpose is to remove any remanent magnetization in the sample.

Table I. Samples for M_s and H_c measurement.

Sample	Description
A	Inland, plate steel, hot rolled, ultra-low carbon
B	Inland, cold rolled, H parallel to rolling direction
C	Inland, cold rolled, H perpendicular to rolling direction
D	Armco, cold rolled, ZnP coating, H parallel to rolling direction
E	Armco, cold rolled, ZnP coating, H perpendicular to rolling direction

Table II. Intrinsic coercivity at 296 and 76 K.

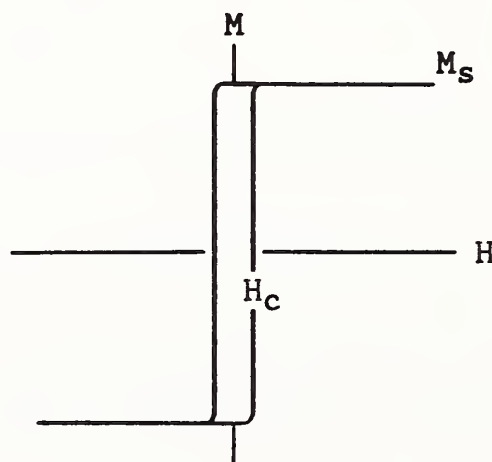| Sample	296 K		76 K	
	H_c (A/m)	H_c (Oe)	H_c (A/m)	H_c (Oe)
A	160	2.0	170	2.1
B	110	1.4	130	1.6
C	100	1.3	110	1.4
D	100	1.3	110	1.4
E	100	1.3	110	1.4

Figure 1. Idealized hysteresis loop of magnetization (M) vs. magnetic field (H), showing saturation magnetization (M_s) and intrinsic coercivity (H_c).
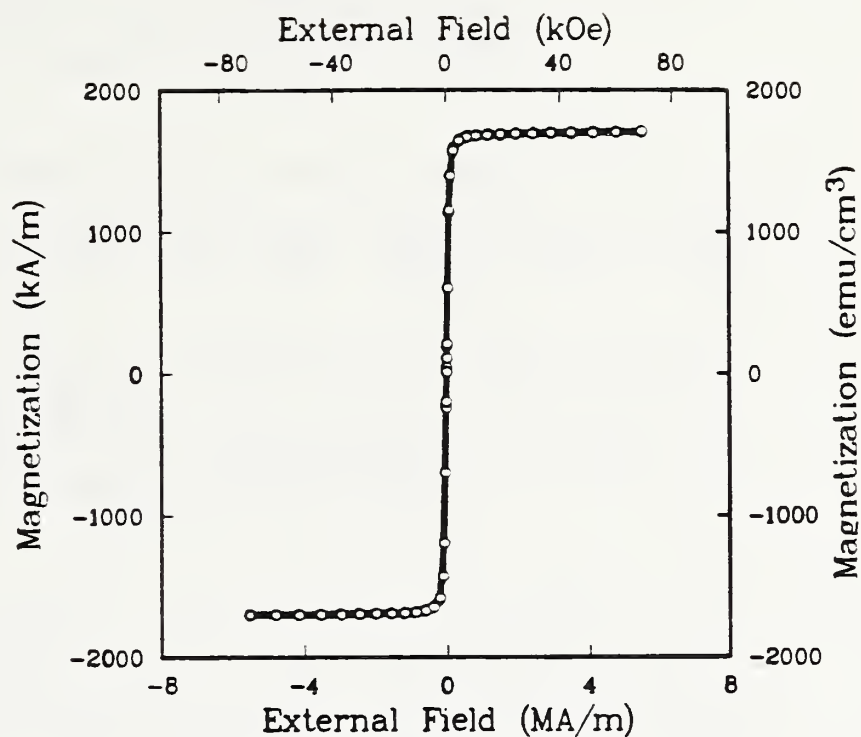
Figure 2. Hysteresis loop of magnetization vs. applied field at liquid-helium temperature for sample E. Curves for the other samples are similar.
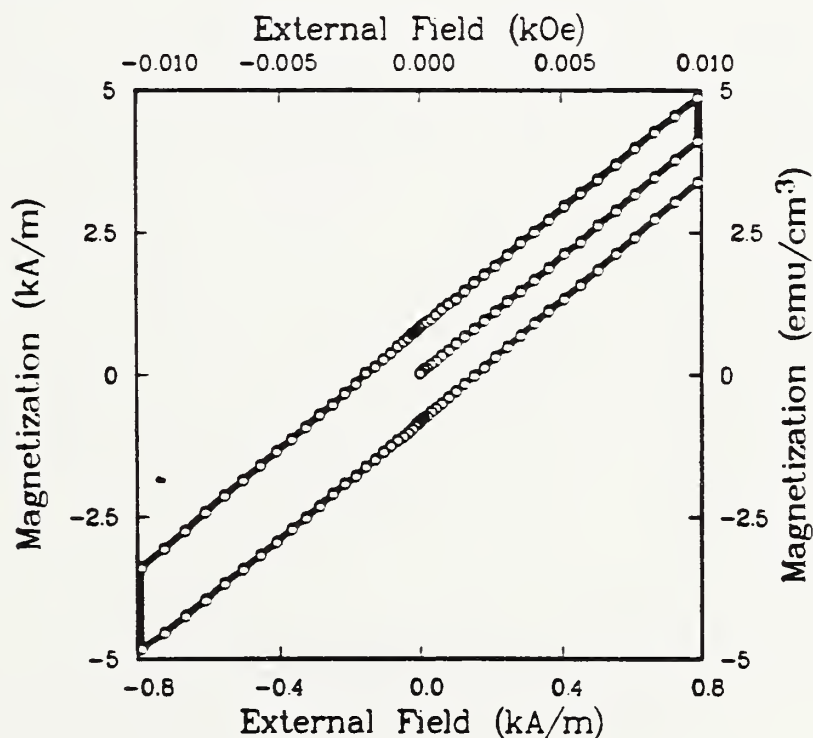

Figure 3. Plot of magnetization vs. applied field (±1 mT maximum field) at room temperature for sample A. Curves for the other samples at room temperature and liquid-nitrogen temperature are similar. Upon reaching ±1 mT, the sample was exposed to a field of ±0.1 T.

Appendix: Publications

Irregularity in Nb-Ti Filament Area and Electric
Field Versus Current Characteristics
J.W. Ekin, Cryogenics 27, 603 (1987)

Relationships Between Critical Current and Stress
in NbTi
J.W. Ekin, IEEE Trans. Mag., MAG-23, 1634 (1987)

Studies of NbTi Strands Extracted From Coreless
Rutherford Cables
L.F. Goodrich, E.S. Pittman, and J.W. Ekin, IEEE
Trans. Mag., MAG-23, 1642 (1987)

Current Capacity Degradation in Superconducting
Cable Strands
L.F. Goodrich and S.L. Bray, Applied Superconduc-
tivity Conference, ASC, San Francisco, California,
Aug. 1988, IEEE Trans. Mag., MAG-25, 1949 (1989)

Irregularity in Nb–Ti filament area and electric field *versus* current characteristics

J.W. Ekin

Electromagnetic Technology Division, Center for Electronics and Electrical Engineering, National Bureau of Standards, Boulder, CO 80303, USA

There is a correlation between irregularity in filament area ('sausaging') and the shape of a superconductor's electric field (E) *versus* current (I) relationship. The shape of the E–I characteristic is quantified in terms of the resistive transition parameter, n, defined by $E \propto I^n$. Low values of n less than about 20 correlate with a wide filament diameter distribution, while n values over 50 correspond to a distribution more than 2.5 times smaller. It is proposed that the low-field (constant) value of n be used as an index of filament quality in evaluating different superconductors for practical applications. A model is also suggested to explain this effect in terms of a locally depressed filament critical current, which forces current to transfer across the normal matrix material into neighbouring filaments. The relationship between n and the statistical distribution of filament diameters may be useful as an easy method of estimating the extent of sausaging in practical multifilamentary Nb–Ti superconductors from measurements of n.

Keywords: superconductors; Nb–Ti; sausaging; multifilamentary superconductors

In a multifilamentary superconductor a correlation exists between irregularity in filament cross-sectional area (sometimes called 'necking' or 'sausaging') and the shape of a superconductor's electric field *versus* current characteristic[1]. Measurements show that the greater the extent of irregularity in filament cross-sectional area, the more gradual is the rise in the electric field *versus* current (E–I) characteristic. The shape of the E–I curve is quantified in terms of the resistive transition parameter, n, defined by $E \propto I^n$. Low values of n indicate significant filament irregularity. The first part of this article proposes that the parameter n be used as an *index of filament quality* in evaluating different superconductors for practical applications.

A model is also suggested to explain this effect: filament necking depresses the critical current, I_c, of a filament locally; this forces current to transfer across the normal matrix material into (unnecked) neighbouring filaments. The current transfer is intrinsic to the wire and occurs continuously along its length wherever the filaments are necked down to a smaller cross-sectional area. These currents crossing the matrix generate significant voltage at transport current levels well below the critical current, which causes the reduction in the value of n. (According to this model, filaments that are uniform along their length but with different cross-sectional areas do not cause intrinsic current transfer. It is only when filaments neck that significant current transfer occurs and the value of n is degraded.)

The second part of this article presents a quantitative relationship between n and the statistical distribution of filament diameters[2] measured for the Nb Ti superconductors studied in the first part. The relationship may be useful as a quick method for estimating the extent of sausaging in practical multifilamentary Nb–Ti superconductors from measurements of n.

This article is based on two internal reports of the Electromagnetic Technology Division of the National Bureau of Standards[1,2]. The two main features of these reports – the correlation of n with filament sausaging and the filament-necking model – have been confirmed by subsequent research at several laboratories[3–9]. The sausaging model and data should aid in present efforts to produce high critical current density multifilamentary conductors and to develop a theory treating I_c inhomogeneity. They also help explain and quantify some observations of a preliminary nature, which noted a concurrence of filament sausaging and a lowering of I_c[10–12].

The transition parameter, n, was introduced some time ago by Voelker[13] in another connection relating to filament breakage rather than sausaging. The n value ($n \approx 3$) he measured was significantly lower than the n values reported here; in a sense, his work represents an extension of filament sausaging to the extreme case of filament breakage. We suspect that filament necking may have also contributed to the relatively low n values ($7 \leq n \leq 12$) in some of the 'good' multifilamentary samples he measured, since n-values are typically much greater than 30 in multifilamentary superconductors with little filament necking.

The model of Jones *et al.*[14], which has formed the basis

for much I_c inhomogeneity analysis[8,14-17], does not include the effects of current transfer between sausaged filaments. as described in the model[1]. The data and model presented here show that filament sausaging. rather than chemical or intrinsic material inhomogeneity, is the dominant source of I_c inhomogeneity that needs to be considered at low and medium fields in many practical multifilamentary Nb-Ti superconductors. The effective sausaging length is several filament diameters, which makes filament-to-filament current transfer an important consideration in I_c inhomogeneity theory. Recently, Evetts and Plummer[8] have incorporated current transfer effects into a unified analysis of sausaging effects in multifilamentary conductors. A preliminary comparison indicates that these data are in reasonable agreement with their model.

The following two sections are based, respectively, on References 1 and 2; the third section contains an addendum that summarizes the statistical data in convenient form. The identities of the superconductors have been relabelled, but otherwise the internal reports appear in their original form.

Effect of superconductor filament irregularity

During critical current testing of several Nb-Ti conductors, it was noticed that the electric field *versus* current ($E-I$) characteristic for one conductor did not show the sharp take-off behaviour normally observed in other Nb-Ti: copper superconductors we have tested. Instead, the rise in voltage in this conductor started well below the critical current, I_c, showing a gradual rise as I approached I_c rather than a sharp rise right at I_c (see sample A in *Figure 1*). This limits the usefulness of the conductor in magnet applications. since a significant electric field in the conductor below I_c leads to heating and decreased stability. Several tests were consequently undertaken to determine the source of this electric field.

The effect may be quantified by describing the superconductor $E-I$ characteristic in terms of the equation
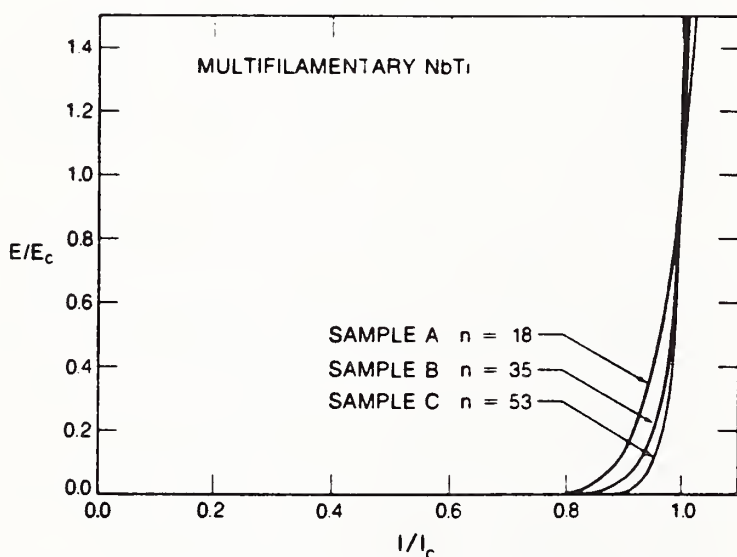
$$\frac{E}{E_c} = \left(\frac{I}{I_c}\right)^n$$

Figure 1 Normalized electric field *versus* current plots for three multifilamentary Nb-Ti superconductors, showing the more gradual resistive transition in sample A compared with samples B and C
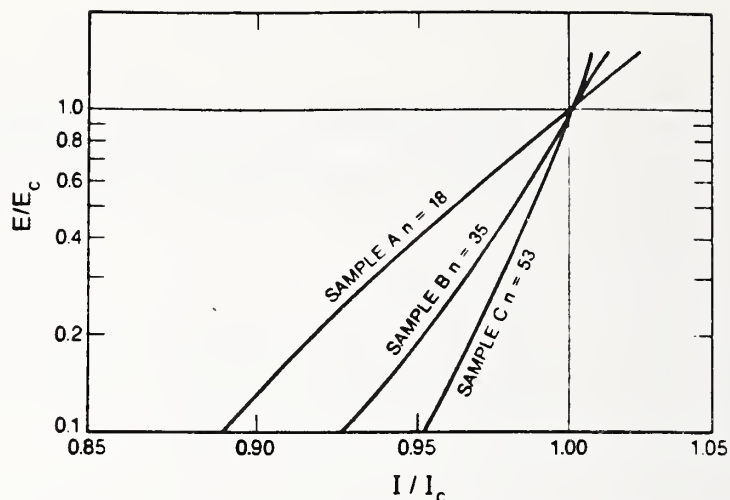

Figure 2 Logarithmic plot of electric field *versus* current for the curves in *Figure 1*, showing the low value of *n* in sample A compared with samples B and C (*n* is defined by the relationship $V \propto I^n$)

where: I_c = critical current; and E_c = electric field criterion at which I_c is determined. The larger the exponent n, the sharper the $E-I$ take-off at I_c. Thus, large n is desirable for magnet applications.

In *Figure 2*, log E/E_c is plotted *versus* I/I_c for sample A as well as another previously tested conductor, sample B. to determine comparative values of n. As seen from the curves in *Figure 2*, sample B has an *n*-value of ≈ 35, whereas sample A has an *n*-value of only ≈ 18.

One possible source of the low n in sample A is filament irregularity. If there is sausaging in the filaments, current will transfer out of a filament where it necks down. into a neighbouring filament which can carry the extra current. When the current in the neighbouring filament encounters a necked region, it too will be forced out of that filament through the matrix material and into another filament (perhaps back into the original filament if its diameter is back to average size or greater). In this manner, filament irregularity forces current transfer through the resistive matrix material continuously. causing significant electric fields along the conductor well below I_c. resulting in a low value of n.

To test this hypothesis a series of scanning electron micrographs were made of the filaments in each conductor. The copper matrix of each conductor was chemically removed and the filaments photographed longitudinally. The results are shown in *Figures 3a* and *4a*. Significantly greater filament irregularities were found in sample A than in sample B. As shown in *Table 1*, the average diameter fluctuations, ΔD, for sample A amounted to $\approx 9 \mu m$, or $\approx 33\%$ of its average filament diameter $\langle D \rangle$. In sample A, in contrast. ΔD was less than $7 \mu m$, or $\approx 20\%$ of its average filament diameter. The relative amount of filament irregularity, $\Delta D/\langle D \rangle$, in these conductors thus correlates well with degradation in the value of n characterizing their $E-I$ curves.

To see if this large filament irregularity is a characteristic of conductors containing a large volume fraction of copper, a third conductor, sample C, was also tested. The conductor contained a large amount of copper similar to sample A but had a somewhat larger filament diameter. As shown in *Figure 5* and *Table 1*, ΔD for this conductor was only $\approx 6\%$ of its $\langle D \rangle$. The $E-I$ characteristic of this conductor was correspondingly sharper, with a measured n value of 46, which is more than twice that of sample A. Thus, large values of ΔD need not be an inherent

Figure 3 Longitudinal (a) and cross-sectional (b) views of the filaments in sample A

Relationship between *n* and the statistical distribution of filament sizes

In the preceding section, it was reported that the electric field *versus* current characteristics for sample A did not show the sharp take-off normally found in other Nb–Ti:copper conductors we have tested. The effect was quantified in terms of a parameter, *n*, which for sample A was only ≈ 18, compared with values of $n = 35$ for sample B and $n = 53$ for sample C (another high copper to Nb–Ti ratio superconductor). The low value of *n* was ascribed to irregularities (sausaging) in the filament diameter of sample A as observed in SEM longitudinal micrographs of isolated filaments.

To quantify these preliminary observations, a series of SEM micrographs of the complete cross-section of the conductor has been obtained (shown in *Figures 3b–5b*).
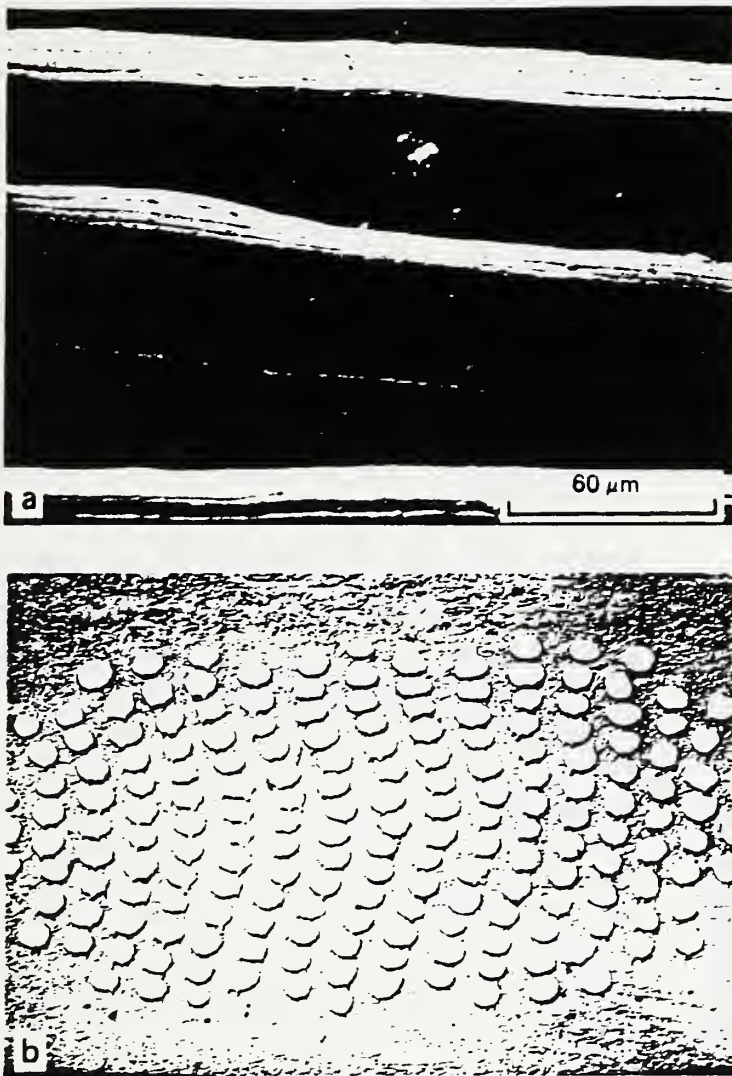

Figure 4 Longitudinal (a) and cross-sectional (b) views of the filaments in sample B

characteristic of conductors containing high percentages of copper stabilizer.

In summary, these results show that the degradation in the value of *n* for these multifilamentary Nb–Ti conductors correlates well with the relative amount of filament irregularity observed in each and that such irregularities need not be a characteristic of conductors containing a large fraction of copper. The value of *n* measured for sample A is significantly lower than that measured for other Nb–Ti conductors and these data would suggest it could be substantially improved by reducing the large filament diameter irregularities observed in this conductor. Furthermore, it would seem that the parameter *n* could be used as a valuable index of filament quality in evaluating different superconductors. Certainly, *n* should be an extremely useful parameter in characterizing the quality of a superconductor's *E–I* characteristics, complementing the I_c value usually supplied with commercial conductors.
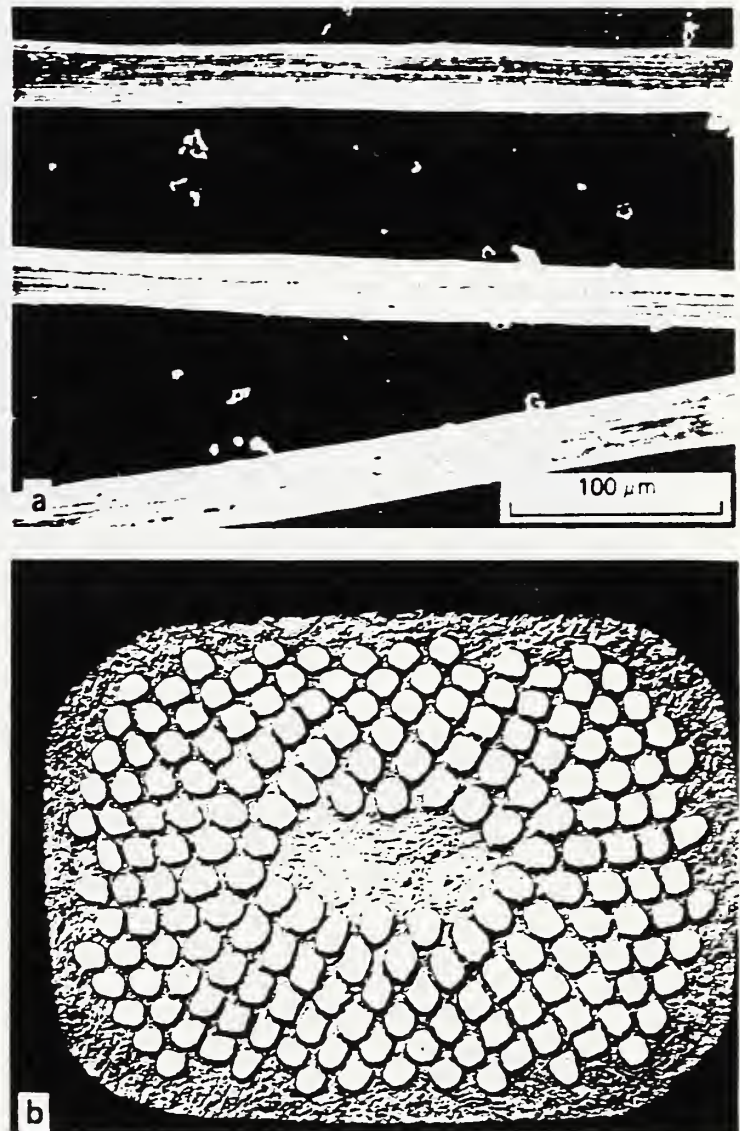
Table 1 Filament diameter variations for three Nb–Ti conductors

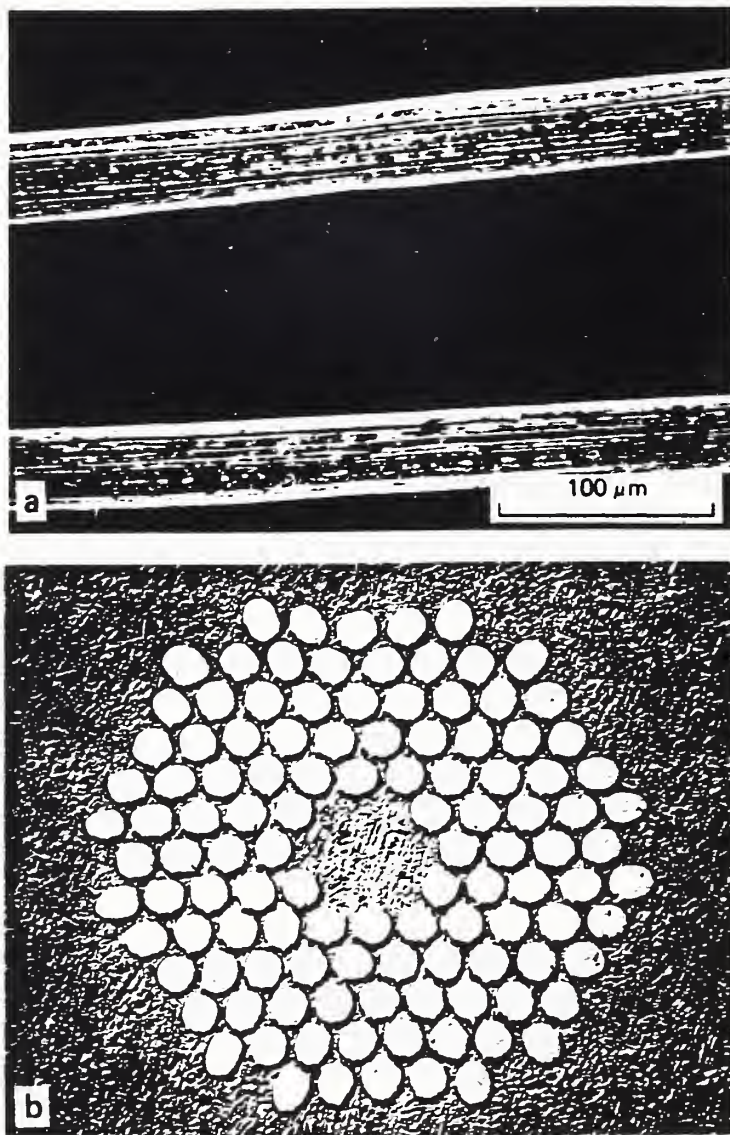| Conductor	Size (mm)	Number of filaments	Twist pitch (cm)	Cu:Nb-Ti	Average filament diameter, $\langle D \rangle$ (μm)	$\dfrac{D_{max}}{D_{min}}$	ΔD (μm)	Deformation length $(\langle D \rangle)^{*}$	n
Sample A	0.51 × 1.02	187	1.8	4.77	27	1.33	8.9	4	18
Sample B	0.56 × 0.71	180	1.3	1.8	33	1.20	6.5	8	35
Sample C	1.00 diameter	114	2.5	5.5	37	1.06	2.2	6	53

Figure 5 Longitudinal (a) and cross-sectional (b) views of the filaments in sample C
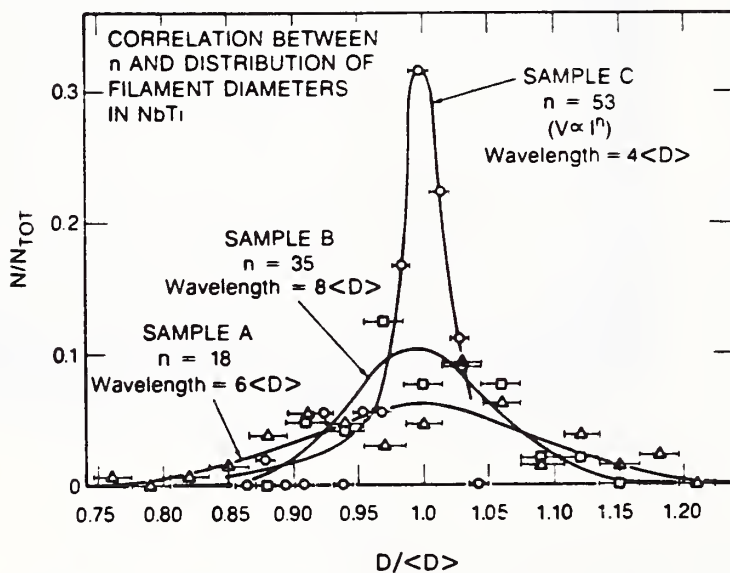

Figure 6 Distribution of filament diameters in samples A, B and C. Horizontal bars indicate the sampling interval for each histogram. Irregularities in the cross-sectional area of each filament mainly determine *n*, rather than variations in the *average* filament diameter from filament to filament. In these samples, the average filament diameter varied with radial position in the composite. The radial effect was eliminated from the plotted distribution by determining the variation in diameter of each filament relative to the average diameter of other filaments at the same radial position

From many measurements of the individual filament diameter in these micrographs, a *statistical distribution* of the filament diameters in each conductor has been obtained. *Figure 6* shows the distribution of filament diameters, *D*, about the average filament diameter of each ring of filaments, $\langle D \rangle$. The spread in the distribution for sample A is much broader than for samples B or C, confirming the earlier qualitative treatment given the filament irregularities. The half-width of the filament diameter distribution correlates very nicely with the variations in the parameter *n*. This evidence is consistent with the current transfer hypothesis advanced in the previous report as the explanation for the relatively large electric field appearing in sample A at currents below the critical current.

In the SEM micrographs in *Figures 3b–5b* note the presence of the large centre island of copper in conductor samples B and C, compared with the lack of this feature in sample A. It is believed this centre copper island is a significant factor in minimizing the filament irregularity problem (particularly in conductors having a high copper to superconductor volume ratio).

Addendum

The *n* values reported above were nearly independent of magnetic field from 3 to 7 T. Over this field range they varied by less than $\approx 5\%$. A graph of the standard deviation of the filament diameter distributions shown in *Figure 6* is plotted as a function of *n* in *Figure 7*. The
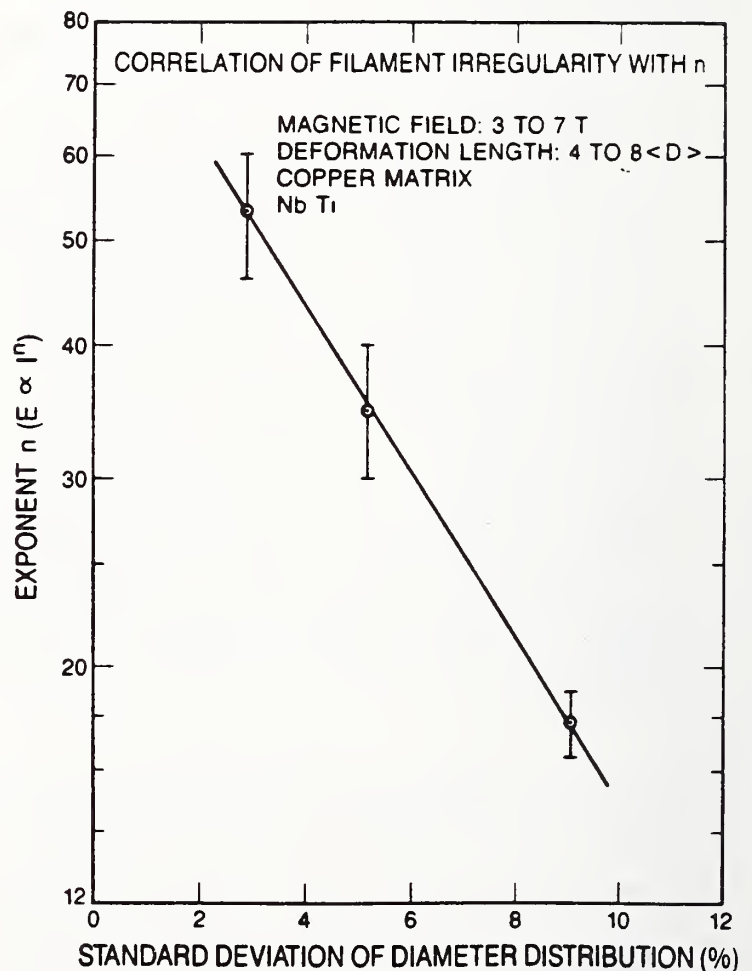

Figure 7 Approximate relationship between *n* and the standard deviation of the filament diameter distribution for several multifilamentary Nb–Ti superconductors (from *Figure 6*)

approximate relationship shown in *Figure 7* may be useful for quickly estimating the extent of filament irregularity in practical multifilamentary Nb–Ti superconductors from measurements of *n*.

Acknowledgements

References

1 Ekin, J.W. *Superconducting Coil Characterization* Quarterly Progress Report No. SR-724-13-82, Div. 724.05, National Bureau of Standards, Boulder, Colorado, USA (March 1982) unpublished. Distributed at the First Workshop on Nb–Ti Superconductors, University of Wisconsin, Madison, Wisconsin, USA (July 1983)
2 Ekin, J.W. *Superconducting Coil Characterization* Quarterly Progress Report No. SR-724-26-82, Div. 724.05, National Bureau of Standards, Boulder, Colorado, USA (June 1982) unpublished. Distributed at the First Workshop on Nb–Ti Superconductors, University of Wisconsin, Madison, Wisconsin, USA (July 1983)
3 Garber, M., McInturff, A. and Larbalestier, D. presentations made at the Second Workshop on Nb–Ti Superconductors, University of Wisconsin, Madison, Wisconsin, USA (July 1984)
4 Gregory, E., Hemachalam, K., Hong, M., Garber, M., Sampson, W., Suenaga, M., McInturff, A., Warnes, W.H., Larbalestier, D. and Scanlon, R. presentations made at the Third Workshop on Nb–Ti Superconductors, Lawrence Berkeley Laboratory, Berkeley, California, USA (January 1985)
5 Garber, M., Suenaga, M., Sampson, W.B. and Sabatini, R.L. *Adv Cryog Eng* Plenum Press, New York, USA (1986) 32 707
6 Larbalestier, D.C. and West, A.W. *Acta Met* (1984) 32 1871
7 Warnes, W.H. and Larbalestier, D.C. *Proc Int Symp Flux Pinning and Electromagnetic Properties in Superconductors* (Ed Matsushita, T., Yamafuji, K. and Irie, F.) Matsukuma Press, Japan (1986) 156
8 Evetts, J.E. and Plummer, C.J.G. *Proc Int Symp Flux Pinning and Electromagnetic Properties in Superconductors* (Ed Matsushita, T., Yamafuji, K. and Irie, F.) Matsukuma Press, Japan (1986) 146
9 Plummer, C.J.G. and Evetts, J.E. *IEEE Trans Magn* (1987) MAG-23 1179
10 Smathers, D.B., Marken, K.R., Larbalestier, D.C. and Scanlan, R.M. *IEEE Trans Magn* (1983) MAG-19 1417
11 West, A.W., Warnes, W.H., Moffat, D.L. and Larbalestier, D.C. *IEEE Trans Magn* (1983) MAG-19 749
12 Evetts, J.E. *IEEE Trans Magn* (1983) MAG-19 1109
13 Voelker, F. *Particle Accelerators* (1970) 1 205
14 Jones, R.G., Rhoderick, E.H. and Rose-Innes, A.C. *Phys Lett* (1967) 24A 318
15 Warnes, W.H. and Larbalestier, D.C. *Appl Phys Lett* (1986) 48 1403
16 Warnes, W.H. and Larbalestier, D.C. *Cryogenics* (1986) 26 643
17 Warnes, W.H. and Larbalestier, D.C. *IEEE Trans Magn* (1987) MAG-23 1183

RELATIONSHIPS BETWEEN CRITICAL CURRENT AND STRESS IN NbTi

J. W. Ekin
Electromagnetic Technology Division
National Bureau of Standards
Boulder, Colorado 80303

ABSTRACT

The effects of various types of stress on the critical current of a multifilamentary NbTi superconductor are reported. Degradation of critical current due to axial tension applied at 4 K, transverse compression applied at 4 K, and hairpin bending strain applied at room temperature has been measured. The degradation from axial tension is much greater than from transverse compression in many practical cases because the soft copper matrix limits the build-up of transverse compression. The degradation from typical levels of transverse compression is only about 4% at 8 T, for example. For axial tension, on the other hand, higher stresses can occur that will degrade the critical current by 24%, for example, at 7 T and 2.7% strain. Both the axial-tensile and the transverse-compressive stress effects are about 98% reversible; thus the degradation will be seen only when the conductor is under operational stress. The results indicate that a primary origin of the critical current degradation in NbTi is a stress-induced reversible decrease in the upper critical field.

INTRODUCTION

In the initial phase of this study, reported here, several types of mechanical tests were made on the same conductor material to evaluate the critical-current degradation from different types of stress. Once identified, the most important stress tests will be performed on many different conductors in a later phase of testing to obtain a data base useful for minimizing critical-current degradation in magnet design.

In this paper, measurements of the effect of 4-K transverse compressive stress on the critical current of NbTi are reported. These results are compared with the effects of axial tension applied at 4 K and severe hairpin bending strain applied at 295 K, all measured on samples of the same NbTi conductor. The conductor chosen for these first tests was the strand material used to make many of the 30-strand Rutherford cables in the Lawrence Berkeley Laboratory (LBL) cable-development program.

TRANSVERSE COMPRESSION TESTS

The effect of axial tension on the critical current of practical multifilamentary NbTi superconductors was first studied about ten years ago.[1] Little electromechanical research has been made on NbTi superconductors since then, and this has been mostly axial stress studies.[2] Less is known about the effects of stress components other than the axial component.[3] In practical superconducting magnets, however, the superconductor is subjected to three-dimensional stress. Typically the transverse component of stress is compressive. For example, in solenoidal magnets the transverse component arises from hoop stress which compresses the magnet winding radially. In dipole magnets it arises from Lorentz force compression of the magnet windings at the midplane.

To obtain data on the effects of this component of stress on the critical current of practical superconductors, a transverse-stress apparatus was designed and built. It simultaneously applies mutually perpendicular components of current, high magnetic field, and transverse compressive stress to a single strand superconductor in a 4-K liquid helium bath.

The sample is prepared in the shape of a flat sided hairpin. Compressive load is applied by sandwiching the central flat section of the hairpin between two stainless-steel anvil heads. Magnetic field is applied mutually perpendicular to both the directions of the force and the sample current with a radial access magnet. The field is also perpendicular to the hairpin legs of the sample to minimize current-transfer effects. (Otherwise, if the hairpin legs were parallel to the applied magnetic field, a large difference in critical current would arise between the legs and the central section.) Further details and pictures of the apparatus are given in Ref. 4.

The first test results were obtained on an unused segment of NbTi strand material similar to that used to make many of the 30-strand Rutherford cables in the LBL cable development programs. The NbTi strand characteristics are given in Table 1. The sample was manufactured using a single stack technique without a diffusion barrier around the filaments.

Figure 1 shows the degradation of critical-current by transverse stress applied to the sample at 4 K. The ordinate in Fig. 1 is the measured critical current normalized by its starting (zero-stress) value. The abscissa is transverse force per unit sample length, F/L (top scale). A second abscissa scale is also shown (bottom scale) which is an effective overall transverse stress obtained by dividing the applied load by the projected area of the sample in the direction of the applied load. This projected area is simply taken as the length over which compressive load is applied (9.5 mm) multiplied by the starting sample diameter (0.648 mm).
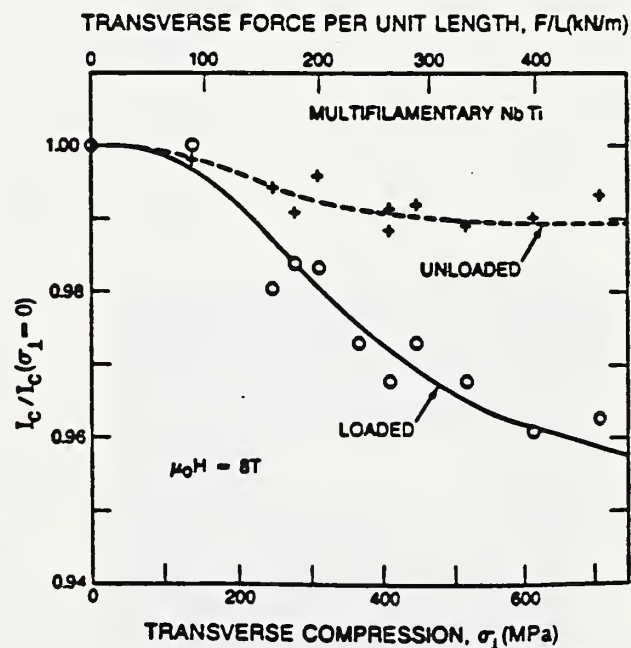

Figure 1. Effect of transverse compressive force on the critical current a NbTi conductor at 8 T.

Table 1. Characteristics of the multifilamentary NbTi sample studied in this paper.

Strand diameter	0.648 mm
Filament diameter	16 μm
Number of filaments	648
Copper-to-superconductor volume ratio	1.77
Twist pitch	1.27 cm
Superconductor area	0.1189 mm^2
Total area	0.3295 mm^2

This effective stress is given for comparative purposes only. In the experiment, the anvil heads were flat and the sample round, so this simple method of determining stress does not take into account the small initial contact area, nor the increase in contact area between the anvil heads and the sample as the sample is progressively deformed. However, it represents reasonably well the approximate average stress experienced by the NbTi filaments within the composite.

The overall sample strain was quite great because of deformation of the soft copper matrix. It amounted to about 24% at the maximum value of force-per-sample-length (F/L) of 458 kN/m. This overall sample strain, however, is typically much greater than the actual NbTi filament strain because the copper matrix material yields at a relatively low stress. A picture of the deformed sample after the maximum loading (F/L = 458 kN/m) at 4 K is shown in Fig. 2.

The separation of the voltage taps was relatively small, 8.7 mm. Consequently a relatively high critical-current voltage criterion was used, corresponding to an electric field of 5 μV/cm. The critical-current values at more sensitive criteria are easily calculated, however, using the measured values of the exponent n given in Fig. 3 [$I_{c1}/I_{c2} = (E_{c1}/E_{c2})^{1/n}$]. Note that for this sample, which was fabricated using a single stack technique with relatively large filaments (16 μm), n reached values of about 80 at low magnetic fields. This is relatively high for multifilamentary NbTi superconductors.

As seen from the results at 8 T in Fig. 1, little degradation (≤ 0.5%) was observed for this particular sample up to a F/L value of about 100 kN/m (corresponding to an approximate transverse compressive stress, $\sigma\perp$, of about 150 MPa). The degradation effect then increased monotonically to about 4% as F/L was increased to 460 kN/m ($\sigma\perp$ = 700 MPa). Because the yield stress of the copper matrix is so low, it is difficult to generate much higher stress without severe sample deformation; see Figure 2. Thus, the maximum critical-current degradation from transverse stress is about 4% at 7 T.
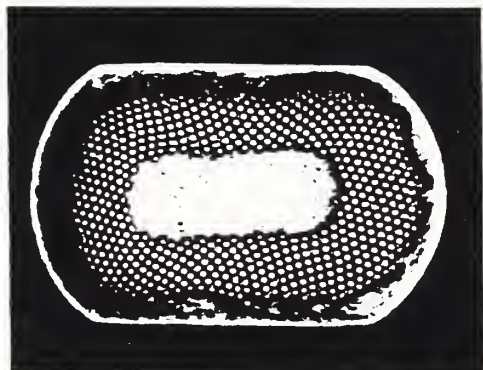

Figure 2. Cross section view of the NbTi conductor after application of 458 kN/m transverse load at 4 K.

The effect was almost completely reversible. Upon unloading from F/L = 460 kN/m, the critical current recovered to within 0.5% of its original value. This recovery took place even though the sample was permanently deformed by about 25%.

The transverse stress degradation was largest at high magnetic field. At lower fields (5 T and 3 T) the effect was less than 0.5 % at a F/L value of 460 kN/m.

AXIAL TENSION TESTS

Tests at Magnetic Fields Up to 7 T

To compare the relative magnitudes of the effects of transverse compression with axial tension, another sample of the same starting material (see Table 1) was tested in an axial tensile mode. The experiments were carried out using an apparatus described in Ref. 6.

Results corresponding to a 5 μV/cm criterion (the same as that used for the transverse compression tests) are given in Fig. 4 as a function of stress and strain. Stress was calculated using the overall conductor cross sectional area. The results of Fig. 4 compared with Fig. 1 show that the effect of axial tensile stress applied at 4 K is significantly greater than the effect of transverse compression at 4 K, in terms of the overall stress on the conductor. For example, the degradation of the critical current at 7 T is about 24% at an average tensile stress of 700 MPa (tensile strain of 2.7%). This compares with an 8 T degradation of about 4% at 700 MPa transverse stress, about one sixth.

However, because the copper matrix has a relatively low yield stress (about 130 MPa), the axial stress in the NbTi filaments is actually higher (about 2.1 times higher) than the overall stress on the conductor. Accounting for this, the degradation from axial tension at 700 MPa in the NbTi filaments corresponds to about 340 MPa overall conductor stress, or a degradation of only about 7% at 8 T. Thus, the two effects (axial and transverse) are nearly comparable in terms of actual NbTi filament stress. The slight difference in critical-current degradation between the two components of stress may arise from texturing of the filaments introduced during fabrication.

Much more stress can be developed in the NbTi filaments from axial tension than from transverse
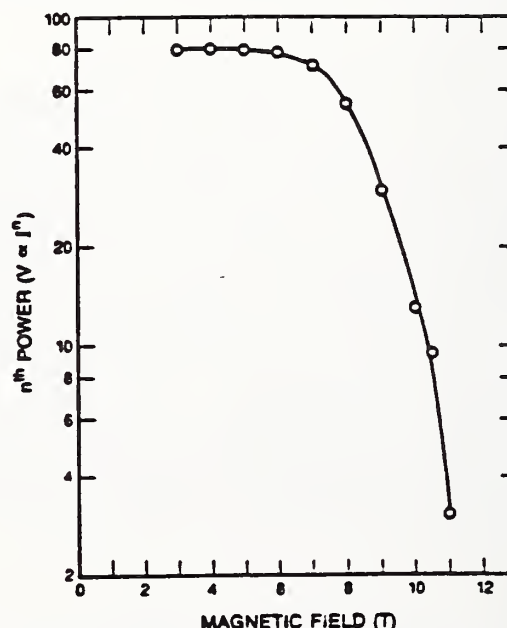

Figure 3. Magnetic field dependence of the exponent n.

compression because the soft copper matrix limits the buildup of transverse compression. Thus, in many practical cases, axial tensile stress is the more important source of critical-current degradation.

In other respects the two types of stress effects (axial and transverse) are similar. Both stress effects increase with increasing magnetic field. For example, the degradation at an axial stress of 700 MPa (2.7% strain) was 19% at 3 T, and increased to 26% at 7 T. For transverse stress, the degradation was negligible (≤0.5%) below 5 T, and increased to 4% at 8T.

Both types of stress effects are also highly reversible. For example, upon unloading from an applied axial stress of about 700 MPa (strain of 2.7%), the critical current at 5 T recovered to within 1% of its original value. This extreme reversibility persisted up to the fracture point of the sample, which occurred at a strain of 4.06%. Just before the sample fractured, the critical current still recovered to within 1.5% of its original value upon unloading.

A significant serrated yield event (load drop of 10%) took place at a tensile strain of 3.0%. Figure 4 shows that this did not significantly affect the smooth monotonic decrease of the critical current with stress and strain.

However, a thermal runaway event, a "quench" took place while the sample was under high stress, 842 MPa (3.5% strain), which did significantly affect the critical current degradation. As shown in Fig. 4, the critical current rose significantly after the transient heating that accompanied the thermal runaway and current-supply shutdown. During this quench the strain in the sample was maintained constant, but the stress decreased about 15% due to annealing. Thus, the event indicates that critical-current degradation in NbTi is predominantly stress controlled rather than strain controlled, since strain was constant while both the stress and critical current recovered. The event suggests that strain and deformation alone are

not the prime causes of degradation in NbTi, but rather the stress that accompanies deformation is the major cause, at least at 4 K. Thus, stress annealing the conductor might be a method for improving the critical current.

Tests at Magnetic Fields Above 7 T

To measure the effect at magnetic fields approaching the upper critical field, another series of tests was made at fields above 7 T using an apparatus described in Ref. 7. The results are given in Fig. 4 along with the low-field results.

These data show that the relative magnitude of the stress effect becomes much larger as the magnetic field approaches the upper critical field. At 2.14% strain, for example, the critical-current degradation is 19% at 8 T, 24% at 9 T, 42% at 10 T, and rises to 60% at 10.5 T.

HAIRPIN BEND TEST AT 295 K

To compare these 4 K stress effects with room-temperature bending-strain effects, the same superconductor strand material was subjected to a severe bending strain test. The conductor was bent into a hairpin shape at 295 K and placed transversely to the bore of a 9 T solenoidal magnet. This field orientation was chosen to reduce current-transfer effects.

The sample was subjected to bending strain, starting at about 15% and increasing to a little over 100%. This was done progressively in the same sample by bending it at room temperature, cooling the sample to 4 K, measuring I_c, warming the sample to room temperature, bending the sample into a tighter radius, and repeating the whole process. The critical current was measured at each radius until the radius was reduced to nearly zero.

The I_c results corresponding to a 5μV/cm criterion are shown in Fig. 5. In this figure, the relative critical-current degradation is plotted as a function of bending strain in the outer filaments, ε_B. Critical current was measured for current flowing
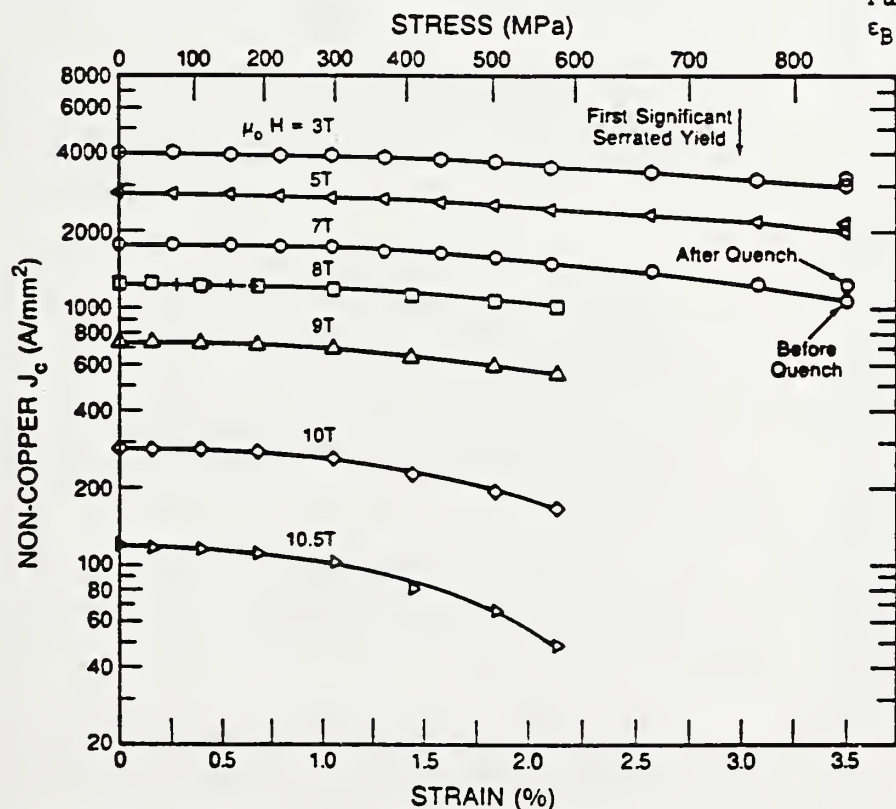

Figure 4. Effect of axial tensile strain and stress on the critical current of a NbTi conductor at magnetic fields from 3 T to 10.5 T. A much coarser scale was used here than in Figs. 1 and 5.
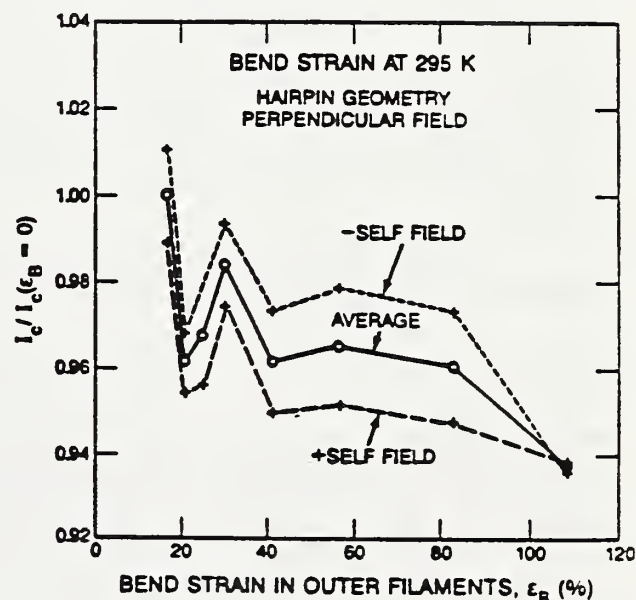

Figure 5. Effect of room-temperature bend strain on the critical current of a NbTi conductor at 8 T. The abscissa is the calculated bending strain in the outermost filaments.

in two directions in the hairpin sample, one direction where the self field of the sample added to the background field (marked +) and the other where the self field subtracted from the background field (marked -). The average of the two critical-current values is plotted with open circles in Fig. 5.

The magnitude of the degradation at the high bending strains shown in Fig. 5 is small. The effect of room temperature bending strain on the critical current is less than 4% at bending strains of over 100%. All bending was done at room temperature, and there was no stress applied to the sample when it was cooled for the critical-current measurement. Further bend tests need to be made to better simulate cabling conditions. Note that the conductor strand was not under tension when it was bent, nor was it bent around a mandrel or severely pressed. The critical current under bending strain also needs to be measured at lower electric fields.

CONCLUSION

The main results of these measurements are summarized below:

1. The magnitude of critical-current degradation in NbTi from transverse compression applied at 4 K is much less than from axial tension in terms of overall conductor stress, but the two are comparable in terms of stress in the NbTi filaments.

2. Much more stress can be developed in NbTi filaments from axial tension than from transverse compression, because the soft copper matrix limits the buildup of transverse compression to low levels. At such levels the I_c degradation is only about 4% at 8 T, for example. Thus, in many practical cases, axial tensile stress (from tension or bending strain) is the more important source of critical-current degradation. For example, the I_c degradation is 24% at 7T when the NbTi filaments are axially strained 2.7%.

3. The I_c degradation from both types of stress is about 98% reversible, indicating that the effects of stress in NbTi will be seen only when the conductor is under stress.

4. The data indicate that a primary origin of the critical-current degradation in NbTi is a stress induced reversible decrease in the upper critical field. This is true for degradation due to both transverse-compression and axial-tension degradation. It is shown by the large relative increase in the critical-current degradation from both types of stress as the magnetic field approaches the upper critical field.

There are several practical consequences of these preliminary findings for cable fabrication:

1. In Rutherford cables, not much transverse stress is generated in the NbTi filaments along the cable faces because of yielding of the soft copper matrix material surrounding the filaments. Much more stress can be developed in the NbTi filaments from axial tension at the cable edges where they are bent around the cable. This may explain the relatively small degradation measured along conductor strands extracted from the face of Rutherford cables compared to the edge region.[8]

2. The potentially large effect of axial tension indicates that tension on the cable strands should be set at the minimum level needed for cable integrity.

3. Stress annealing the conductor may improve the critical current under some circumstances.

Additional measurements will be needed to determine whether the effect is predominantly a very low temperature (4-K) stress phenomenon or also arises from stress applied at higher temperatures. The consistency of the effects among different NbTi superconductors needs to be tested and further bend testing is needed to relate this to the axial tension results.

ACKNOWLEDGEMENTS

REFERENCES

1. J. W. Ekin, F. R. Fickett, and A. F. Clark, "Effect of Stress on the Critical Current of NbTi Multifilamentary Composite Wire," Proc. Int'l. Cryog. Mat. Conf. (Aug. 1975), Adv. Cryo. Eng. 22, 449 (1977).

2. For a review, see J. W. Ekin, "Mechanical Properties and Strain Effects in Superconductors," in Superconducting Materials Science: Metallurgy, Fabrication, and Applications, edited by S. Foner and B. B. Schwartz, Plenum Press, New York, p. 455-510 (1981).

3. The effect of critical-current anisotropy introduced by room-temperature flattening has been studied by Garber, unpublished, and by L. F. Goodrich, W. P. Dube, E. S. Pittman, and A. F. Clark, Adv. Cryog. Eng. 32, 833 (1986).

4. J. W. Ekin, L. F. Goodrich, J. Moreland, E. S. Pittman, and A. F. Clark, "Electromechanical Properties of Superconductors for High Energy Physics Applications," NBS Internal Report, NBSIR #86-3061 (1986), in press.

5. J. Royet and R. M. Scanlan, "Manufacture of Keystoned Flat Superconducting Cables for Use in SEC Dipoles," Paper LB-1 of these conference proceedings.

6. J. W. Ekin, "Superconductors," Chapt. 13 in Materials at Low Temperatures, edited by R. P. Reed and A. F. Clark, American Soc. for Metals, p. 465-513 (1983.)

7. J. W. Ekin, "Strain Scaling Law for Flux Pinning in Practical Superconductors, Part I: Basic Relationship and Application to Nb_3Sn Conductors," Cryogenics 20, 611-624 (1980).

8. L. F. Goodrich, E. S. Pittman, J. W. Ekin, and R. M. Scanlan, "Electromechanical Properties of NbTi Strands Extracted From Cables," Paper MH-8 of these conference proceedings.

STUDIES OF NbTi STRANDS EXTRACTED FROM CORELESS RUTHERFORD CABLES

L. F. Goodrich, E. S. Pittman, and J. W. Ekin
National Bureau of Standards
Boulder, Colorado 80303

and

R. M. Scanlan
Lawrence Berkeley Laboratory
Berkeley, California 94720

Abstract

The electromechanical properties of NbTi strands extracted from coreless Rutherford cables were studied to clarify the relative effects of strand location and field angle on current degradation that occurs in cables that have been compacted into a keystone shape. Detailed critical-current measurements were made on two samples which were fabricated under controlled conditions. These are prototype cables for high energy physics applications. Specific factors that are addressed are the nature, location, and amount of degradation. This information is intended to lead to methods for reducing the amount of critical-current degradation in cable manufacture.

Introduction

The measurements reported here were made on two samples, denoted as Sample A (billet 5914, cable SC 305) and Sample B (billet 5212, cable SC 297). Sample A was a strand from a cable that was commonly used for cable studies late in 1985 and early 1986. Sample B was a strand from a cable that was re-rolled through the turkshead (to re-size it) after it had been cabled. This re-rolling may have been done in the direction opposite the original cabling and roll direction. The re-rolled cable Sample B was a worst-case situation that was studied to more clearly identify the degradation features. The comparison of the results of measurements on these two cables indicated significant similarities and differences. The critical current, I_c, of strands extracted from cables was measured as a function of position along the cable and magnetic field orientation. A more complete report on this work can be found in Ref. 1. Information on the cable fabrication and current density with high homogeneous NbTi alloy can be found in Refs. 2, 3 and 4.

Experimental Details

The samples were from 30-strand cables and started as 0.65-mm-diameter round wires with a right hand filament twist of about 0.8 twist/cm. The cable had a left hand lay with a 69-mm pitch and a cable width of 9.7 mm, mid-thickness of 1.17 mm, and a keystone angle of about 1.24°. Sample A had a Nb diffusion barrier on each of the 6006, 5-μm-diameter filaments. Sample B had 648, 16-μm-diameter filaments and did not have a diffusion barrier. The Sample A billet was double stacked; Sample B was single stack. The starting-wire critical currents (before the cabling process) were determined at 5 T and 4.02 K using a 0.1 μV/cm criterion (Sample A, 320 A; Sample B, 347 A). The critical-current density was calculated using the NbTi cross-sectional area (Sample A, 2500 A/mm^2; Sample B, 2900 A/mm^2), which was determined using the copper-to-superconductor volume ratio (Sample A, 1.64;

Sample B, 1.77). The critical-current density at 4.22 K would be about 6% less than the values listed at 4.02 K.

A number of voltage taps were placed along the length of the strand to determine its local electrical properties after it had been deformed by the cabling process. Three regions of the cable were studied: the thin edge, the face (top or bottom), and the thick edge. Each of these regions was divided with voltage taps into three approximately equal-length, adjacent segments. The three segments of each cable edge were denoted as the central flat edge and the two corners (bent portion). These edge voltage taps had separations of 2 to 2.5 mm (thin edge) and 2.5 to 3 mm (thick edge). The voltage taps along the face of the cable had separations of about 9 mm and they did not include any of the cable corner regions. The precision and accuracy of the critical current measurements were limited by the low voltage for these closely spaced voltage taps and the fact that the sample would quench before very much voltage drop could be developed between some voltage taps. The precision was about ±1% and the accuracy was about ±2%.

The effective critical current was defined as the critical current determined by adding the voltage contributions of each strand segment, taking into account that the positions along the face need to be counted twice for one pitch length. This total voltage was then converted to an effective electric field by dividing by one pitch length. This was useful because it related more directly to measurements made on the whole cable where several pitch lengths were included between the voltage taps.

Results

The data presented here are preliminary in that they may not represent averages of a number of specimens. There is no reason to believe, however, that these two specimens were not typical. Independent measurements on the cables[5] indicated that Sample A was degraded by about 9% and had a field anisotropy of about 11% and Sample B was degraded by 22% and had an anisotropy of -11%. Anisotropy refers to 1 minus the ratio of perpendicular I_c (90°) to parallel I_c (0°) and degradation refers to 1 minus the ratio of perpendicular I_c to starting wire I_c (see Ref. 6). These results are consistent with those presented here. These additional data presented here on the nature, location, and amount of degradation are intended to lead to methods for reducing the degradation.

In the first run of Sample B, the thin edge had the lowest critical curent, and this region was limiting the current. For the second run, a short section of the thin edge was shunted with a 0.7-cm length of

another cable strand. This allowed the current to get slightly higher and enabled testing of the other regions of the strand before the sample quenched. The data presented for Sample B are a combination of these two runs, not shunted and shunted.

The critical current as a function of position along the strand at 0° and 90° field angle is given in Figs. 1 and 2 for Sample A. The critical current was defined as the current at which the electric field strength was 0.1 µV/cm. The zero angle was defined as the orientation with the magnetic field parallel to the wide face of the cable. The critical current values varied by as much as 27% from the maximum at 0° and 11% at 90°. At 0° the central flat portion of the thin edge had the lowest I_c. The central flat portion of the thick edge was less degraded. The corners of both edges had a higher I_c and had some asymmetry in the same cable lay direction. This may be due to mass flow away from the cable edge during the cable fabrication. The difference between 0 and 90° is due to the effect of the conductor aspect ratio[7] and the fact that the applied magnetic field is not exactly perpendicular to the current for all portions of the strand at all angles. The cable pitch is about 17°, which would increase I_c at 0° by about 8% for the portions across the cable face.[8] At 90° the applied magnetic field is perpendicular to the cable face, but it is not perpendicular to portions of the cable edges. The major deformation direction for the cable edge is 90° from that for the cable face. The edges have their lowest I_c at 0°. The central region of the cable face does not have very much change in I_c between 0 and 90° because the strand is almost round there.

The critical current as a function of position at 0° and 90° for the Sample B is given in Figs. 3 and 4. The critical current values varied by as much as 35% from the maximum at 0° and 33% at 90°. At 0° the

central flat of the thin edge had the lowest I_c, and unlike Sample A, it did not increase very much at 90°. For both samples the difference between the thin and thick edges were similar, as were the corner values. The central flat region of the thin edge is the weak link and would appear to have a degraded I_c rather than a large aspect ratio effect.[6]

A relevant question at this point is: What is the effective critical current of these strands as a function of orientation? One possibility is the current at which the average electric field strength is equal to some value (see experimental section). The effective critical current and quench current for Sample A are plotted as a function of angle in Fig. 5. The effective critical current at various electric field criteria had an angular dependence very similar to the quench current. This was not expected considering that the quench current should be strongly dominated by the degraded section (or weak link) of the strand and consequently lower at 0°. This suggests that the average E does give a relevant critical current. The end cooling around the weak link must have been sufficient such that the local heating did not have an adverse effect on I_c. The weak link at 0° contributed about 55% of the total voltage even though it only represented 5% of the total length. For the effective critical current, the weak link region is at a high electric field where the effect of a single bend is not as large (See Ref. 9 for effect of bending).

The effective critical currents and quench current for Sample B are plotted as a function of angle in Fig. 6. There are two curves without symbols. The upper was the quench current after a shunt was placed on the thin edge. The lower was the quench current before the shunt was placed on the thin edge. The lowest curve is the effective I_c at 0.1 µV/cm. The
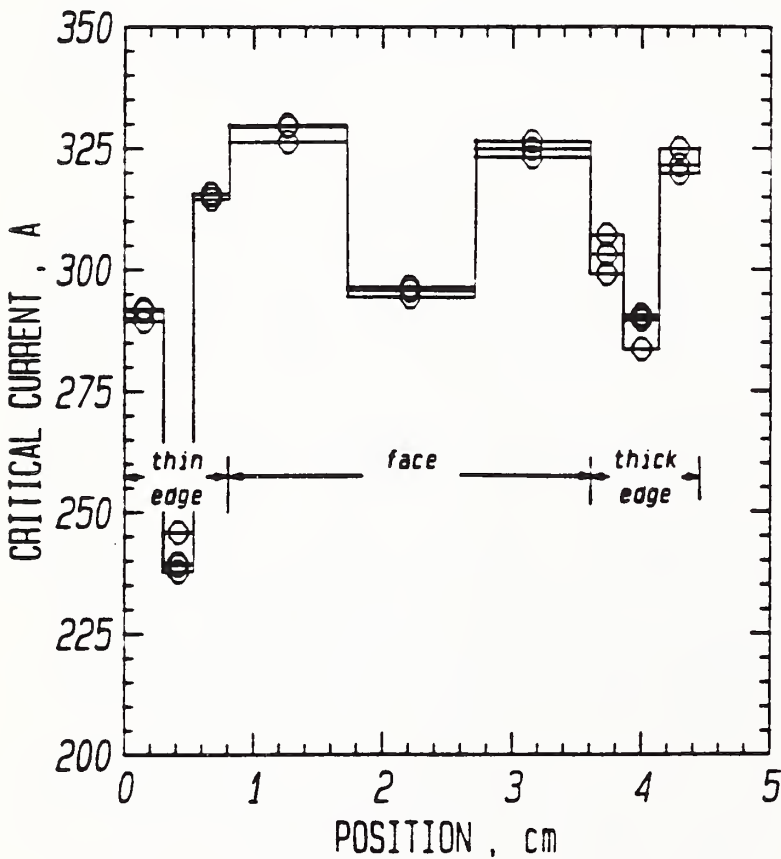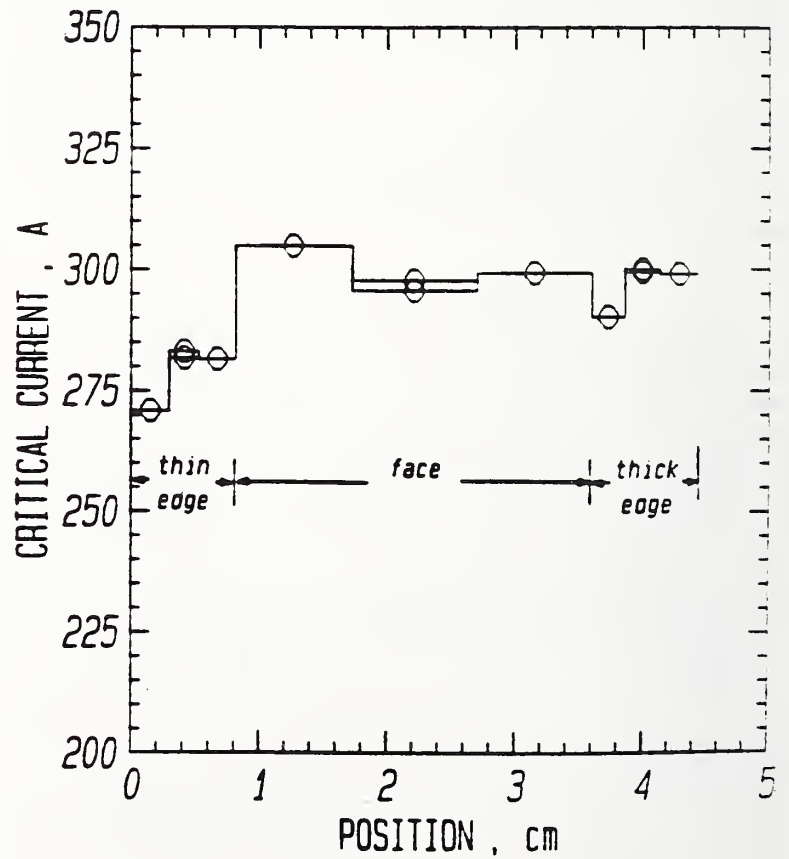

Figure 1. Sample A, I_c vs. position at 0°.

Figure 2. Sample A, I_c vs. position at 90°.
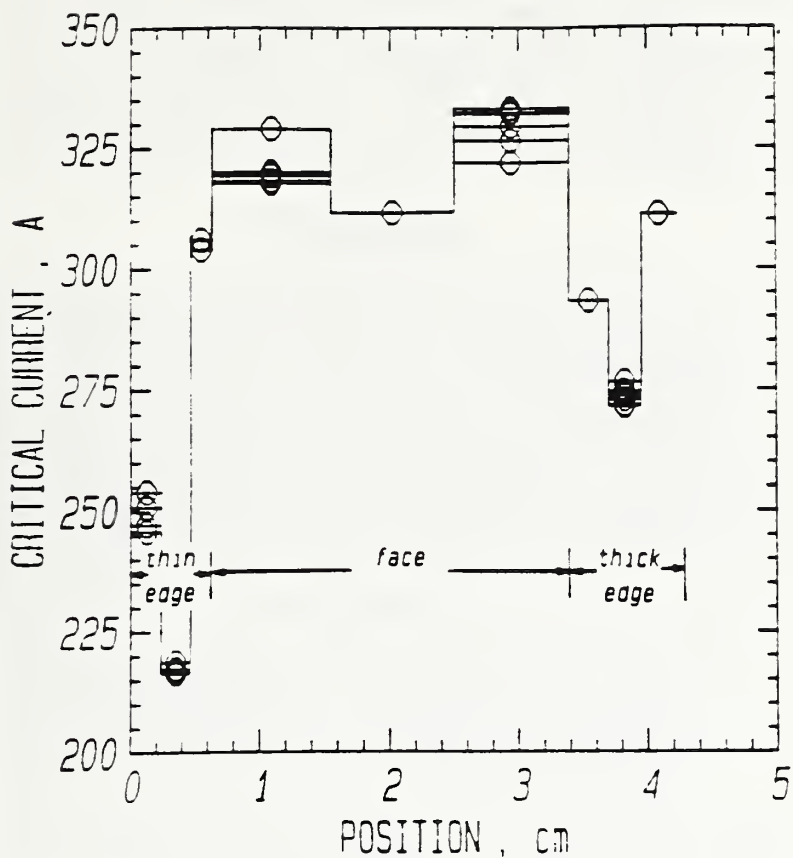
Figure 3.   Sample B, I_c vs. position at 0°.

weak link at 0° contributed about 95% of the total voltage even though it represented only 5% of the total length.

    Table 1 snows the percent differences of the I_c's from the starting wire (before cabling) values. The starting wire I_c's are approximate because they
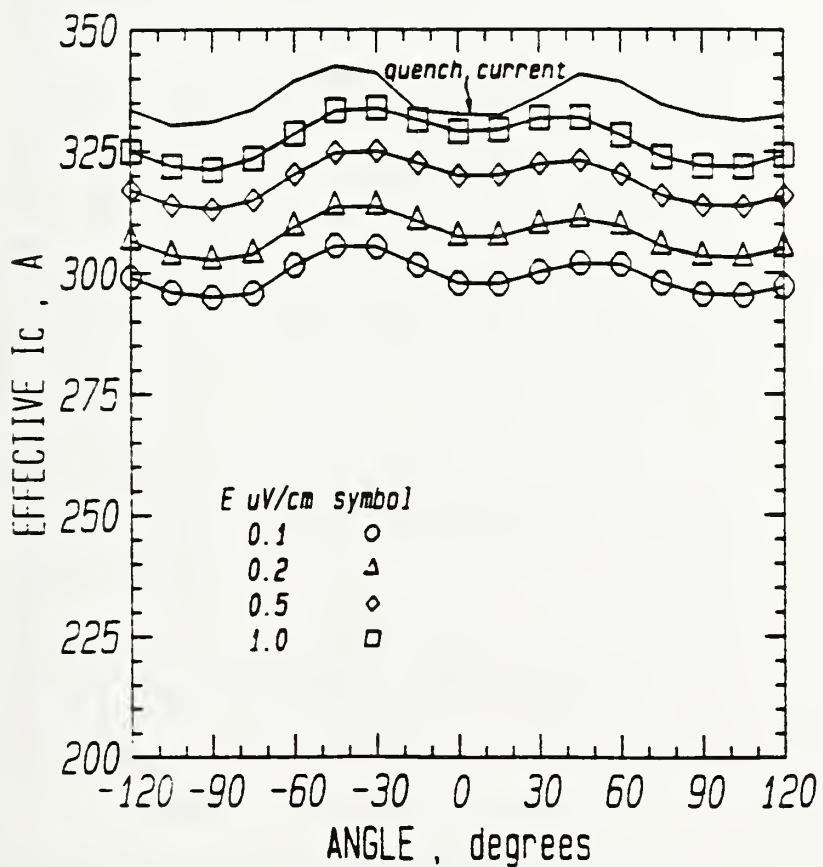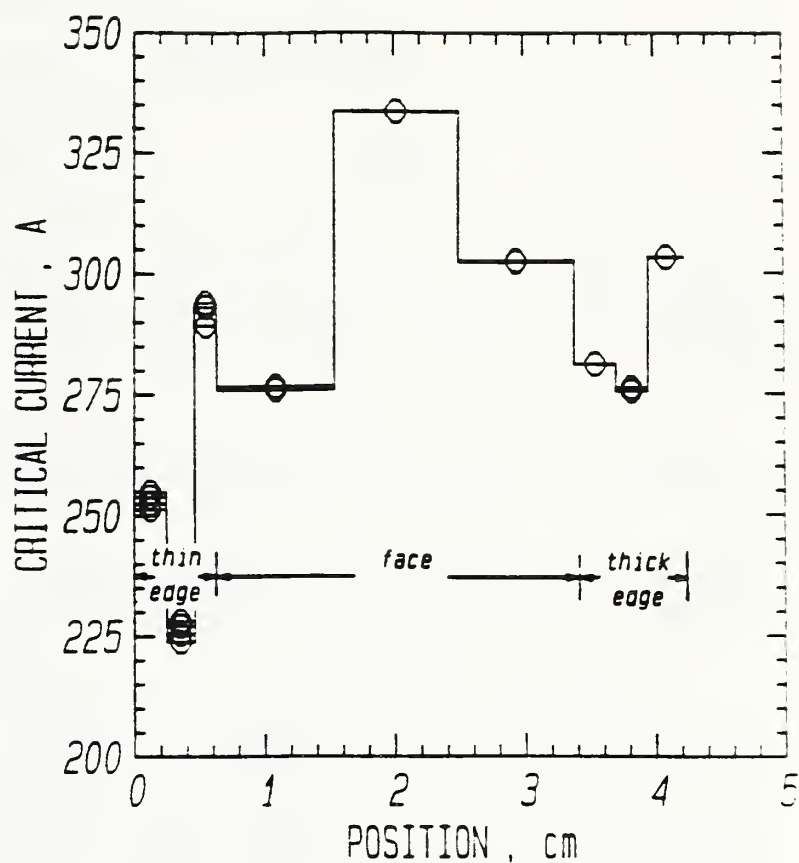

Figure 4.   Sample B, I_c vs. position at 90°.

were measured as another part of this program in another magnet.[9] The additional lowering of the weak-link I_c for Sample B resulted in a much lower effective I_c. In fact, the difference in effective I_c's was greater than the difference in weak link I_c's at 0.1 µV/cm. At 0°, I_c of Sample B was an additional

Figure 5.   Sample A, effective I_c and quench I vs. angle.
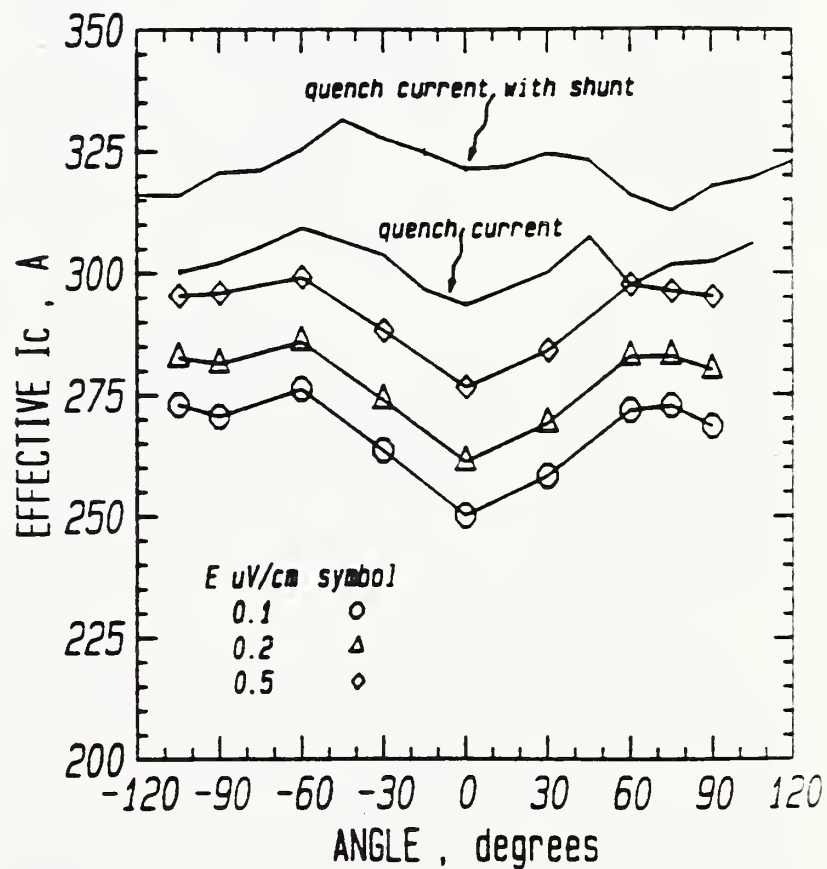

Figure 6.   Sample B, effective I_c and quench I vs. angle.

Table 1. Percent differences in I_c from starting wire I_c's at 5 T, 4.0 K, and 0.1 μV/cm

Starting Wire I_c	Sample A 320 A		Sample B 347 A	
Field Angle	0°	90°	0°	90°
highest segment	+ 2.8%	- 4.7%	- 4.6%	- 4.0%
lowest segment	-25.3%	-15.3%	-37.5%	-34.9%
effective I_c	- 6.9%	- 7.5%	-27.7%	-22.8%

12% lower than that of Sample A but the effective I_c was 20% lower. The difference in I_c's at higher electric fields, however, was more than 12%. This increased effect may show that the local heating had an adverse effect on I_c for Sample B.

Discussion

Understanding the relationship between the mechanical deformation in the cabling process and the electrical performance may lead to improvements in the critical current of a cable. Comparisons of these two samples should be tempered by the fact that the starting wires were not the same but were similar enough to support the conclusions drawn from each sample. Additional current sharing that can take place in the cable will help reduce the effects of local changes in critical current. However, the experiment of shunting Sample B by soldering another strand to it (with no transport current of its own) may indicate that the best case would only be a 7% improvement. On the other hand, any compromise in end cooling could have a significant effect.

These results have two implications for short-sample critical-current testing of cables. First, the data indicate that both magnetic-field orientations need to be tested in order to determine the limiting case for the critical current. As shown above, for more degraded cables, the parallel-field case may limit. In the less degraded cables, the perpendicular case limits. The amount of degradation is not known beforehand, so both orientations need to be measured.

Second, the difference between thick and thin edge degradation shown in these data indicates that changing the direction of the test current (for each field orientation) will affect the critical current. This is because the location of the peak magnetic field changes with current direction (see Fig. 3 in Ref. 6). Thus, the peak field location relative to the thin edge should be recorded. The conservative approach in short-sample cable tests would be to make the measurement for both directions of the test current and use the critical current for the worst case. The additional measurements will help increase the understanding of cable degradation.

Conclusions

Cabling can lead to very localized reduction in critical current within a single strand. The lowest critical current was observed for the central flat part of the thin edge and this segment contributes most of the overall voltage drop. The widest spread in local critical current values along the cable strands occurs with the magnetic field perpendicular to the cable edge. Unfortunately in the dipole magnet application, this orientation is near the critical orientation. The relevant critical-current criteria

for local measurements may be based on a spatial average. This is because of the extreme localization of damage, limited extent of the voltage, and strong end cooling effect which all limit the local temperature rise. Any compromise in sample stability may lower the critical current to that of the weak link.

References

1. J. W. Ekin, L. F. Goodrich, J. Moreland, E. S. Pittman, and A. F. Clark, "Electro-Mechanical Properties of Superconductors for High Energy Physics Applications," NBSIR 86-3061, National Bureau of Standards, Boulder, Colorado.

2. J. Royet and R. M. Scanlan, "Manufacture of Keystoned Flat Superconducting Cables for Use in SSC Dipoles," these proceedings, paper LB-1.

3. R. Scanlan, J. Royet, and C. E. Taylor, "Superconducting Materials for the SSC," Adv. Cryog. Eng. - Materials, Vol. 32, 697, Plenum Press, New York (1986).

4. D. C. Larbalestier, A. W. West, W. Starch, W. Warnes, P. Lee, W. K. McDonald, P. O'Larey, K. Hemachalam, B. Zeitlin, R. Scanlan, and C. Taylor, "High Critical Current Densities in Industrial Scale Composites Made From High Homogeneity Nb 46.5 Ti," IEEE Trans. on Magnetics, MAG 21, 269, 1985.

5. W. B. Sampson, Brookhaven National Laboratory., Upton, New York, private communications (1986).

6. M. Garber and W. B. Sampson, "Critical Current Anisotropy in NbTi cables," IEEE Trans. on Magnetics, MAG 21, 336, 1985.

7. L. F. Goodrich, W. P. Dube, E. S. Pittman, and A. F. Clark, "The Effect of Aspect Ratio on Critical Current in Multifilamentary Superconductors," Adv. Cryog. Eng. - Materials, Vol. 32, 833, Plenum Press, New York (1986).

8. A. F. Clark, L. F. Goodrich, F. R. Fickett, and J. V. Minervini, "Development of Standards for Superconductors, Interim Report Oct. 1980 to Jan. 1982," NBSIR 82-1678, National Bureau of Standards, Boulder, Colorado (July 1982), pp 17-36.

9. J. W. Ekin, "Critical Current vs. Stress Relationships in NbTi Superconductors," these proceedings, paper MH-6.

CURRENT CAPACITY DEGRADATION IN SUPERCONDUCTING CABLE STRANDS

L. F. Goodrich and S. L. Bray
National Bureau of Standards
Boulder, Colorado 80303

Abstract

The electromagnetic properties of NbTi strands extracted from Rutherford cables were studied to clarify the effect of mechanical deformation, caused by the cabling process, on the current capacity of the strands. Three different cables were studied, all of which are prototypes for the Superconducting Super Collider's dipole magnets. The extracted cable strands were instrumented to allow measurement of the voltage across several key regions of mechanical deformation as a function of current and the orientation of the applied magnetic field. The resulting data are presented in terms of the strand's voltage profile as well as its critical current in order to more thoroughly characterize the conductor's electromagnetic properties. The cable strands show very localized reductions in current capacity that are well correlated with the regions of high mechanical deformation. For example, at a particular field orientation, the voltage across a portion of the strand that is only 3% of the total strand length contributes 90% of the total strand voltage. Two applied magnetic field orientations, parallel and perpendicular to the cable's width, have pronounced effects on the electrical properties of the strand. Both of these magnetic field orientations will arise in applications.

Introduction

The measurements presented here are a continuation of earlier studies[1] of NbTi cable strands extracted from Rutherford cables (cables provided by the Lawrence Berkeley Laboratory). These are prototype cables for high energy physics applications. Specifically, they were designed for use in the outer windings of the Superconducting Super Collider's (SSC) dipole magnets. The main emphasis of these studies is the effect of mechanical deformation, during manufacture, on the cable's current capacity. In addition to the bending deformation required to achieve the cable's twist pitch, the cables are compacted into a keystone shape. These mechanical deformations result in a very localized degradation in the electrical properties of the cable strands. The deformation of the cable strands results in a periodic geometry with the various segments of the strands defined by the degree and type of deformation. The desired product of this work is information that will lead to methods for reducing the current-capacity degradation associated with the manufacture of superconducting cables.

For all the measurements, the orientation of the applied magnetic field was perpendicular to the cable's longitudinal axis. The angle of the applied field about this axis was set at either the 0° (parallel to the cable width) or 90° (perpendicular) orientation. The reasons for emphasizing these field directions are twofold. First, there is a pronounced effect on the strand's electrical properties in these orientations and, second, both of these field orientations arise in a dipole magnet. The experimental details of this work will be reported in a future publication.[2]

The mechanical deformation of the cable strands during the cabling process results in localized variations in the conductor's current capacity. The sources of this variation fall into two categories: cross-sectional area differences and angular effects. The cross-sectional variation of the superconducting filaments is due to necking and serrated yielding of the NbTi filaments. Under the second category, angular effects, the orientation of the applied magnetic field with respect to the conductor's longitudinal axis (pitch angle effect) and its mechanically deformed cross section (aspect ratio effect[3]) vary along the strand.

Three different cables, manufactured with different virgin wire (source wire for the cable strands) and cabling techniques, were studied. These data allow comparisons among the cables. The strand critical current (strand I_c) is defined as the current at which the sum of the voltages from each of the strand segments divided by the sum of the segment lengths is equal to a selected electric field criterion. The strand I_c is presented for both magnetic field orientations, 0° and 90°. This information is useful in examining the cumulative effect of variations in spatial orientation and aspect ratio of different strand segments at different field angles. The concept of a strand I_c is also useful for comparing the strand's I_c with the I_c of the virgin wire from which the cable was manufactured. These comparisons indicate the amount of I_c degradation introduced by the cabling process. In order to assess the relative contribution to the total voltage of different strand segments, the voltage distribution along the conductor's length, at both magnetic field angles, is also presented.

Three different cables, denoted as W, X, and Y, were studied. Cable W was re-rolled through a turkshead (for resizing) after it had been cabled. The re-rolled cable is a worst-case situation that was studied to more clearly identify the degradation features. Cable X is similar to W; however, it was not subjected to as much mechanical deformation and is a more typical example of late 1985 to early 1986 prototype outer cables. Cable Y (1987) is an evolution of cable X where the cabling techniques were refined in an attempt to reduce current-capacity degradation.

Results

The conductors measured in this study represent an evolution in the cable fabrication process aimed at reducing its detrimental effect on the critical-current density (J_c) of the finished cable in comparison to that of the virgin wire.[4] An evolution has also occurred in the design and processing of the virgin wire.[5] This evolution can be characterized by a decrease in filament size aimed at reducing ac losses while attempting to maintain the J_c. Initially, the increased wire drawing that was used to reduce the filament size of wire X in comparison with wire W resulted in a lower J_c. Later, improved manufacturing processes that were used for wire Y resulted in a substantial restoration of the J_c of the virgin wire.

Strand Critical Current

I_c measurements were made on the virgin wires from which each respective cable was manufactured. Three pairs of voltage taps, with each pair spanning about 10 mm, were connected to the specimens. This allowed

for a check of I_c homogeneity with position. I_c measurements were also made as a function of the applied magnetic field angle. This allowed for a test of I_c homogeneity with respect to field angle. The average I_c of the virgin wire was used to determine the relative degradation of each cable. The typical I_c variation among voltage taps was ±0.3% at 5 T and ±0.5% at 8 T for all of the virgin wire samples. For samples X and Y, the I_c variation of a given tap with respect to field angle (0° to 360°) was measured to be about ±0.6% at 5 T.

Figures 1 and 2 show comparisons between the J_c of the extracted cable strands (strand J_c) and the virgin wires from which they were constructed. Figure 1 shows this comparison for each of the three conductors for applied magnetic field angles of 0° and 90° at 5 T. There is a consistent increase in the J_c at 0° from cable W to cable Y although the virgin wire's J_c decreased between wires W and X. Since cable W is a worst-case situation with respect to the cabling operation, the higher J_c for strand X is due to the reduced mechanical deformation of the strand. Cable Y shows a greater mechanical degradation of its J_c than cable X, but, again, it shows an increased strand J_c due to its high virgin wire J_c. For cable strand X, the mechanical degradation of the J_c was somewhat higher at 90° than at 0° and, consequently, there was a decrease in the J_c of strand X as compared with the J_c of strand W. This increased degradation at 90° was not present in strand Y and strand Y showed an increased J_c in comparison with its two predecessors.

The 8 T plot, Fig. 2, shows an increase in the strand's J_c between W and Y but there is a decrease between W and X. Comparison between the 5 and 8 T J_c degradation for all of the strands shows a reduced sensitivity to mechanical deformation at the higher magnetic field for all the strands. The virgin wire W, which has larger diameter filaments, had a higher relative J_c at 8 T than do wires X and Y. This lower sensitivity of wire W to magnetic field results in a higher strand J_c for W than for X.

Differential Voltage Profile

Figures 3 and 4 show the electrical properties of the cable strand as a function of the position along its length. At the top of each plot, located outside the axes, is an outline of the cable strand's geometry positioned so as to correlate with the horizontal or position axis. The cable outline is labeled to indicate the position of the thin edge, the face, and the thick edge relative to the horizontal axis. The differential voltage across the various strand segments is plotted as a function of position. The plateaus, or peak levels, in the curves represent the voltage across the indicated strand segments at the indicated strand I_c. The lines connecting the data are only a visual aid and they are not intended as an interpolation between the data points. The current levels for each of the different samples is not the same in these plots (current levels for each of the strands is given in the figure captions); however, the overall voltage level is the same for each of the samples. In other words, the data in these plots represents the same strand I_c criterion (0.1 $\mu V/cm$) for each of the samples.

The plots show that there is a considerable variation in the lengths of the various strand segments. Herein lies the significance of these plots, which show the relative contribution of the separate strand segments to the overall voltage.

For the samples and conditions existing in these measurements, the total voltage seems to determine the
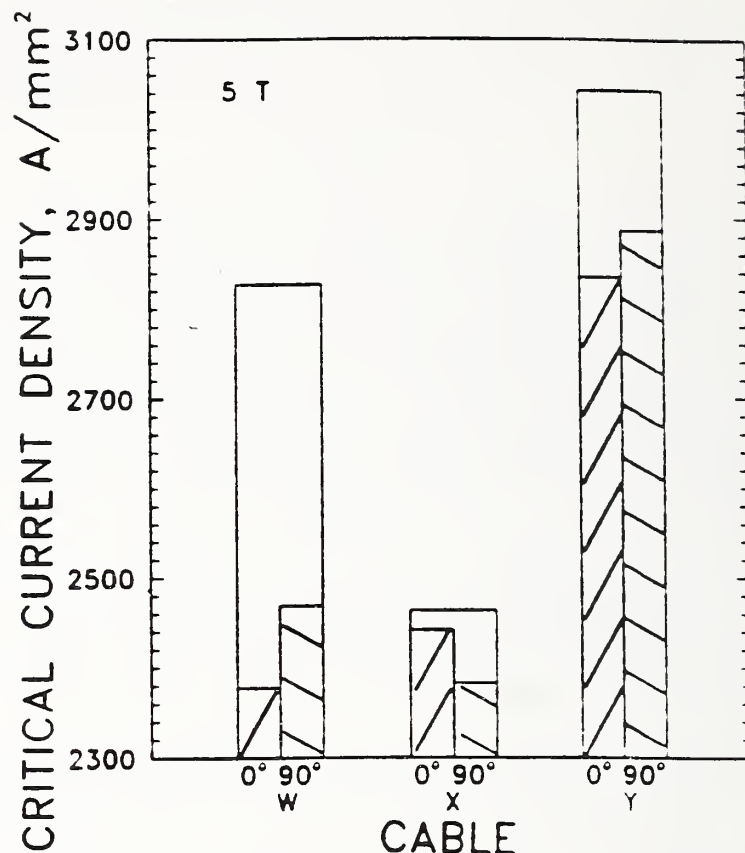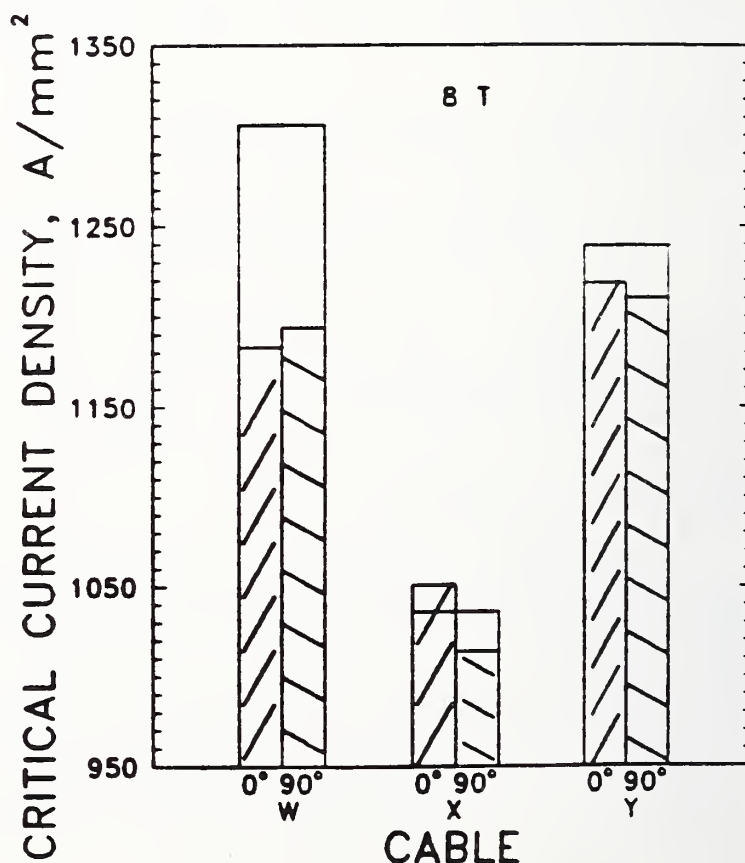

Figure 1. Critical current density of cable strands and their respective virgin wires for 0 and 90° at 5 T. The virgin wire J_c is represented by the continuous line segment spanning 0 to 90° for each cable. The strand J_c values at 0 and 90° are represented by the shaded bars for each cable.

Figure 2. Critical current density of cable strands and their respective virgin wires for 0 and 90° at 8 T. The virgin wire J_c is represented by the continuous line segment spanning 0 to 90° for each cable. The strand J_c values at 0 and 90° are represented by the shaded bars for each cable.
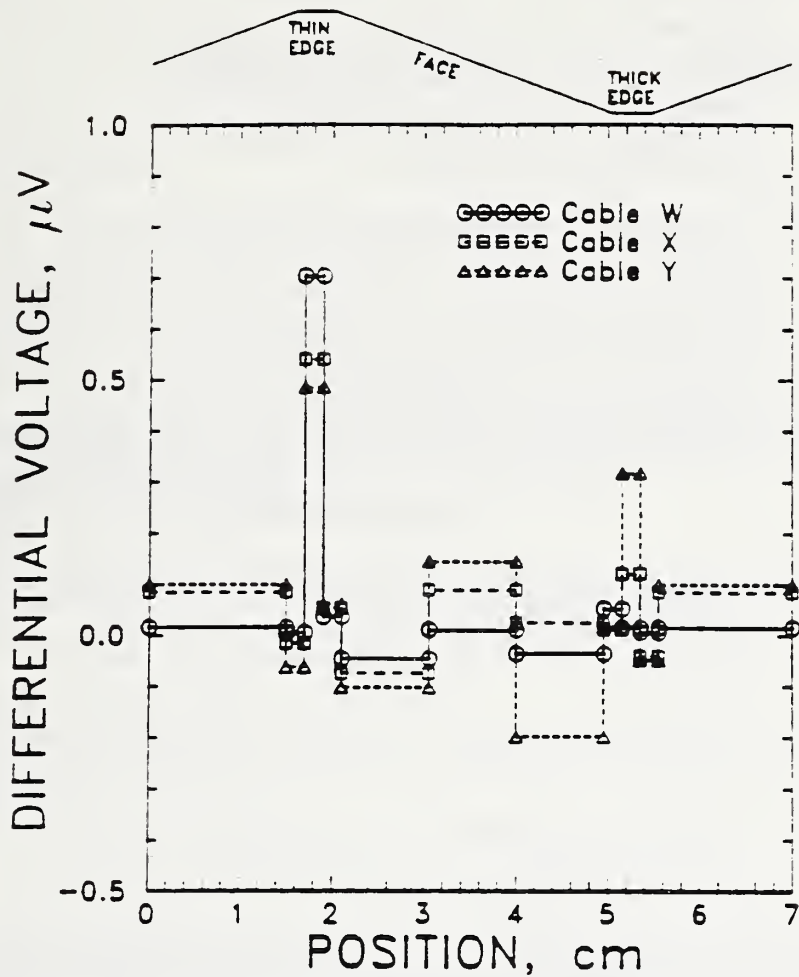
Figure 3. Differential voltage profiles at 5 T and an applied magnetic field angle of 0° for cables W, X, and Y at currents of 285 A, 307 A, and 339 A respectively.

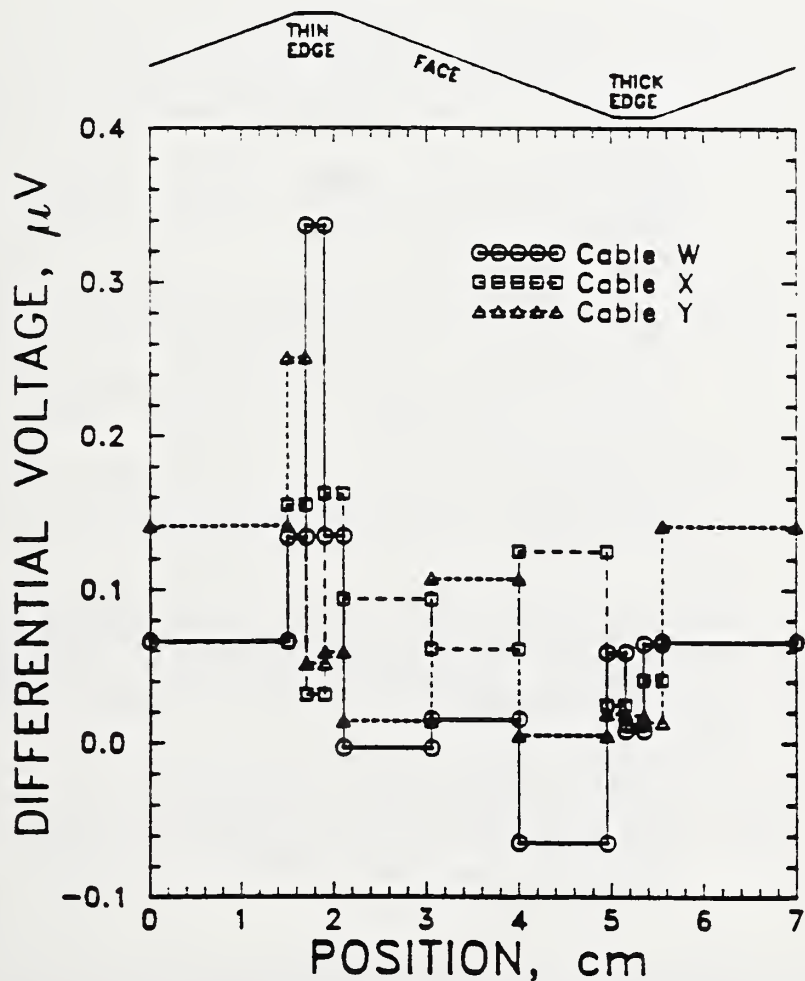Figure 4. Differential voltage profiles at 5 T and an applied magnetic field angle of 90° for cables W, X, and Y at currents of 296 A, 300 A, and 345 A respectively.

current capacity of the conductor. This is evidenced by a close agreement between the measured strand critical currents and the maximum achieved currents (quench currents). For a sample that has poor longitudinal thermal conductivity, the short edge segments might act as weak links, limiting the current capacity to a value below that required to reach the strand I_c criterion. For all cables and the 0° orientation, the majority of the voltage is concentrated at the edges of the cable with the central portions being dominant. At 90°, the voltage concentration increases at the corners of the edges in comparison with the centers.

The negative voltages shown in the plots are projection voltages[6,7] associated with current redistribution among the filaments. The strongest evidence of intrinsic (not associated with the location of the current contact) transverse currents within the strand is a region of negative voltage bounded by regions of large positive voltages. The curve for cable Y is the best example of this structure. This type of structure is present in the center of these plots. This indicates that the current redistribution is caused by the longitudinal variation in the relative current carrying capacity of the filaments rather than being caused by current injection at the current contact. Thus, voltages associated with this type of redistribution will occur periodically along the entire length of the cable strand.

Although the negative voltages are the most obvious indication of current redistribution, there are other indicators. These indicators have the same general character as the negative voltages with the exception of polarity. The positive current transfer voltages are evident when observing a series of differential voltage plots in which the sample current is increasing. There are portions of the differential voltage profile that rise abruptly, like a flux flow voltage, and then level off with increasing current until the actual flux flow region is reached. These transitory positive voltages, like the negative voltages, are indicative of intrinsic current redistribution within the cable strand.

Discussion

The main objective of this work is to determine the current capacity of several different cable strands with the ultimate goal being an increased understanding of the sources and degree of current capacity degradation in these conductors. Typically, the I_c of a conductor is an accepted practical measure of its current capacity. However, for these particular conductors, there are some difficulties in relating I_c to the actual current capacity of the cable strands. Owing to the electrical inhomogeneity of the strands caused by the cabling operation, there is a large variation in the I_c along the strand's length. The problem is determining what current level in this fairly broad range of critical currents best reflects the strand's practical current capacity.

One approach is to assume a weak link situation where the strand segment that has the lowest I_c determines the overall current capacity of the strand. A comparison between the actual quench currents (the maximum observed current prior to thermal runaway) and the weak link I_c shows that the current capacity of the strand is significantly higher than the weak link I_c. This enhanced current capacity, above the weak link I_c, is due to the strand's relatively good stability.

At the other extreme, the current capacity of the strands could be assumed to be equal to the strand I_c. For the conductors tested here, this would not be a bad

assumption, as evidenced by the close agreement between the strand I_c and the quench currents. However, there are two problems associated with simply measuring the strand I_c and assuming this to be the strand's practical limit. First, the strand I_c gives no information about the voltage distribution along the strand's length and, consequently, it is not useful in understanding the sources of current degradation in the cable. Also, for conductors that are less stable than those tested here, the actual current limit might be close to the weak link I_c and, in this case, the strand I_c level could not be achieved.

Another factor associated with the I_c measurements for these cable strands is the presence of intrinsic current-transfer voltages that are caused by periodic current redistribution along the strand's length. This current transfer is apparently caused by the periodic mechanical deformation of the strand and, thus, it is not limited to the current contact area. Due to its intrinsic nature, these current transfer voltages play a role in determining the current capacity of the cable, not only in testing but in application as well. It is clear that I_c data alone are insufficient for characterizing these conductors. For this reason the differential voltage data were also presented.

Conclusions

Based on these measurements, some general conclusions can be stated regarding the electromagnetic character of these cables and its effect on their current capacities. Also, the measurements have implications regarding short sample testing of these cables.

The mechanical deformation of the cable strands associated with the cabling process can lead to very localized reductions in their current capacity. The widest spread in local current capacity occurs with the applied magnetic field parallel to the cable's width. Despite large local variations in the cable strand's current capacity, the quench current and the strand I_c do not vary much with the angle of the applied magnetic field. The deformation geometry of the cable is such that the interaction between the applied magnetic field and a strand segment's aspect ratio or its pitch angle have the same tendency. In other words, a field angle that is detrimental (beneficial) to a strand segment's current capacity due to its aspect ratio is also detrimental (beneficial) due to its pitch angle. However, the various strand segments have different critical orientations such that the detrimental and beneficial effects of the field angle on the various segments tend to cancel one another over the total length of the strand. For these particular conductors, the relevant I_c criteria may be a spatial average (the strand I_c) because the degradation in current capacity is concentrated over short regions of the cable strand and local temperature rises are limited by strong end cooling. Any compromise in sample stability may lower the I_c to that of the weak link segment of the cable strand.

These results have two implications for short-sample I_c testing of cables. First, the data indicate that both magnetic field orientations, parallel to the cable's width and perpendicular to its width, need to be tested to determine the limiting orientation for the I_c. The limiting magnetic-field orientation can be parallel or perpendicular to the cable's width and the limiting orientation is not known beforehand. Second, a large difference in current capacity degradation can exist between the thick and thin cable edges; thus, changing the direction of the test current (for each field orientation) can affect the measured I_c. This is due to a self field effect where the location of the

peak magnetic field depends on the current direction. Thus, the peak field location should be part of the data recorded for short sample measurements of these conductors. Consequently, these more detailed cable measurements should be made periodically as part of the cable development process.

The wire from which these cables are made has evolved to the point where they have a high virgin current capacity and a relatively high tolerance to mechanical deformation. Considering the amount of mechanical deformation of the strands caused by the cabling process, the resulting degradation in current capacity is surprisingly low. In the case of the latest outer winding cable, sample Y, the maximum observed degradation in its strand I_c was only 6.8%.

References

[1] L. F. Goodrich, E. S. Pittman, J. W. Ekin, and R. M. Scanlan, "Studies of NbTi Strands Extracted from Coreless Rutherford Cables," IEEE Trans. on Magnetics, MAG 23, 1642, 1987.

[2] J. W. Ekin, L. F. Goodrich, and S. L. Bray, NBSIR, National Bureau of Standards, Boulder, Colorado (to be published).

[3] L. F. Goodrich, W. P. Dube, E. S. Pittman, and A. F. Clark, "The Effect of Aspect Ratio on Critical Current in Multifilamentary Superconductors," Adv. Cryog. Eng. -Materials, Vol. 32, 833, Plenum Press, New York (1986).

[4] J. Royet and R. M. Scanlan, "Manufacture of Keystoned Flat Superconducting Cables for Use in SSC dipoles," IEEE Trans. on Magnetics, MAG 23, 480, 1987.

[5] D. C. Larbalestier et al., "High Critical Current Densities in Industrial Scale Composites Made From High Homogeneity Nb 46.5 Ti", IEEE Trans. on Magnetics, MAG 21, 269, 1985.

[6] L. F. Goodrich, J. W. Ekin, F. R. Fickett, "Effect of Twist Pitch on Short-Sample V-I Characteristics of Multifilamentary Superconductors," Adv. Cryog. Eng. - Materials, Vol. 28, Plenum Press, New York (1981), p. 571-580.

[7] L. F. Goodrich, "The Effect of Field Orientation on Current Transfer in Multifilamentary Superconductors," IEEE Trans. Mag. MAG-19, 244-247 (1983).

4. TITLE AND SUBTITLE

ELECTROMECHANICAL PROPERTIES OF SUPERCONDUCTORS FOR HIGH ENERGY PHYSICS APPLICATIONS
PART II

5. AUTHOR(S)

J. W. Ekin, L. F. Goodrich, S. L. Bray, N. F. Bergren, and R. B. Goldfarb

11. ABSTRACT (A 200-WORD OR LESS FACTUAL SUMMARY OF MOST SIGNIFICANT INFORMATION. IF DOCUMENT INCLUDES A SIGNIFICANT BIBLIOGRAPHY OR LITERATURE SURVEY, MENTION IT HERE.)

This report presents data on superconductor performance under mechanical load. The data are needed for setting mechanical design constraints and measuring the electromechanical perform-ance of NbTi superconductors for DOE high-energy physics magnet applications. The effect of axial tensile stress, applied at room temperature, on the critical current of NbTi superconduc-tor strands has been measured.. The data show a simple result that the effect on the critical current is independent of the temperature at which the stress is applied; this allows the exis-ting 4 K data base to be used to determine critical current degradation from room temperature fabrication stress, from cool-down stress introduced by differential contraction, and from 4 K stress generated by the Lorentz force when the magnet is energized. A study of the critical current variations along NbTi strands extracted from a Rutherford cable has been made also. The results show that the principal mechanical degradation is extremely localized at the re-gions where the NbTi strand is bent around the edge of the cable. For example, only 3% of the total strand length can contribute 92% of the total strand voltage. A further study has been made of the effects of bending strain on the critical current of NbTi conductors. The degra-dation of the critical current from bending strain is much greater at low values of electrical field than at high, suggesting that irregularity of the filament cross-sectional area intro-duced by bending may be the source of the I_c degradation. The bend tolerance of a NbTi conduc-tor can be enhanced by increasing the local copper-to-superconductor area ratio. Measurements of the permeability, saturation magnetization, and intrinsic coercivity of several high-perme-ability steel alloys were made. The overall differences of saturation magnetization and in-trinsic coercivity between cold-rolled steel samples were not significant.

12. KEY WORDS (6 TO 12 ENTRIES; ALPHABETICAL ORDER; CAPITALIZE ONLY PROPER NAMES; AND SEPARATE KEY WORDS BY SEMICOLONS)

bending strain; cable; coercivity; critical current; electromechanical; magnetic properties; mechanical properties; NbTi; permeability; Rutherford cable; saturation magnetization; SSC; stress effect; Superconducting Super Collider